PHYSICAL REVIEW D **87,** 094031 (2013)

Flavor-phenomenology of two-Higgs-doublet models with generic Yukawa structure

Andreas Crivellin, Christoph Greub, and Ahmet Kokulu

Albert Einstein Center for Fundamental Physics, Institute for Theoretical Physics, University of Bern, CH-3012 Bern, Switzerland

(Received 3 April 2013; published 28 May 2013)

In this article, we perform an extensive study of flavor observables in a two-Higgs-doublet model with generic Yukawa structure (of type III). This model is interesting not only because it is the decoupling limit of the minimal supersymmetric standard model but also because of its rich flavor phenomenology which also allows for sizable effects not only in flavor-changing neutral-current (FCNC) processes but also in tauonic B decays. We examine the possible effects in flavor physics and constrain the model both from tree-level processes and from loop observables. The free parameters of the model are the heavy Higgs mass, $\tan\beta$ (the ratio of vacuum expectation values) and the ''nonholomorphic'' Yukawa couplings $\epsilon^f_{ij}(f = u, d, \ell)$. In our analysis we constrain the elements ϵ^f_{ij} in various ways: In a first step we give order of magnitude constraints on ϵ^f_{ij} from 't Hooft's naturalness criterion, finding that all ϵ^f_{ij} must be rather small unless the third generation is involved. In a second step, we constrain the Yukawa structure of the type-III two-Higgs-doublet model from tree-level FCNC processes ($B_{s,d} \to \mu^+\mu^-$, $K_L \to \mu^+\mu^-$, $\bar{D}^0 \to \mu^+\mu^-$, $\Delta F = 2$ processes, $\tau^- \to \mu^-\mu^+\mu^-$, $\tau^- \to e^-\mu^+\mu^-$ and $\mu^- \to e^-e^+e^-$) and observe that all flavor off-diagonal elements of these couplings, except $\epsilon^u_{32,31}$ and $\epsilon^u_{23,13}$, must be very small in order to satisfy the current experimental bounds. In a third step, we consider Higgs mediated loop contributions to FCNC processes [$b \to s(d)\gamma$, $B_{s,d}$ mixing, $K - \bar{K}$ mixing and $\mu \to e\gamma$] finding that also ϵ^u_{13} and ϵ^u_{23} must be very small, while the bounds on ϵ^u_{31} and ϵ^u_{32} are especially weak. Furthermore, considering the constraints from electric dipole moments we obtain constrains on some parameters $\epsilon^{u,\ell}_{ij}$. Taking into account the constraints from FCNC processes we study the size of possible effects in the tauonic B decays ($B \to \tau\nu$, $B \to D\tau\nu$ and $B \to D^*\tau\nu$) as well as in $D_{(s)} \to \tau\nu$, $D_{(s)} \to \mu\nu$, $K(\pi) \to e\nu$, $K(\pi) \to \mu\nu$ and $\tau \to K(\pi)\nu$ which are all sensitive to tree-level charged Higgs exchange. Interestingly, the unconstrained $\epsilon^u_{32,31}$ are just the elements which directly enter the branching ratios for $B \to \tau\nu$, $B \to D\tau\nu$ and $B \to D^*\tau\nu$. We show that they can explain the deviations from the SM predictions in these processes without fine-tuning. Furthermore, $B \to \tau\nu$, $B \to D\tau\nu$ and $B \to D^*\tau\nu$ can even be explained simultaneously. Finally, we give upper limits on the branching ratios of the lepton flavor-violating neutral B meson decays ($B_{s,d} \to \mu e$, $B_{s,d} \to \tau e$ and $B_{s,d} \to \tau\mu$) and correlate the radiative lepton decays ($\tau \to \mu\gamma$, $\tau \to e\gamma$ and $\mu \to e\gamma$) to the corresponding neutral current lepton decays ($\tau^- \to \mu^-\mu^+\mu^-$, $\tau^- \to e^-\mu^+\mu^-$ and $\mu^- \to e^-e^+e^-$). A detailed Appendix contains all relevant information for the considered processes for general scalar-fermion-fermion couplings.

DOI: 10.1103/PhysRevD.87.094031 PACS numbers: 13.20.He, 12.60.−i, 14.80.Da

I. INTRODUCTION

Two-Higgs-doublet models (2HDMs) [1] have been under intensive investigation for a long time (see for example Ref. [2] for an introduction or Ref. [3] for a recent review article). There are several reasons for this great interest in 2HDMs: First, 2HDMs are very simple extensions of the standard model (SM) obtained by just adding an additional scalar $SU(2)_L$ doublet to the SM particle content. This limits the number of new degrees of freedom and makes the model rather predictive. Second, motivation for 2HDMs comes from axion models [4] because a possible CP-violating term in the QCD Lagrangian can be rotated away [5] if the Lagrangian has a global $U(1)$ symmetry which is only possible if there are two Higgs doublets. Also the generation of the baryon asymmetry of the Universe motivates the introduction of a second Higgs doublet because in this way the amount of CP violation can be large enough to accommodate for this asymmetry, while the CP violation in the SM is too small [6]. Finally, probably the best motivation for studying 2HDMs is the minimal supersymmetric standard model (MSSM) where supersymmetry enforces the introduction of a second Higgs doublet [7] due to the holomorphic superpotential. Furthermore, the 2HDM of type III is also the effective theory obtained by integrating out all superpartners of the SM-like particles (the SM fermion, the gauge boson and the Higgs particles of the 2HDM) from MSSM.

2HDMs are not only interesting for direct searches for additional Higgs bosons at colliders. In addition to these high energy searches at the LHC also low-energy precision flavor observables provide a complementary window to physics beyond the SM, i.e., to the 2HDMs. In this respect, flavor-changing neutral-current (FCNC) processes, e.g., neutral meson decays to muon pairs ($B_{s(d)} \to \mu^+\mu^-$, $D \to \mu^+\mu^-$ and $K_L \to \mu^+\mu^-$) are especially interesting because they are very sensitive to flavor changing neutral Higgs couplings. However, also charged current processes

like tauonic B-meson decays are affected by the charged Higgs boson and $b \to s\gamma$ provides currently the best lower limit on the charged Higgs mass in the 2HDM of type II.

Recently, tauonic B decays received special attention because the *BABAR* collaboration performed an analysis of the semileptonic B decays $B \to D\tau\nu$ and $B \to D^*\tau\nu$ reporting a discrepancy of 2.0σ and 2.7σ from the SM expectation, respectively. The measurements of both decays exceed the SM predictions, and combining them gives a 3.4σ deviation from the SM [8,9] expectation, which constitutes first evidence for new physics in semileptonic B decays to tau leptons. This evidence for the violation of lepton flavor universality is further supported by the measurement of $B \to \tau\nu$ by *BABAR* [10,11] and BELLE [12,13] which exceeds the SM prediction by 1.6σ using V_{ub} from the global fit [14]. Assuming that these deviations from the SM are not statistical fluctuations or underestimated theoretical or systematic uncertainties, it is interesting to ask which model of new physics can explain the measured values. Since a 2HDM of type II cannot explain $B \to \tau\nu$, $B \to D\tau\nu$ and $B \to D^*\tau\nu$ simultaneously [8], one must look at 2HDMs with more general Yukawa structures. Also 2HDMs of type III with minimal flavor violation (MFV) [15] cannot explain these deviations from the SM but a 2HDM of type III (where both Higgs doublets couple to up quarks and down quarks as well) with flavor violation in the up sector, is capable of explaining $B \to \tau\nu$, $B \to D\tau\nu$ and $B \to D^*\tau\nu$ without fine-tuning [16].

These points motivate us to perform a complete analysis of flavor violation in 2HDMs of type III in this article. For this purpose we take into account all relevant constraints from FCNC processes (both from tree-level contributions and from loop-induced effects) and consider afterwards the possible effects in charged current processes.

This article is structured as follows: In Sec. II, we review the Yukawa Lagrangian of the 2HDM of type III. In Sec. III we give a general overview on the constraints on 2HDMs and update the bounds on the 2HDM of type II. The following sections discuss in detail the constraints on the 2HDM of type-III parameter space from 't Hooft's naturalness argument (Sec. IV), from tree-level FCNC processes (Sec. V) and from loop-induced charged and neutral Higgs mediated contributions to the flavor observables (Sec. VI). Section VII studies the possible effects in charged current decays ($B \to \tau\nu$, $B \to D\tau\nu$, $B \to D^*\tau\nu$, $D_{(s)} \to \tau\nu$, $D_{(s)} \to \mu\nu$, $K(\pi) \to e\nu$, $K(\pi) \to \mu\nu$, $\tau \to K(\pi)\nu$) and Sec. VIII is denoted to the study of the upper limits on the branching ratios $B_{s,d} \to \tau\mu, B_{s,d} \to \tau e, B_{s,d} \to \mu e$ and the correlations among $\tau^- \to \mu^-\mu^+\mu^-, \tau^- \to e^-\mu^+\mu^-$, $\mu^- \to e^-e^+e^-$ and $\tau \to \mu\gamma$, $\tau \to e\gamma$, $\mu \to e\gamma$. Finally, we conclude. A detailed Appendix contains some of the input parameters used in our analysis, general expressions for some branching ratios as well as all the relevant Wilson coefficients for $b \to s(d)\gamma$, $\Delta F = 2$ processes, leptonic neutral meson decays ($\Delta F = 1$), lepton flavor violating (LFV) transitions, electric dipole moments (EDMs), anomalous magnetic moment (AMM) of muon and (semi)leptonic charged meson decays for general charged and/or neutral scalar-fermion-fermion couplings.

II. SETUP

The SM contains only one scalar weak-isospin doublet, the Higgs doublet. After electroweak symmetry breaking its vacuum expectation value ("vev") gives masses to up quarks, down quarks and charged leptons. The charged (CP-odd neutral) component of this doublet becomes the longitudinal component of the W (Z) boson, and thus we have only one physical CP-even neutral Higgs particle in the SM. In a 2HDM we introduce a second Higgs doublet and obtain four additional physical Higgs particles (in the case of a CP conserving Higgs potential): the neutral heavy CP-even Higgs H^0, a neutral CP-odd Higgs A^0 and the two charged Higgses $H^\pm$.

As outlined in the Introduction we consider a 2HDM with generic Yukawa structure (2HDM of type III). One motivation is that a 2HDM with natural flavor conservation (like type I or type II) cannot explain $B \to D\tau\nu$, $B \to D^*\tau\nu$ and $B \to \tau\nu$ simultaneously, while the type-III model is capable of doing this [16]. Beside this, our calculations in the 2HDM III are the most general ones in the sense that they can be applied to models with specific flavor structures like 2HDMs with MFV [15,17,18]. In this sense also our bounds are model independent, because they apply to any 2HDM with specific Yukawa structures as well (in the absence of large cancellations which are unlikely). Finally, the type-III 2HDM is the decoupling limit of the MSSM and the calculated bounds can be translated to limits on the MSSM parameter space.

The fact that the 2HDM III is the decoupling limit of the MSSM also motivates us to choose for definiteness a MSSM like Higgs potential[1] which automatically avoids dangerous CP violation. The matching of the MSSM on the 2HDM Yukawa sector has been considered in detail. For the MSSM with MFV it was calculated in Refs. [19–24] and for the MSSM with generic flavor structure in Ref. [25] (neglecting the effects of the A-terms) and in Ref. [26] (including the A terms). Even the next-to-leading order corrections were calculated for the flavor-conserving case in [27] and for the flavor-changing one in the general MSSM in Ref. [28]. Also the one-loop corrections to the Higgs potential have been considered [29–37], but their effects on flavor observables were found to be small [38].

[1]If we would require that the Higgs potential possesses a Z_2 symmetry the results would be very similar (for $v \ll m_H$). The heavy Higgs masses squared would still differ by terms of the order of v^2 and only Higgs self-couplings would be different, but they do not enter the flavor processes at the loop level under consideration.

Following the notation of Refs. [26,28,39] we have the following Yukawa Lagrangian in the 2HDM of type III starting in an electroweak basis:

$$\mathcal{L}_Y = \bar{Q}^a_{fL}[Y^{d\,\mathrm{ew}}_{fi}\epsilon_{ba}H^{b\star}_d - \epsilon^{d\,\mathrm{ew}}_{fi}H^a_u]d_{iR} + \bar{Q}^a_{fL}[Y^{u\,\mathrm{ew}}_{fi}\epsilon_{ab}H^{b\star}_u - \epsilon^{u\,\mathrm{ew}}_{fi}H^a_d]u_{iR} + \mathrm{H.c.} \tag{1}$$

Here a, b denote $SU(2)_L$ indices, ϵ_{ab} is the two-dimensional antisymmetric tensor with $\epsilon_{12} = -1$ and the Higgs doublets are defined as

$$H_d = \begin{pmatrix} H^1_d \\ H^2_d \end{pmatrix} = \begin{pmatrix} H^0_d \\ H^-_d \end{pmatrix} \quad \text{with} \quad \langle H_d \rangle = \begin{pmatrix} v_d \\ 0 \end{pmatrix},$$
$$H_u = \begin{pmatrix} H^1_u \\ H^2_u \end{pmatrix} = \begin{pmatrix} H^+_u \\ H^0_u \end{pmatrix} \quad \text{with} \quad \langle H_u \rangle = \begin{pmatrix} 0 \\ v_u \end{pmatrix}. \tag{2}$$

Apart from the holomorphic Yukawa couplings $Y^{u\,\mathrm{ew}}_{fi}$ and $Y^{d\,\mathrm{ew}}_{fi}$, we included the nonholomorphic couplings $\epsilon^{q\,\mathrm{ew}}_{fi}$ ($q = u, d$) as well.

As a next step we decompose the $SU(2)$ doublets into their components and switch to a basis in which the holomorphic Yukawa couplings are diagonal:

$$\begin{aligned}\mathcal{L}_Y = &-\bar{d}_{fL}[Y^{d_i}\delta_{fi}H^{0\star}_d + \tilde{\epsilon}^d_{fi}H^0_u]d_{iR} \\ &- \bar{u}_{fL}[Y^{u_i}\delta_{fi}H^{0\star}_u + \tilde{\epsilon}^u_{fi}H^0_d]u_{iR} \\ &+ \bar{u}_{fL}V_{fj}[Y^{d_i}\delta_{ji} - \cot\beta\tilde{\epsilon}^d_{ji}]H^{2\star}_d d_{iR} \\ &+ \bar{d}_{fL}V^\star_{jf}[Y^{u_i}\delta_{ji} - \tan\beta\tilde{\epsilon}^u_{ji}]H^{1\star}_u u_{iR} + \mathrm{H.c.},\end{aligned} \tag{3}$$

where $\tan\beta = v_u/v_d$ is the ratio of the vacuum expectation values v_u and v_d acquired by H_u and H_d, respectively. We perform this intermediate step, because this is the basis which corresponds to the super–Cabibbo-Kobayashi-Maskawa (CKM) basis of the MSSM and the couplings $\tilde{\epsilon}^d_{ij}$ can be directly related to loop-induced nonholomorphic Higgs coupling. The wave-function rotations $U^{qL,R}_{fi}$ necessary to arrive at the physical basis with diagonal quark mass matrices are defined by

$$U^{qL\star}_{jf}m^q_{jk}U^{qR}_{ki} = m_{q_i}\delta_{fi}. \tag{4}$$

They modify the Yukawa Lagrangian as follows:

$$\begin{aligned}\mathcal{L}_Y = &-\bar{d}_{fL}\left[\left(\frac{m_{d_i}}{v_d}\delta_{fi} - \epsilon^d_{fi}\tan\beta\right)H^{1\star}_d + \epsilon^d_{fi}H^2_u\right]d_{iR} \\ &- \bar{u}_{fL}\left[\left(\frac{m_{u_i}}{v_u}\delta_{fi} - \epsilon^u_{fi}\cot\beta\right)H^{2\star}_u + \epsilon^u_{fi}H^1_d\right]u_{iR} \\ &+ \bar{u}_{fL}V_{fj}\left[\frac{m_{d_i}}{v_d}\delta_{ji} - (\cot\beta + \tan\beta)\epsilon^d_{ji}\right]H^{2\star}_d d_{iR} \\ &+ \bar{d}_{fL}V^\star_{jf}\left[\frac{m_{u_i}}{v_u}\delta_{ji} - (\tan\beta + \cot\beta)\epsilon^u_{ji}\right]H^{1\star}_u u_{iR} \\ &+ \mathrm{H.c.}\end{aligned} \tag{5}$$

Here, m_{q_i} are the physical running quark masses, H^1_q and H^2_q are the components of the Higgs doublets, and

$$V_{fi} = U^{uL*}_{jf}U^{dL}_{ji} \tag{6}$$

is the CKM matrix. The Higgs doublets H_u and H_d project onto the physical mass eigenstates H^0 (heavy CP-even Higgs), h^0 (light CP-even Higgs), A^0 (CP-odd Higgs) and $H^\pm$ in the following way:

$$\begin{aligned}H^0_u &= \frac{1}{\sqrt{2}}(H^0\sin\alpha + h^0\cos\alpha + iA^0\cos\beta), \\ H^0_d &= \frac{1}{\sqrt{2}}(H^0\cos\alpha - h^0\sin\alpha + iA^0\sin\beta), \\ H^1_u &= \cos\beta H^+, \qquad H^2_d = \sin\beta H^-,\end{aligned} \tag{7}$$

where α is the mixing angle necessary to diagonalize the neutral CP-even Higgs mass matrix (see, e.g., [40]).[2] Since we assume a MSSM-like Higgs potential[3] we have

$$\begin{aligned}&\tan\beta = \frac{v_u}{v_d}, \qquad \tan 2\alpha = \tan 2\beta\frac{m^2_{A^0} + M^2_Z}{m^2_{A^0} - M^2_Z}, \\ &m^2_{H^\pm} = m^2_{A^0} + M^2_W, \qquad m^2_{H^0} = m^2_{A^0} + M^2_Z - m^2_{h^0},\end{aligned} \tag{8}$$

with $\frac{-\pi}{2} < \alpha < 0$ and $0 < \beta < \frac{\pi}{2}$.

This means that in the phenomenologically interesting and viable limit of large values of $\tan\beta$ and $v \ll m_{A^0}$ we have to a good approximation[4]

$$\tan\beta \approx -\cot\alpha, \qquad m_{H^0} \approx m_{H^\pm} \approx m_{A^0} \equiv m_H. \tag{9}$$

Without the nonholomorphic corrections ϵ^q_{ij}, the rotation matrices $U^{qL,R}_{fi}$ would simultaneously diagonalize the mass terms and the neutral Higgs couplings in Eq. (5). However, in the presence of nonholomorphic corrections, this is no longer the case and flavor changing neutral Higgs couplings are present in the basis in which the physical quark mass matrices are diagonal.

The Yukawa Lagrangian in Eq. (5) leads to the following Feynman rules[5] for Higgs-quark-quark couplings:

$$i(\Gamma^{LRH}_{q_fq_i}P_R + \Gamma^{RLH}_{q_fq_i}P_L) \tag{10}$$

with

[2]Note that we defined α as common in the MSSM. In the 2HDM also a convention with a doubled range for α is used.

[3]MSSM-like Higgs potential implies that in the large $\tan\beta$ limit and for $v \ll m_H$ the charged Higgs mass $m_{H^\pm}$, the heavy CP even Higgs mass m_{H^0} and the CP odd Higgs mass m_{A^0} are equal.

[4]For the SM-like Higgs boson h^0 we use $m_{h^0} \approx 125$ GeV in our numerical analysis.

[5]Hermiticity of the Lagrangian implies the relation $\Gamma^{RLH}_{q_fq_i} = \Gamma^{LRH\star}_{q_iq_f}$.

$$\Gamma^{LRH^0_k}_{u_f u_i} = x^k_u\left(\frac{m_{u_i}}{v_u}\delta_{fi} - \epsilon^u_{fi}\cot\beta\right) + x^{k\star}_d\epsilon^u_{fi},$$
$$\Gamma^{LRH^0_k}_{d_f d_i} = x^k_d\left(\frac{m_{d_i}}{v_d}\delta_{fi} - \epsilon^d_{fi}\tan\beta\right) + x^{k\star}_u\epsilon^d_{fi},$$
$$\Gamma^{LRH^\pm}_{u_f d_i} = \sum_{j=1}^{3}\sin\beta V_{fj}\left(\frac{m_{d_i}}{v_d}\delta_{ji} - \epsilon^d_{ji}\tan\beta\right), \quad (11)$$
$$\Gamma^{LRH^\pm}_{d_f u_i} = \sum_{j=1}^{3}\cos\beta V^\star_{jf}\left(\frac{m_{u_i}}{v_u}\delta_{ji} - \epsilon^u_{ji}\tan\beta\right).$$

Similarly, for the lepton case, the nonvanishing effective Higgs vertices are

$$\Gamma^{LRH^0_k}_{\ell_f \ell_i} = x^k_d\left(\frac{m_{\ell_i}}{v_d}\delta_{fi} - \epsilon^\ell_{fi}\tan\beta\right) + x^{k\star}_u\epsilon^\ell_{fi},$$
$$\Gamma^{LRH^\pm}_{\nu_f \ell_i} = \sum_{j=1}^{3}\sin\beta V^{\mathrm{PMNS}}_{fj}\left(\frac{m_{\ell_i}}{v_d}\delta_{ji} - \epsilon^\ell_{ji}\tan\beta\right). \quad (12)$$

Here, $H^0_k = (H^0, h^0, A^0)$ and the coefficients x^k_q are given by

$$x^k_u = \left(-\frac{1}{\sqrt{2}}\sin\alpha, -\frac{1}{\sqrt{2}}\cos\alpha, \frac{i}{\sqrt{2}}\cos\beta\right),$$
$$x^k_d = \left(-\frac{1}{\sqrt{2}}\cos\alpha, \frac{1}{\sqrt{2}}\sin\alpha, \frac{i}{\sqrt{2}}\sin\beta\right). \quad (13)$$

This means that flavor violation (beyond the one already present in the 2HDM of type II) is entirely governed by the couplings $\epsilon^{q,\ell}_{ij}$. If one wants to make the connection to the MSSM, the parameters $\epsilon^{q,\ell}_{ij}$ will depend only on supersymmetry (SUSY) breaking parameters and $\tan\beta$.

III. CONSTRAINTS ON THE 2HDM PARAMETER SPACE—GENERAL DISCUSSION AND OVERVIEW

In this section we give an overview on flavor observables sensitive to charged Higgs contributions. We review the constraints on the 2HDM of type II and discuss to which extent these bounds will hold in the 2HDM of type III. A detailed analysis of flavor constraints on the type-III 2HDM parameter space will be given in the following sections.

The most common version of 2HDMs, concerning its Yukawa sector, is the 2HDM of type II which respects natural flavor conservation [41] by requiring that one Higgs doublet couples only to up-quarks while the other one gives masses to down-type quarks and charged leptons (like the MSSM at tree level). Flavor observables in 2HDMs of type II have been studied in detail [42–44]. In the type-II model there are no tree-level flavor-changing neutral currents and all flavor violation is induced by the CKM matrix entering the charged Higgs vertex. In this way the constraints from FCNC processes can be partially avoided. This is true for $\Delta F = 2$ processes where the charged Higgs contribution is small, for $K_L \to \mu^+\mu^-$, $D^0 \to \mu^+\mu^-$ (due to the tiny Higgs couplings to light quarks) and all flavor observables in the lepton sector. However, the FCNC processes $b \to s\gamma$ (also to less extent $b \to d\gamma$) and $B_s \to \mu^+\mu^-$ are sensitive the charged Higgs contributions. In addition, direct searches at the LHC and charged current processes restrict the type-II 2HDM parameter space.

Among the FCNC processes, the constraints from $b \to s\gamma$ are most stringent due to the necessarily constructive interference with the SM contribution [45–48]. The most recent lower bound on the charged Higgs mass obtained in Ref. [49] is $m_{H^\pm} \geq 360$ GeV which includes next-to-next-to leading-order (NNLO) QCD corrections and is rather independent of $\tan\beta$. In the type-III 2HDM this lower bound on the charged Higgs mass can be weakened due to destructive interference with contributions involving ϵ^q_{ij}. Also in $B_s \to \mu^+\mu^-$ (and $B_d \to \mu^+\mu^-$) a sizable loop-induced effect is possible in the 2HDM II, but the constrains are still not very stringent even if the new LHCb measurement are used. The reason for this is that, taking into account the constraints from $b \to s\gamma$ on the charged Higgs mass, the branching ratio for $B_s \to \mu^+\mu^-$ in the 2HDM II is even below the SM expectation for larger values of $\tan\beta$ [50–52] due to the destructive interference between the charged Higgs and the SM contribution.

Regarding charged current processes, tauonic B decays are currently most sensitive to charged Higgs effects. Here, the charged-Higgs contribution in the type-II 2HDM to $B \to \tau\nu$ interferes destructively with the SM contribution [53,54]. The same is true for $B \to D^*\tau\nu$ [55] and $B \to D\tau\nu$ [42,56,57]. As outlined in the Introduction this leads to the fact that the 2HDM II cannot explain $B \to \tau\nu$, $B \to D\tau\nu$ and $B \to D^*\tau\nu$ simultaneously [8]. Other charged current observables sensitive to charged Higgses are $D_{(s)} \to \mu\nu$, $D_{(s)} \to \tau\nu$ [58–60], $\tau \to K(\pi)\nu$ and $K \to \mu\nu/\pi \to \mu\nu$ [61] (see [44] for a global analysis).

Figure 1 shows our updated constraints on the 2HDM II parameters space from $b \to s\gamma$, $B \to \tau\nu$, $B \to D\tau\nu$, $B \to D^*\tau\nu$, $B_s \to \mu^+\mu^-$ and $K \to \mu\nu/\pi \to \mu\nu$. We see that in order to get agreement within 2σ between the theory prediction and the measurement of $B \to D^*\tau\nu$, large values of $\tan\beta$ and light Higgs masses would be required which is in conflict with all other processes under consideration.

Concerning direct searches the bounds on the charged Higgs mass are rather weak due to the large background from W events. The search for neutral Higgs bosons is easier and the CMS bounds[6] on m_{A^0} from $A^0 \to \tau^+\tau^-$ are shown in Fig. 2. These bounds were obtained in the MSSM, but since the MSSM corrections to $A^0 \to \tau^+\tau^-$ are rather small and since we consider a MSSM-like Higgs potential,

[6]Note that we did not use the bounds from unpublished CMS update of the $A^0 \to \tau^+\tau^-$ analysis.

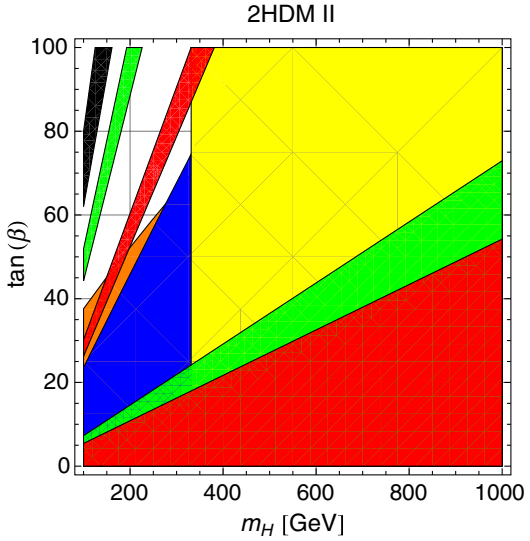

FIG. 1 (color online). Updated constraints on the 2HDM of type-II parameter space. The regions compatible with experiment are shown (the regions are superimposed on each other): $b \to s\gamma$ (yellow), $B \to D\tau\nu$ (green), $B \to \tau\nu$ (red), $B_s \to \mu^+\mu^-$ (orange), $K \to \mu\nu/\pi \to \mu\nu$ (blue) and $B \to D^*\tau\nu$ (black). Note that no region in parameter space is compatible with all processes. Explaining $B \to D^*\tau\nu$ would require very small Higgs masses and large values of $\tan\beta$ which is not compatible with the other observables. To obtain this plot, we added the theoretical uncertainty linear on the top of the 2σ experimental error.

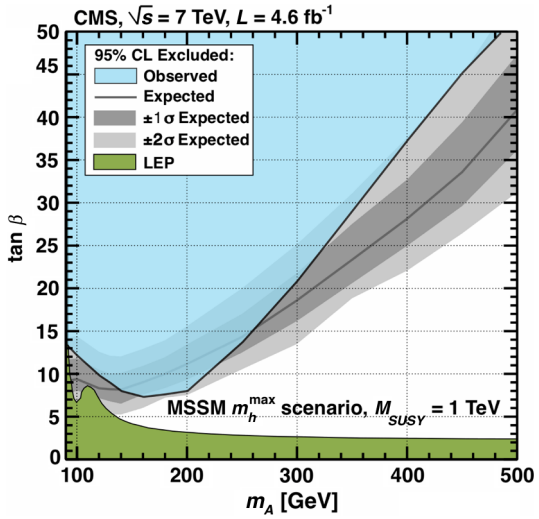

FIG. 2 (color online). Plot from the CMS collaboration taken from Ref. [165]: Exclusion limits in the $m_{A^0} - \tan\beta$ plane from $A^0 \to \tau^+\tau^-$. The analysis was done in the MSSM, but since we consider a 2HDM with MSSM-like Higgs potential and the MSSM corrections to the $A^0\tau\tau$ vertex are small, we can apply this bound to our model. However, a large value of ϵ^{ℓ}_{33} in the 2HDM of type III could affect the conclusions. Note that in the limit $v \ll m_H$ all heavy Higgs masses (m_{H^0}, m_{A^0} and $m_{H^\pm}$) are approximately equal.

these bounds also hold in the 2HDM III as long as the Peccei-Quinn symmetry breaking in the lepton sector is small.[7]

Going beyond the simple Yukawa structure of the 2HDM of type II, also 2HDMs of type III with MFV [15,17,18], alignment [63,64] or natural flavor conservation [17,41] have been analyzed in detail. However, flavor observables in type-III models with generic flavor structure have received much less attention. Reference [65] considered the possible effects of the flavor-diagonal terms and Ref. [66] considers leptonic observables. As outlined in the Introduction, 2HDMs of type II (or type III with MFV) cannot explain $B \to D\tau\nu$ and $B \to D^*\tau\nu$ simultaneously [8] (and for $B \to \tau\nu$ fine-tuning is needed [18]).

In the following sections we will study in detail the flavor observables in the 2HDM with generic flavor structure [67], but for definiteness, with MSSM-like Higgs potential. For this purpose, all processes described above are relevant. In addition, $\Delta F = 2$ processes, lepton flavor violating observables (LFV), EDMs, $\tau \to K(\pi)\nu/K(\pi) \to \mu\nu$ and $K \to \mu(e)\nu/\pi \to \mu(e)\nu$ will turn out to give information on the flavor structure of the 2HDM of type III. Furthermore, we will investigate to which extent contributions to $B_{s,d} \to \tau\mu$, $B_{s,d} \to \tau e$, $B_{s,d} \to \mu e$ and muon anomalous magnetic moment are possible.

IV. CONSTRAINTS FROM 'T HOOFT'S NATURALNESS CRITERION

The naturalness criterion of 't Hooft states that the smallness of a quantity is only natural if a symmetry is gained in the limit in which this quantity is zero. This means on the other hand that large accidental cancellations, which are not enforced by a symmetry, are unnatural and thus not desirable. Let us apply this reasoning to the fermion mass matrices in the 2HDM. We recall from the last section the expressions for the fermion mass matrices in the electroweak basis:

$$m^d_{ij} = v_d Y^{d\,\mathrm{ew}}_{ij} + v_u \epsilon^{d\,\mathrm{ew}}_{ij}, \qquad m^u_{ij} = v_u Y^{u\,\mathrm{ew}}_{ij} + v_d \epsilon^{u\,\mathrm{ew}}_{ij},$$
$$m^\ell_{ij} = v_d Y^{\ell\,\mathrm{ew}}_{ij} + v_u \epsilon^{\ell\,\mathrm{ew}}_{ij}. \tag{14}$$

Diagonalizing these fermion mass matrices gives the physical fermion masses and the CKM matrix. Using 't Hooft's naturalness criterion we can demand the absence of fine-tuned cancellations between $v_d Y^{d,\ell}_{ij}$ ($v_u Y^u_{ij}$) and $v_u \epsilon^{d,\ell}_{ij}$ ($v_d \epsilon^u_{ij}$). Thus, we require that the contributions of $v_u \epsilon^{d,\ell}_{ij}$ and $v_d \epsilon^u_{ij}$ to the fermion masses and CKM matrix do not exceed the physical measured quantities.

In first order of a perturbative diagonalization of the fermion mass matrices, the diagonal elements m^f_{ii} give rise to the fermion masses, while (in our conventions) the

[7]For a global analysis of electroweak precision constraints see for example Ref. [62].

elements m^f_{ij} with $i<j$ ($i>j$) affect the left-handed (right-handed) rotations necessary to diagonalize the fermion mass matrices. The left-handed rotations of the quark fields are linked to the CKM matrix and can therefore be constrained by demanding that the physical CKM matrix is generated without a significant degree of fine-tuning. However, the right-handed rotations of the quarks are not known and the mixing angles of the PMNS matrix are big so that for these two cases we can only demand that the fermion masses are generated without too large accidental cancellations. Note that in Eq. (14) the elements $\epsilon^{f\,\mathrm{ew}}_{ij}$ enter, while the elements ϵ^f_{ij} which we want to constrain from flavor observables are given in the physical basis with diagonal fermion masses. This means that in order to constrain ϵ^f_{ij} from 't Hooft's naturalness criterion we have to assume in addition that no accidental cancellation occur by switching between the electroweak basis and the physical basis. In conclusion this leads to the following upper bounds:

$$\begin{aligned}
|v_{u(d)}\epsilon^{d(u)}_{ij}| &\leq |V^{\mathrm{CKM}}_{ij}| \times \max\left[m_{d_i(u_i)}, m_{d_j(u_j)}\right] \quad \text{for } i<j,\\
|v_{u(d)}\epsilon^{d(u)}_{ij}| &\leq \max\left[m_{d_i(u_i)}, m_{d_j(u_j)}\right] \quad \text{for } i\geq j,\\
|v_u\epsilon^{\ell}_{ij}| &\leq \max\left[m_{\ell_i}, m_{\ell_j}\right].
\end{aligned} \tag{15}$$

In the large $\tan\beta$ limit, inserting the quark masses $m_q(\mu)$ at the Higgs scale (which we choose here to be $\mu_{\mathrm{Higgs}}=500$ GeV), we can immediately read off the upper bounds on $\epsilon^{u,d,\ell}_{ij}$ from Eq. (15):

$$\begin{aligned}
|\epsilon^d_{ij}| &\leq \begin{pmatrix} 1.3\times10^{-4} & 5.8\times10^{-5} & 5.1\times10^{-5}\\ 2.6\times10^{-4} & 2.6\times10^{-4} & 5.9\times10^{-4}\\ 1.4\times10^{-2} & 1.4\times10^{-2} & 1.4\times10^{-2}\end{pmatrix}_{ij},\\
|\epsilon^u_{ij}| &\leq (\tan\beta/50)\begin{pmatrix} 3.4\times10^{-4} & 3.2\times10^{-2} & 1.6\times10^{-1}\\ 1.4\times10^{-1} & 1.4\times10^{-1} & 1.9\\ - & - & -\end{pmatrix}_{ij},\\
|\epsilon^{\ell}_{ij}| &\leq \begin{pmatrix} 2.9\times10^{-6} & 6.1\times10^{-4} & 1.0\times10^{-2}\\ 6.1\times10^{-4} & 6.1\times10^{-4} & 1.0\times10^{-2}\\ 1.0\times10^{-2} & 1.0\times10^{-2} & 1.0\times10^{-2}\end{pmatrix}_{ij}.
\end{aligned} \tag{16}$$

Of course, these constraints are not strict bounds in the sense that they must be respected in any viable model. Anyway, big violation of naturalness is not desirable and Eq. (16) gives us a first glance on the possible structure of the elements ϵ^f_{ij}. As we will see later, it is possible to explain $B\to\tau\nu$, $B\to D\tau\nu$ and $B\to D^*\tau\nu$ using $\epsilon^u_{31,32}$ without violating Eq. (16), while if one wants to explain $B\to\tau\nu$ with ϵ^d_{33} 't Hooft's naturalness criterion is violated.

V. CONSTRAINTS FROM TREE-LEVEL NEUTRAL-CURRENT PROCESSES

The flavor off-diagonal elements ϵ^f_{ij} (with $i\neq j$) give rise to flavor-changing neutral currents (FCNCs) already at the tree level. Comparing the Higgs contributions to the loop-suppressed SM contributions, large effects are in principle possible. However, all experimental results are in very good agreement with SM predictions, which put extremely stringent constraints on the nonholomorphic terms ϵ^f_{ij}.

In this section we consider three different kinds of processes:

(i) Muonic decays of neutral mesons ($B_{s,d}\to\mu^+\mu^-$, $K_L\to\mu^+\mu^-$ and $\bar{D}^0\to\mu^+\mu^-$).
(ii) $\Delta F=2$ processes ($D-\bar{D}$, $K-\bar{K}$, $B_s-\bar{B}_s$ and $B_d-\bar{B}_d$ mixing).
(iii) Flavor changing lepton decays ($\tau^-\to\mu^-\mu^+\mu^-$, $\tau^-\to e^-\mu^+\mu^-$ and $\mu^-\to e^-e^+e^-$).

As we will see in detail in Sec. V A, the leptonic neutral meson decays $B_{s,d}\to\mu^+\mu^-$, $K_L\to\mu^+\mu^-$ and $\bar{D}^0\to\mu^+\mu^-$ put constraints on the elements ϵ^d_{ij} (with $i\neq j$) and $\epsilon^u_{12,21}$ already if one of these elements is nonzero, while $B_d-\bar{B}_d$, $B_s-\bar{B}_s$, $K-\bar{K}$ and $D-\bar{D}$ mixing only provide constraints on the products $\epsilon^d_{ij}\epsilon^{d\star}_{ji}$ and $\epsilon^u_{12}\epsilon^{u\star}_{21}$ (Sec. V B). This means that the constraints on $\Delta F=2$ processes can be avoided if one element of the product $\epsilon^q_{ij}\epsilon^{q\star}_{ji}$ is zero, while the constraints from the leptonic neutral meson decays can only be avoided if the Peccei-Quinn symmetry breaking for the leptons is large such that $\epsilon^{\ell}_{22}\approx m_\mu/v_u$ is possible.

In Sec. V C we will consider the flavor changing lepton decays $\tau^-\to\mu^-\mu^+\mu^-$, $\tau^-\to e^-\mu^+\mu^-$ and $\mu^-\to e^-e^+e^-$ which constrain the off-diagonal elements $\epsilon^{\ell}_{23,32}$, $\epsilon^{\ell}_{13,31}$ and $\epsilon^{\ell}_{12,21}$, respectively.

A. Leptonic neutral meson decays: $B_{s,d}\to\mu^+\mu^-$, $K_L\to\mu^+\mu^-$ and $\bar{D}^0\to\mu^+\mu^-$

Muonic decays of neutral mesons ($B_s\to\mu^+\mu^-$, $B_d\to\mu^+\mu^-$, $K_L\to\mu^+\mu^-$ and $\bar{D}^0\to\mu^+\mu^-$) are strongly suppressed in the SM for three reasons: they are loop induced, helicity suppressed and they involve small CKM elements. Therefore, their branching ratios (in the SM) are very small and in fact only $K_L\to\mu^+\mu^-$ and recently also $B_s\to\mu^+\mu^-$ [68] have been measured, while for the other decays only upper limits on the branching ratios exist (see Table I). We do not consider decays to electrons (which are even stronger helicity suppressed) nor $B_{d,s}\to\tau^+\tau^-$ (where the tau leptons are difficult to reconstruct) because the experimental limits are even weaker. The study of meson decays to lepton flavor-violating final states is postponed to Sec. VIII.

We see from Fig. 3 that the off-diagonal elements of $\epsilon^d_{13,31}$, $\epsilon^d_{23,32}$, $\epsilon^d_{12,21}$ and $\epsilon^u_{12,21}$ directly give rise to tree-level

TABLE I. Experimental values and SM predictions for the branching ratios of neutral meson decays to muon pairs. For $K_L \to \mu^+\mu^-$ we only give the upper limit on the computable short distance contribution [69] extracted from the experimental value $(6.84 \pm 0.11) \times 10^{-9}$ (90% C.L.) [70]. The SM prediction for $D^0 \to \mu^+\mu^-$ cannot be reliably calculated due to hadronic uncertainties.

Process	Experimental value	SM prediction
$\mathcal{B}[B_s \to \mu^+\mu^-]$	$3.2^{+1.5}_{-1.2} \times 10^{-9}$ [68]	$(3.23 \pm 0.27) \times 10^{-9}$ [71]
$\mathcal{B}[B_d \to \mu^+\mu^-]$	$\leq 9.4 \times 10^{-10}$ (95% C.L.) [68]	$(1.07 \pm 0.10) \times 10^{-10}$ [71]
$\mathcal{B}[K_L \to \mu^+\mu^-]_{\text{short}}$	$\leq 2.5 \times 10^{-9}$ [69]	$\approx 0.9 \times 10^{-9}$ [69]
$\mathcal{B}[D^0 \to \mu^+\mu^-]$	$\leq 1.4 \times 10^{-7}$ (90% C.L.) [70]	...

neutral Higgs contributions to $B_d \to \mu^+\mu^-$, $B_s \to \mu^+\mu^-$, $K_L \to \mu^+\mu^-$ and $\bar{D}^0 \to \mu^+\mu^-$, respectively.

In principle, the constraints from these processes could be weakened, or even avoided, if $\epsilon^{\ell}_{22} \approx m_{\ell_2}/v_u$. Anyway, in this section we will assume that the Peccei-Quinn breaking for the leptons is small and neglect the effect of ϵ^{ℓ}_{22} in our numerical analysis for setting limits on ϵ^{q}_{ij}.

1. $B_{s,d} \to \mu^+\mu^-$

For definiteness, consider the decay of a neutral $B_s(\bar{b}s)$ meson (the corresponding decay of a B_d meson follow trivially by replacing s with d and 2 with 1) to a muon pair. The effective Hamiltonian governing this transition is[8]

$$\mathcal{H}^{B_s\to\mu^+\mu^-}_{\text{eff}} = -\frac{G_F^2 M_W^2}{\pi^2}[C_A^{bs}O_A^{bs} + C_S^{bs}O_S^{bs} + C_P^{bs}O_P^{bs} + C_A'^{bs}O_A'^{bs} + C_S'^{bs}O_S'^{bs} + C_P'^{bs}O_P'^{bs}] + \text{H.c.}, \tag{17}$$

where the operators are defined as

$$O_A^{bs} = (\bar{b}\gamma_\mu P_L s)(\bar{\mu}\gamma^\mu\gamma_5\mu), \qquad O_S^{bs} = (\bar{b}P_L s)(\bar{\mu}\mu), \qquad O_P^{bs} = (\bar{b}P_L s)(\bar{\mu}\gamma_5\mu), \tag{18}$$

and the primed operators are obtained replacing P_L with P_R. The corresponding expression for the branching ratio in terms of the Wilson coefficients reads

$$\mathcal{B}[B_s \to \mu^+\mu^-] = \frac{G_F^4 M_W^4}{8\pi^5}\sqrt{1-4\frac{m_\mu^2}{M_{B_s}^2}}M_{B_s}f_{B_s}^2 m_\mu^2 \tau_{B_s}\left[\left|\frac{M_{B_s}^2(C_P^{bs}-C_P'^{bs})}{2(m_b+m_s)m_\mu} - (C_A^{bs}-C_A'^{bs})\right|^2 + \left|\frac{M_{B_s}^2(C_S^{bs}-C_S'^{bs})}{2(m_b+m_s)m_\mu}\right|^2 \times\left(1-4\frac{m_\mu^2}{m_{B_s}^2}\right)\right]. \tag{19}$$

[8]The complete expression for the Hamiltonian and the branching ratio including lepton flavor-violating final states is given in the Appendix.

Concerning the running of the Wilson coefficients due to the strong interaction, the operators O_A^{bs} and $O_A'^{bs}$ correspond to conserved vector currents with vanishing anomalous dimensions. This means that their Wilson coefficients are scale independent. The scalar and pseudoscalar Wilson coefficients C_S^{bs} and C_P^{bs} ($C_S'^{bs}$ and $C_P'^{bs}$) have the same anomalous dimension as quark masses in the SM which means that their scale dependence is given by

$$C_{S,P}^{(\prime)bs}(\mu_{\text{low}}) = \frac{m_q(\mu_{\text{low}})}{m_q(\mu_{\text{high}})}C_{S,P}^{(\prime)bs}(\mu_{\text{high}}), \tag{20}$$

where m_q is the running quark mass with the appropriate number of active flavors. In the SM, C_A is the only nonvanishing Wilson coefficient

$$C_A^{bs} = -V_{tb}^\star V_{ts} Y\left(\frac{m_t^2}{M_W^2}\right) - V_{cb}^\star V_{cs} Y\left(\frac{m_c^2}{M_W^2}\right), \tag{21}$$

where the function Y is defined as $Y = \eta_Y Y_0$ such that the NLO QCD effects are included in $\eta_Y = 1.0113$ [71] and the one loop Inami-Lim function Y_0 reads [72]

$$Y_0(x) = \frac{x}{8}\left[\frac{4-x}{1-x} + \frac{3x}{(1-x)^2}\ln(x)\right]. \tag{22}$$

The complete Wilson coefficients for general quark-quark-scalar couplings are given in the Appendix. In the 2HDM of type III, in the case of large $\tan\beta$ and $v \ll m_H$, the terms involving ϵ^{q}_{ij} simplify to

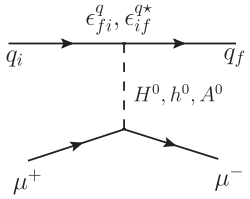

FIG. 3. Feynman diagram showing the neutral Higgs contribution to $B_{s,d} \to \mu^+\mu^-$, $K_L \to \mu^+\mu^-$ and $\bar{D}^0 \to \mu^+\mu^-$.

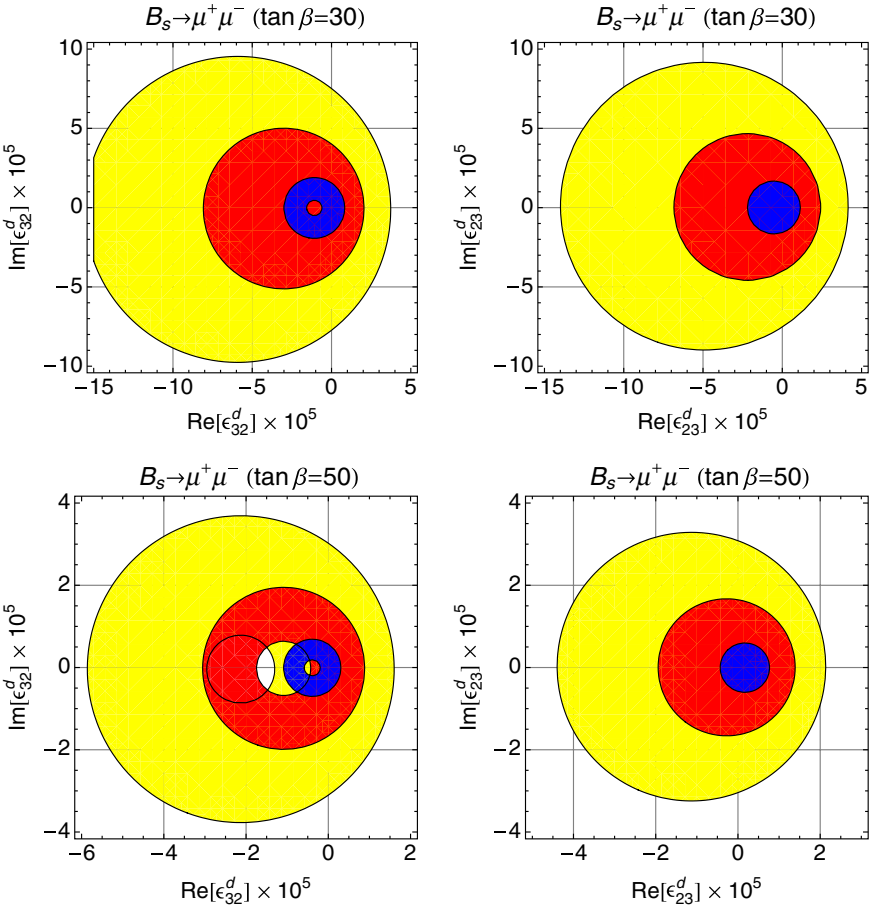

FIG. 4 (color online). Allowed regions in the complex $\epsilon^d_{23,32}$ plane from $B_s \to \mu^+\mu^-$ for $\tan\beta = 30$, $\tan\beta = 50$ and $m_H = 700$ GeV (yellow), $m_H = 500$ GeV (red) and $m_H = 300$ GeV (blue). Note that the allowed regions for the ϵ^d_{32} plane are not full circles because in this case a suppression of $\mathcal{B}[B_s \to \mu^+\mu^-]$ below the experimental lower bound is possible.

$$C_S^{bs} = C_P^{bs} = -\frac{\pi^2}{G_F^2 M_W^2}\frac{1}{2m_H^2}\frac{m_{\ell_2} - v_u \epsilon^\ell_{22}}{v}\epsilon^{d\star}_{23}\tan^2\beta,$$
$$C_S'^{bs} = -C_P'^{bs} = -\frac{\pi^2}{G_F^2 M_W^2}\frac{1}{2m_H^2}\frac{m_{\ell_2} - v_u \epsilon^\ell_{22}}{v}\epsilon^{d}_{32}\tan^2\beta. \quad (23)$$

To these Wilson coefficients the well-known loop-induced type-II 2HDM contributions,[9]

$$C_S^{bs} = C_P^{bs} = -\frac{m_b V_{tb}^\star V_{ts}}{2}\frac{m_\mu}{2M_W^2}\tan^2\beta\frac{\log(m_H^2/m_t^2)}{m_H^2/m_t^2 - 1}, \quad (24)$$

have to be added as well [52]. Note that since we give the Wilson coefficients at the matching scale, also m_b and m_t must be evaluated at this scale.

We can now constrain the elements $\epsilon^d_{23,32}$ and $\epsilon^d_{13,31}$ by demanding that the experimental bounds are satisfied within two standard deviations for $B_s \to \mu^+\mu^-$ or equivalently at the 95% C.L. concerning $B_d \to \mu^+\mu^-$. The results for the constraints on ϵ^d_{23} and ϵ^d_{32} (ϵ^d_{13} and ϵ^d_{31}) from $B_s \to \mu^+\mu^-$ ($B_d \to \mu^+\mu^-$) are shown in Fig. 4 (Fig. 5).

All constraints on $\epsilon^d_{13,31}$ and $\epsilon^d_{23,32}$ are very stringent; of the order of 10^{-5}. Both an enhancement or a suppression of $\mathcal{B}[B_{d,s} \to \mu^+\mu^-]$ compared to the SM prediction is possible. While in the 2HDM II the minimal value for $\mathcal{B}[B_{d,s} \to \mu^+\mu^-]$ is half the SM prediction, in the 2HDM III also a bigger suppression of $B_{d,s} \to \mu^+\mu^-$ is possible if $\epsilon^d_{13,23} \neq 0$. In principle, the constraints on ϵ^d_{23} (ϵ^d_{13}) from $B_{s(d)} \to \mu^+\mu^-$ are not independent of ϵ^d_{32} (ϵ^d_{31}). Anyway, in the next section it will turn out that the constraints from $\Delta F = 2$ processes are more stringent if both ϵ^d_{32} and ϵ^d_{23} are different from zero (the same conclusions hold for $\epsilon^d_{31,13}$, $\epsilon^d_{21,12}$ and $\epsilon^u_{21,12}$).

$B_s \to \mu^+\mu^-$ and $B_d \to \mu^+\mu^-$ can also be used to constrain the leptonic parameter ϵ^ℓ_{22}. We will discuss the corresponding subject in Sec. VI.

2. $K_L \to \mu^+\mu^-$

Concerning $K_L \to \mu^+\mu^-$, the branching ratio and the Wilson coefficients can be obtained by a simple

[9]Since we want to put constraints on the elements $\epsilon^d_{13,23}$ we assume that the loop-induced 2HDM II contribution is not changed by elements ϵ^u_{i3} or ϵ^d_{33}.

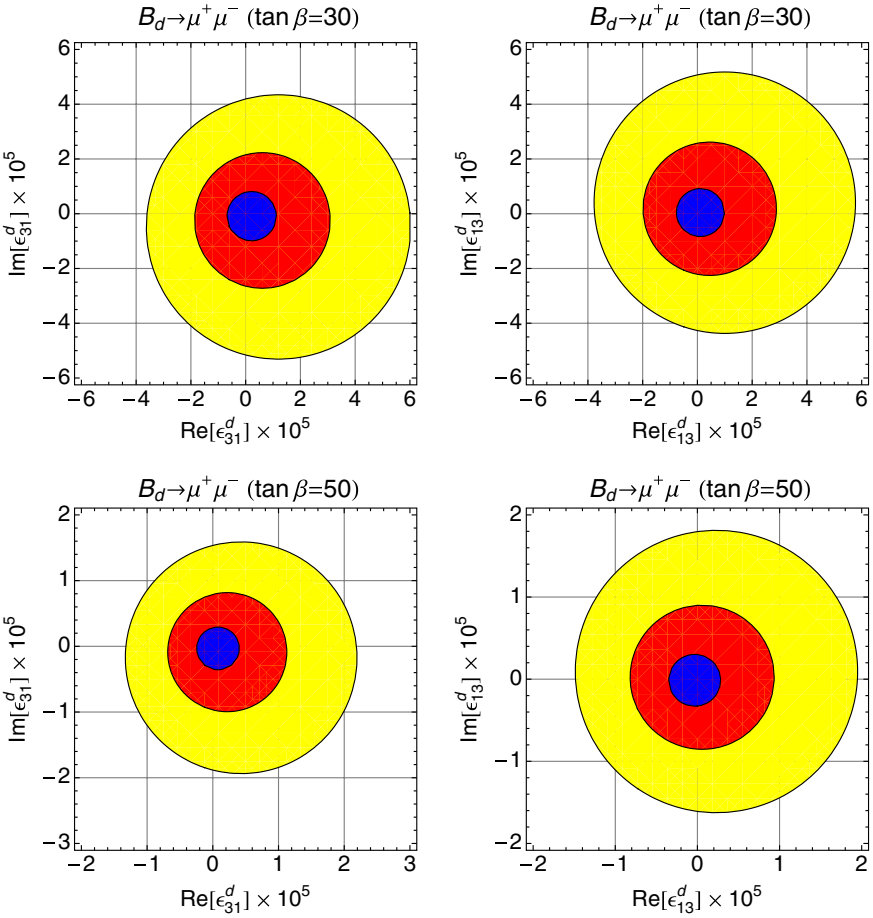

FIG. 5 (color online). Allowed regions in the complex $\epsilon^d_{13,31}$ plane from $B_d \to \mu^+\mu^-$ for $\tan\beta = 30$, $\tan\beta = 50$ and $m_H = 700$ GeV (yellow), $m_H = 500$ GeV (red) and $m_H = 300$ GeV (blue).

replacement of indices from Eqs. (19), (21), and (23). Because of the presence of large nonperturbative QCD effects, we require that the 2HDM III contribution together with the short distance piece of the SM contribution does not exceed the upper limit on the short distance contribution to the branching ratio calculated in Ref. [69]. The resulting constraints on $\epsilon^d_{12,21}$ are shown in Fig. 6. They are found to be extremely stringent (of the order of 10^{-6}).

3. $\bar{D}^0 \to \mu^+\mu^-$

The analogous expressions for the branching ratio for $\bar{D}^0 \to \mu^+\mu^-$ ($\bar{D}^0(\bar{c}u)$ follow by a straightforward replacement of indices in Eq. (19) but the Wilson coefficients in the type-III 2HDM for $\bar{D}^0 \to \mu^+\mu^-$ have a different dependence on $\tan\beta$:

$$C_S^{cu} = -C_P^{cu} = \frac{\pi^2}{G_F^2 M_W^2}\frac{1}{2m_H^2}\frac{m_{\ell_2} - v_u \epsilon^\ell_{22}}{v}\epsilon^{u\star}_{12}\tan\beta,$$
$$C_S^{\prime cu} = C_P^{\prime cu} = \frac{\pi^2}{G_F^2 M_W^2}\frac{1}{2m_H^2}\frac{m_{\ell_2} - v_u \epsilon^\ell_{22}}{v}\epsilon^{u}_{21}\tan\beta. \quad (25)$$

Differently than for $B_{d,s} \to \mu^+\mu^-$ the SM contribution cannot be calculated due to nonperturbative effects and the 2HDM II contribution is numerically irrelevant. Since we do not know the SM contribution, we require that the 2HDM III contribution alone does not generate more than the experimental upper limit on this branching ratio.

It is then easy to express the constraints on $\epsilon^u_{12,21}$ in terms of the parameters m_H and $\tan\beta$:

$$|\epsilon^u_{12,21}| \le 3.0 \times 10^{-2}\,\frac{(m_H/500\ \text{GeV})^2}{\tan\beta/50}. \quad (26)$$

The resulting bounds on $\epsilon^u_{12,21}$ (setting one of these elements to zero) are shown in Fig. 7.

B. Tree-level contributions to $\Delta F = 2$ processes

In the presence of nonzero elements ϵ^q_{ij} neutral Higgs mediated contributions to neutral meson mixing ($B_{d,s} - \bar{B}_{d,s}$, $K - \bar{K}$ and $D - \bar{D}$ mixing) arise (see Fig. 8). In these processes, the 2HDM contribution vanishes if the $U(1)_{\text{PQ}}$ symmetry is conserved. This has the consequence that the leading $\tan\beta$-enhanced tree-level contribution to the $\Delta F = 2$ processes (shown in Fig. 8) is only nonvanishing if ϵ^q_{ij} and ϵ^q_{ji} are simultaneously different from zero (in the approximation $m_{A^0} = m_{H^0}$ and $\cot\beta = 0$). Making use of

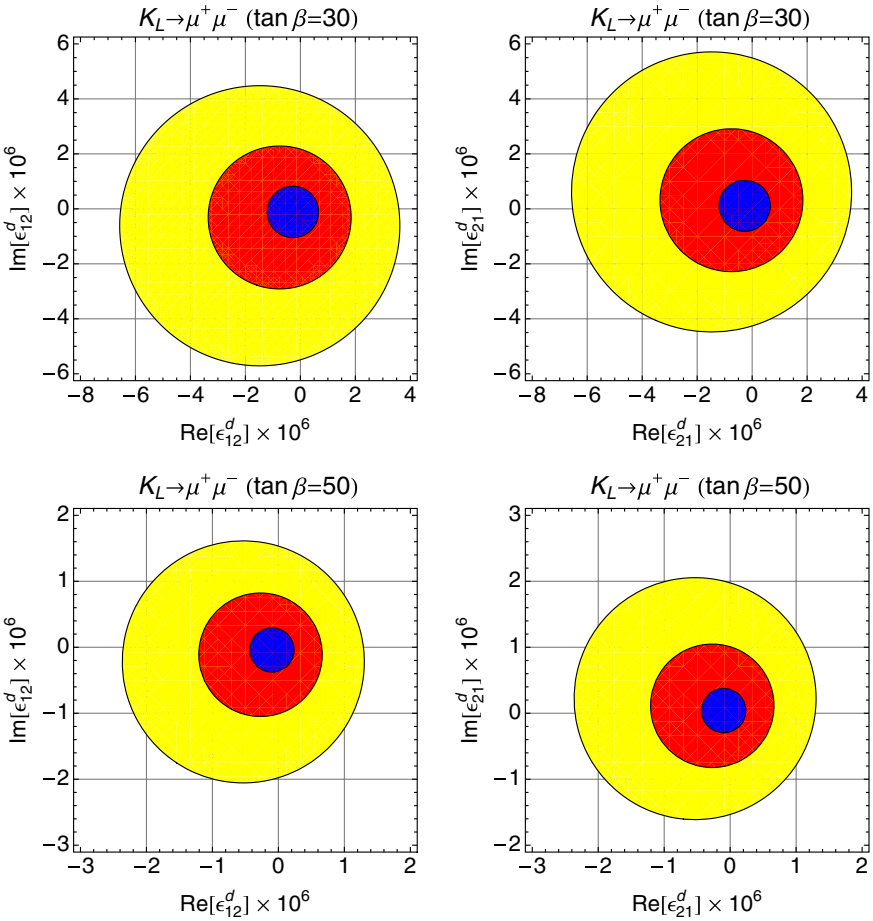

FIG. 6 (color online). Allowed regions in the complex $\epsilon^d_{12,21}$ plane from $K_L \to \mu^+\mu^-$ for $\tan\beta = 30$, $\tan\beta = 50$ and $m_H = 700$ GeV (yellow), $m_H = 500$ GeV (red) and $m_H = 300$ GeV (blue).

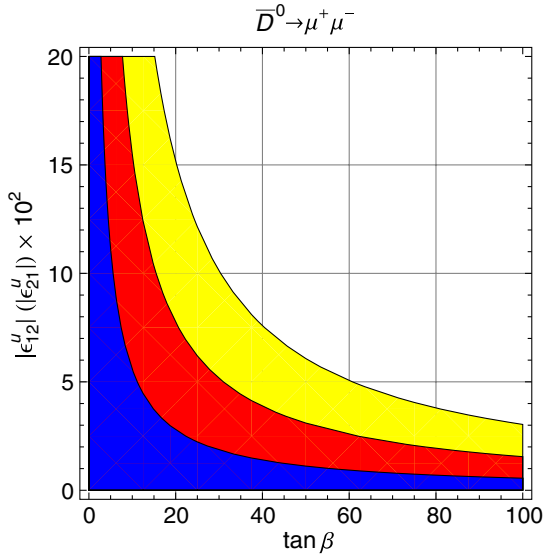

FIG. 7 (color online). Allowed regions in the complex $\epsilon^u_{12,21}$ – $\tan\beta$ plane from $\bar{D}^0 \to \mu^+\mu^-$ for $m_H = 700$ GeV (yellow), $m_H = 500$ GeV (red) and $m_H = 300$ GeV (blue).

the effective Hamiltonian defined in Eq. (A9) of the Appendix we get the following contributions to $B_s - \bar{B}_s$ mixing (the expressions for $B_d - \bar{B}_d$ and $K - \bar{K}$ mixing again follow by a simple replacement of indices):

$$C_4 = -\frac{\epsilon^d_{23}\epsilon^{d\star}_{32}}{m_H^2}\tan^2\beta. \tag{27}$$

All other Wilson coefficients are subleading in $\tan\beta$. For D mixing, again only C_4 is nonzero and given by

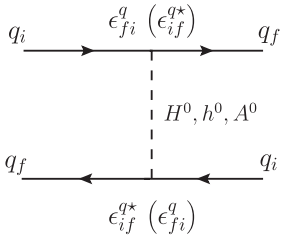

FIG. 8. Feynman diagram contributing to $B_{d,s} - \bar{B}_{d,s}$, $K - \bar{K}$ and $D - \bar{D}$ mixing.

$$C_4 = -\frac{\epsilon^u_{12}\epsilon^{u\star}_{21}}{m_H^2}. \tag{28}$$

After performing the renormalization group evolution [73–77] (here we used $\mu_H = 500$ GeV at the high scale) it turns out that the dominant contribution to the hadronic matrix elements stems from O_4. Inserting the bag factors [78,79] and decay constants from lattice QCD (see Table X), we get for the 2HDM of type-III contribution

$$\begin{aligned}
\langle B^0_d|C_4O_4|\bar{B}^0_d\rangle &\approx 0.26C_4\ \text{GeV}^3,\\
\langle B^0_s|C_4O_4|\bar{B}^0_s\rangle &\approx 0.37C_4\ \text{GeV}^3,\\
\langle K^0|C_4O_4|\bar{K}^0\rangle &\approx 0.30C_4\ \text{GeV}^3,\\
\langle D^0|C_4O_4|\bar{D}^0\rangle &\approx 0.18C_4\ \text{GeV}^3,
\end{aligned} \tag{29}$$

where we used the normalization of the meson states as defined for example in [76]. In Eq. (29) the Wilson coefficients within the matrix elements are at the corresponding meson scale while C_4 on the right-hand side is given at the matching scale m_H. For computing the constraints on $\epsilon^d_{13}\epsilon^{d\star}_{31}$, $\epsilon^d_{23}\epsilon^{d\star}_{32}$ and $\epsilon^d_{12}\epsilon^{d\star}_{21}$ we use the online update of the analysis of the UTfit collaboration [95].[10] For this purpose we define

$$C_{B_q}e^{2i\varphi_{B_q}} = 1 + \frac{\langle B^0_q|\mathcal{H}^{\text{NP}}_{\text{eff}}|\bar{B}^0_q\rangle}{\langle B^0_q|\mathcal{H}^{\text{SM}}_{\text{eff}}|\bar{B}^0_q\rangle}, \tag{30}$$

for $B_d - \bar{B}_d$ and $B_s - \bar{B}_s$ mixing and

$$\begin{aligned}
C_{\epsilon_K} &= 1 + \frac{\text{Im}[\langle K^0|\mathcal{H}^{\text{NP}}_{\text{eff}}|\bar{K}^0\rangle]}{\text{Im}[\langle K^0|\mathcal{H}^{\text{SM}}_{\text{eff}}|\bar{K}^0\rangle]},\\
C_{\Delta M_K} &= 1 + \frac{\text{Re}[\langle K^0|\mathcal{H}^{\text{NP}}_{\text{eff}}|\bar{K}^0\rangle]}{\text{Re}[\langle K^0|\mathcal{H}^{\text{SM}}_{\text{eff}}|\bar{K}^0\rangle]},
\end{aligned} \tag{31}$$

for $K - \bar{K}$ mixing. Using for the matrix elements of the SM Hamiltonian[11] [96]

$$\begin{aligned}
\langle B^0_d|\mathcal{H}^{\Delta F=2}_{\text{SM}}|\bar{B}^0_d\rangle &\approx (1.08 + 1.25i)\times 10^{-13}\ \text{GeV},\\
\langle B^0_s|\mathcal{H}^{\Delta F=2}_{\text{SM}}|\bar{B}^0_s\rangle &\approx (59 - 2.2i)\times 10^{-13}\ \text{GeV},\\
\langle K^0|\mathcal{H}^{\Delta F=2}_{\text{SM}}|\bar{K}^0\rangle &\approx (115 + 1.16i)\times 10^{-17}\ \text{GeV},
\end{aligned} \tag{32}$$

we can directly read off the bounds on C_4 and thus on $\epsilon^d_{12}\epsilon^{d\star}_{21}$, $\epsilon^d_{13}\epsilon^{d\star}_{31}$ and $\epsilon^d_{23}\epsilon^{d\star}_{32}$:

$$-2.0\times10^{-10} \le \text{Re}[\epsilon^d_{23}\epsilon^{d\star}_{32}]\left(\frac{\tan\beta/50}{m_H/500\,\text{GeV}}\right)^2 \le 6.0\times10^{-10}, \tag{33}$$

$$-3.0\times10^{-10} \le \text{Im}[\epsilon^d_{23}\epsilon^{d\star}_{32}]\left(\frac{\tan\beta/50}{m_H/500\,\text{GeV}}\right)^2 \le 7.0\times10^{-10}, \tag{34}$$

$$-3.0\times10^{-11} \le \text{Re}[\epsilon^d_{13}\epsilon^{d\star}_{31}]\left(\frac{\tan\beta/50}{m_H/500\,\text{GeV}}\right)^2 \le 1.5\times10^{-11}, \tag{35}$$

$$-1.5\times10^{-11} \le \text{Im}[\epsilon^d_{13}\epsilon^{d\star}_{31}]\left(\frac{\tan\beta/50}{m_H/500\,\text{GeV}}\right)^2 \le 2.5\times10^{-11}, \tag{36}$$

$$-1.0\times10^{-12} \le \text{Re}[\epsilon^d_{12}\epsilon^{d\star}_{21}]\left(\frac{\tan\beta/50}{m_H/500\,\text{GeV}}\right)^2 \le 3.0\times10^{-13}, \tag{37}$$

$$-4.0\times10^{-15} \le \text{Im}[\epsilon^d_{12}\epsilon^{d\star}_{21}]\left(\frac{\tan\beta/50}{m_H/500\,\text{GeV}}\right)^2 \le 2.5\times10^{-15}. \tag{38}$$

We see that if ϵ^d_{ij} is of the same order as ϵ^d_{ji} these bounds are even more stringent than the ones from $B_{d,s} \to \mu^+\mu^-$ and $K_L \to \mu^+\mu^-$ computed in the last subsection.

For $D - \bar{D}$ mixing, the SM predictions are not known due to very large hadronic uncertainties. In order to constrain the NP effects we demand the absence of fine-tuning, which means that the NP contribution, which are calculable short distance contributions, should not exceed the measured values. Concerning the 2HDM III contribution, there is no $\tan\beta$ enhancement and taking into account the recent analysis of the UTfit collaboration [97] we arrive at the following constraints (for $m_H = 500$ GeV):

$$|\epsilon^u_{12}\epsilon^{u\star}_{21}| < 2.0\times10^{-8}. \tag{39}$$

Note that although these bounds look more stringent than the corresponding $\Delta F = 1$ constraints, they scale differently with $\tan\beta$ and also involve products of pairs of ϵ^u_{ij}. Therefore, contrary to the $\Delta F = 1$ case, in principle all of these limits can be evaded for one of the couplings by suppressing the other one. Figures 9 and 10 show the allowed regions for these parameters obtained from the neutral Higgs contribution to $B_{d,s} - \bar{B}_{d,s}$, $K - \bar{K}$ and $D - \bar{D}$ mixing (see the Feynman diagram in Fig. 8).

C. Lepton-flavor-violating decays: $\tau^- \to \mu^-\mu^+\mu^-$, $\tau^- \to e^-\mu^+\mu^-$ and $\mu \to e^-e^+e^-$

In this section, we investigate the constraints that $\tau^- \to \mu^-\mu^+\mu^-$, $\tau^- \to e^-\mu^+\mu^-$ and $\mu \to e^-e^+e^-$ place on the flavor changing couplings $\epsilon^\ell_{32,23}$, $\epsilon^\ell_{31,13}$ and $\epsilon^\ell_{21,12}$, respectively.

For these decays, the experimental upper limits [98,99] are

[10] See also the online update of the CKMfitter group for an analogous analysis [14].

[11] To obtain a value consistent with the NP analysis of the UTfit collaboration, we also used their input for computing the matrix elements of the SM $\Delta F = 2$ Hamiltonian in Eq. (32).

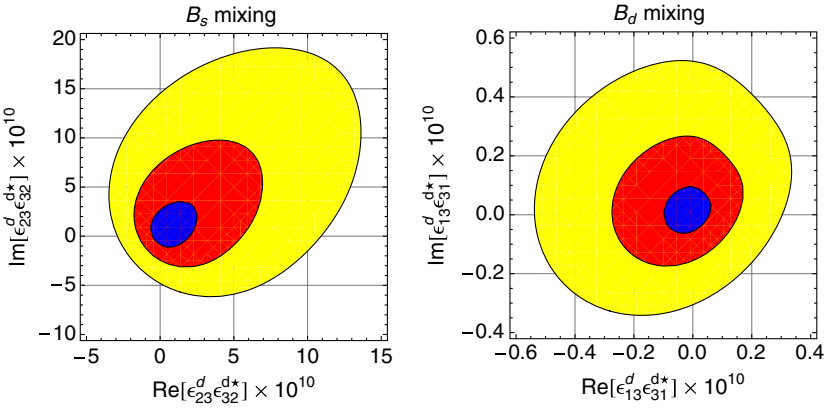

FIG. 9 (color online). Allowed regions in the complex ϵ^d_{ij}-plane from $B_{d,s} - \bar{B}_{d,s}$ mixing for $\tan\beta = 50$ and $m_H = 700$ GeV (yellow), $m_H = 500$ GeV (red) and $m_H = 300$ GeV (blue).

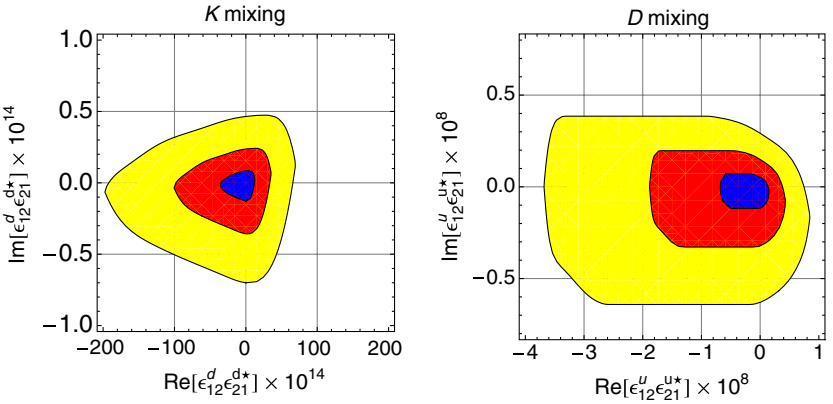

FIG. 10 (color online). Allowed regions in the complex $\epsilon^q_{12}\epsilon^{q\star}_{21}$ plane from $K - \bar{K}$ and $D - \bar{D}$ mixing for $\tan\beta = 50$ and $m_H = 700$ GeV (yellow), $m_H = 500$ GeV (red) and $m_H = 300$ GeV (blue).

$$\begin{aligned}\mathcal{B}[\tau^- \to \mu^-\mu^+\mu^-] &\le 2.1 \times 10^{-8},\\ \mathcal{B}[\tau^- \to e^-\mu^+\mu^-] &\le 2.7 \times 10^{-8},\\ \mathcal{B}[\mu^- \to e^-e^+e^-] &\le 1.0 \times 10^{-12},\end{aligned} \tag{40}$$

at 90% C.L. Let us consider the processes $\tau^- \to \mu^-\mu^+\mu^-$ and $\tau^- \to e^-\mu^+\mu^-$ which are shown in Fig. 11. The expressions for the branching ratio for $\tau^- \to e^-\mu^+\mu^-$ can be written as

$$\begin{aligned}\mathcal{B}[\tau^- \to e^-\mu^+\mu^-] = \frac{m_\tau^5}{12(8\pi)^3\Gamma_\tau}\frac{\tan^4\beta}{m_H^4}\left|\left(\frac{m_\mu}{v} - \varepsilon^\ell_{22}\right)\right|^2 \\ \times (|\varepsilon^\ell_{31}|^2 + |\varepsilon^\ell_{13}|^2),\end{aligned} \tag{41}$$

where Γ_τ is the total decay width of the τ lepton. The branching ratios for $\tau^- \to e^-e^+e^-$ and $\mu^- \to e^-e^+e^-$ can be obtained by an obvious replacement of masses, indices and total decays widths. Note that the full expression for general scalar couplings given in Eq. (A41) of the Appendix is different for $\tau^- \to e^-\mu^+\mu^-$ than for $\tau^- \to \mu^-\mu^+\mu^-$ and only approaches a common expression in the limit of large $\tan\beta$ and large Higgs masses.

Comparing the type-III 2HDM expression with experiment we obtain the following constraints on ϵ^ℓ_{fi} (assuming $\epsilon^\ell_{jj} = 0$):

$$\begin{aligned}|\epsilon^\ell_{12}|^2 + |\epsilon^\ell_{21}|^2 &\le (2.3 \times 10^{-3})^2\left(\frac{m_H/500\ \mathrm{GeV}}{\tan\beta/50}\right)^4 \\ &\times \frac{\mathcal{B}[\mu^- \to e^-e^+e^-]}{1.0 \times 10^{-12}},\\ |\epsilon^\ell_{13}|^2 + |\epsilon^\ell_{31}|^2 &\le (4.2 \times 10^{-3})^2\left(\frac{m_H/500\ \mathrm{GeV}}{\tan\beta/50}\right)^4 \\ &\times \frac{\mathcal{B}[\tau^- \to e^-\mu^+\mu^-]}{2.7 \times 10^{-8}},\\ |\epsilon^\ell_{23}|^2 + |\epsilon^\ell_{32}|^2 &\le (3.7 \times 10^{-3})^2\left(\frac{m_H/500\ \mathrm{GeV}}{\tan\beta/50}\right)^4 \\ &\times \frac{\mathcal{B}[\tau^- \to \mu^-\mu^+\mu^-]}{2.1 \times 10^{-8}}.\end{aligned} \tag{42}$$

These constraints are also illustrated in Fig. 12 for the experimental limits given in Eq. (40).

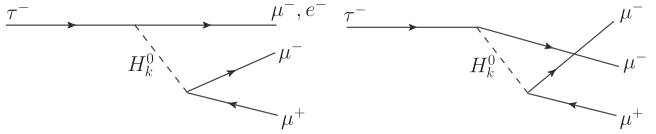

FIG. 11. Feynman diagrams contributing to $\tau^- \to \mu^-\mu^+\mu^-$ and $\tau^- \to e^-\mu^+\mu^-$ via neutral Higgs exchange. Note that for $\tau^- \to \mu^-\mu^+\mu^-$ (or $\mu \to e^-e^+e^-$) two distinct diagrams exist which come with a relative minus sign due to the exchange of the two fermion lines.

VI. LOOP CONTRIBUTIONS TO FCNC PROCESSES

We observed in the previous section that all elements ϵ^d_{ij}, ϵ^ℓ_{ij} (with $i \neq j$) and $\epsilon^u_{12,21}$ must be extremely small due to the constraints from tree-level neutral Higgs contributions to FCNC processes. Furthermore, the constraints on ϵ^q_{ij} and ϵ^q_{ji} get even more stringent if both of them are nonzero at the same time due to the bounds from $\Delta F = 2$ processes. Nevertheless, the elements $\epsilon^u_{13,23}$ and $\epsilon^u_{31,32}$ are still unconstrained because we have no data from neutral current top decays. In addition, also the flavor-conserving elements ϵ^f_{ii} are not constrained from neutral Higgs contributions to FCNC processes.

In this section, we study the constraints from Higgs mediated loop contributions to FCNC observables. First, in Sec. VI A we consider the $\Delta F = 2$ processes, $B_s - \bar{B}_s$, $B_d - \bar{B}_d$ and $K - \bar{K}$ mixing and then examine the constraints on $\epsilon^u_{13,23}$ and $\epsilon^u_{31,32}$ from $b \to s(d)\gamma$. Also ϵ^u_{22} (ϵ^u_{33}) can be constrained from these processes due to the relative $\tan\beta$ enhancement compared to m_c (m_t) in the quark-quark-Higgs vertices. In this analysis, we neglect the effects of the elements ϵ^d_{ij}, which means that we assume the absence of large accidental cancellations between different contributions.

Also $\Delta F = 0$ processes (electric dipole moments) place relevant constraints on the type-III 2HDM parameter space, as we will see in Sec. VI F.

A. $B_s - \bar{B}_s$, $B_d - \bar{B}_d$ and $K - \bar{K}$ mixing

For the charged Higgs contributions to $\Delta F = 2$ processes we calculated the complete set of Wilson Coefficients in a general R_ξ gauge. The result is given, together with our conventions for the Hamiltonian, in the Appendix. For the QCD evolution we used the NLO running of the Wilson coefficients of Refs. [73,74].

For computing the allowed regions in parameter space we used the same procedure as explained in the last section. The results are shown in Figs. 13–15 and can be summarized as follows: $B_s - \bar{B}_s$ ($B_d - \bar{B}_d$) mixing gives constraints on ϵ^u_{23} (ϵ^u_{13}) which are of the order of 10^{-1} (10^{-2}) for our typical values of $\tan\beta$ and m_H. In addition, $B_d - \bar{B}_d$ mixing also constrains ϵ^u_{23} to a similar extent as $B_s - \bar{B}_s$ mixing. The constraints on ϵ^u_{33}, ϵ^u_{32} and ϵ^u_{31} are all very weak (of order one). Also Kaon mixing gives comparable bounds on Abs $[\epsilon^u_{23}]$ and the bounds on Abs $[\epsilon^u_{22}]$ are of the order 10^{-1}.

B. Radiative B meson decays: $b \to s\gamma$ and $b \to d\gamma$

The radiative B decay $b \to s\gamma$ ($b \to d\gamma$) imposes stringent constraints on the element ϵ^u_{23} (ϵ^u_{13}) while also in this case the constraints on ϵ^u_{32} (ϵ^u_{31}) are very weak due to the light charm (up) quark involved (see left diagram in Fig. 16). For these processes both a neutral and a charged Higgs contribution occur. Since the flavor off-diagonal elements $\epsilon^d_{13,23}$ and $\epsilon^d_{31,32}$ are already stringently constrained from tree-level decays we neglect the neutral Higgs contribution here. We give the explicit results for the Higgs contributions to the Wilson coefficients governing $b \to s(d)\gamma$ in the Appendix.

For $B \to X_s\gamma$, we obtain the constraints on the 2HDM of type-III parameters ϵ^u_{ij} by using $\mathcal{B}[B \to X_s\gamma]$ from Ref. [100] (*BABAR*) and Refs. [101,102] (BELLE). Combined and extrapolated to a photon energy cut of 1.6 GeV, the HFAG value is [103]

$$\mathcal{B}[B \to X_s\gamma]^{\rm exp}_{E_\gamma > 1.6\,{\rm GeV}} = (3.43 \pm 0.21 \pm 0.07) \times 10^{-4}. \tag{43}$$

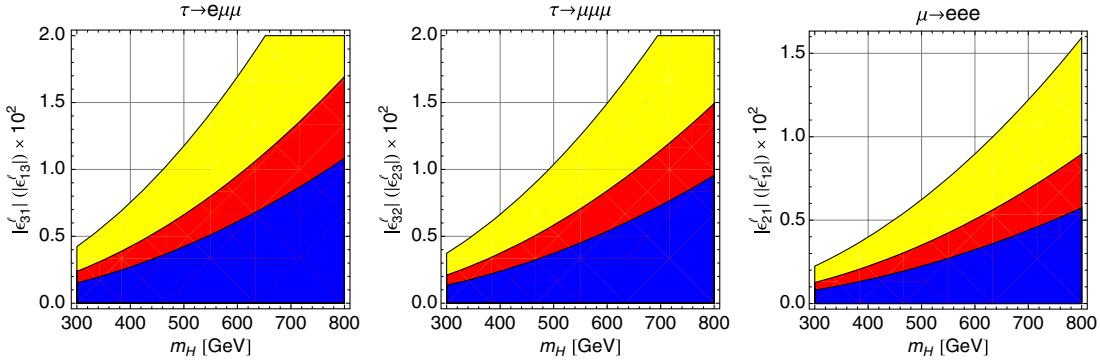

FIG. 12 (color online). Allowed regions for the absolute value of $\epsilon^\ell_{13,31}$, $\epsilon^\ell_{23,32}$ and $\epsilon^\ell_{12,21}$ for $\tan\beta = 30$ (yellow), $\tan\beta = 40$ (red) and $\tan\beta = 50$ (blue) from $\tau^- \to e^-\mu^+\mu^-$, $\tau^- \to \mu^-\mu^+\mu^-$ and $\mu^- \to e^-e^+e^-$, respectively. In each plot only one of the elements ϵ^ℓ_{if} or ϵ^ℓ_{fi} is assumed to be different from zero.

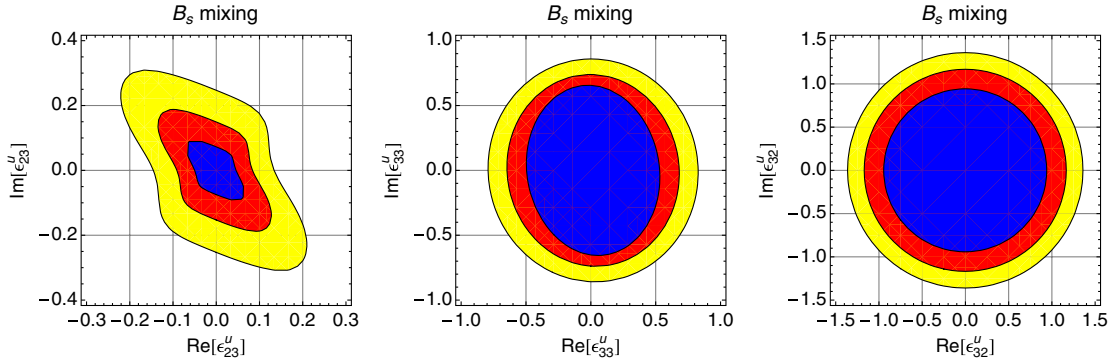

FIG. 13 (color online). Allowed regions in the complex ϵ^u_{ij} plane from B_s mixing for $\tan\beta = 50$ and $m_H = 700$ GeV (yellow), $m_H = 500$ GeV (red) and $m_H = 300$ GeV (blue).

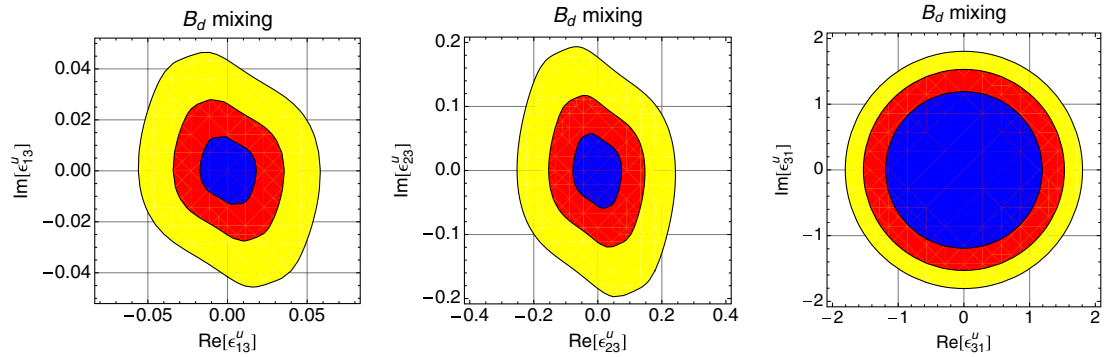

FIG. 14 (color online). Allowed regions in the complex ϵ^u_{ij} plane from B_d mixing for $\tan\beta = 50$ and $m_H = 700$ GeV (yellow), $m_H = 500$ GeV (red) and $m_H = 300$ GeV (blue).

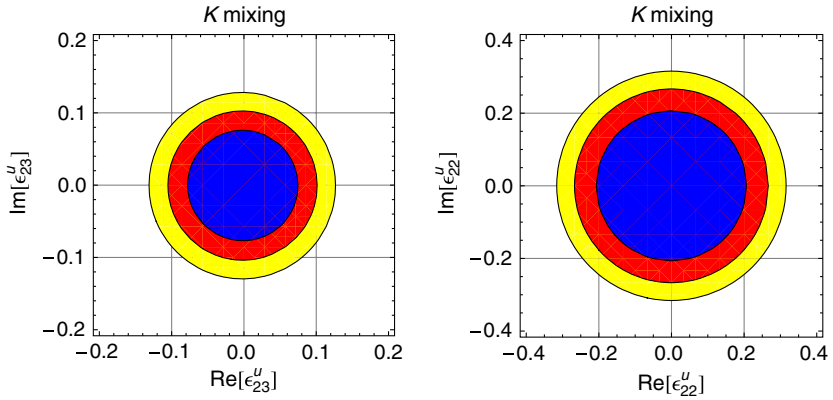

FIG. 15 (color online). Allowed regions in the complex ϵ^u_{ij} plane from $K - \bar{K}$ mixing for $\tan\beta = 50$ and $m_H = 700$ GeV (yellow), $m_H = 500$ GeV (red) and $m_H = 300$ GeV (blue). The constraints are practically independent of $\tan\beta$.

In order to estimate the possible size of NP we use the NNLO SM calculation of Ref. [48] (again for a photon energy cut of 1.6 GeV)

$$\mathcal{B}[B \to X_s\gamma]^{\mathrm{SM}} = (3.15 \pm 0.23) \times 10^{-4}, \tag{44}$$

and calculate the ratio

$$R^{b\to s\gamma}_{\mathrm{exp}} = \frac{\mathcal{B}[B \to X_s\gamma]|^{\mathrm{exp}}}{\mathcal{B}[B \to X_s\gamma]|^{\mathrm{SM}}}. \tag{45}$$

This leads to a certain range for $R^{b\to s\gamma}_{\mathrm{exp}}$. Now, we require that in our leading-order calculation the ratio

$$R^{b\to s\gamma}_{\mathrm{theory}} = \frac{\mathcal{B}[B \to X_s\gamma]|^{\mathrm{2HDM}}}{\mathcal{B}[B \to X_s\gamma]|^{\mathrm{SM}}} \tag{46}$$

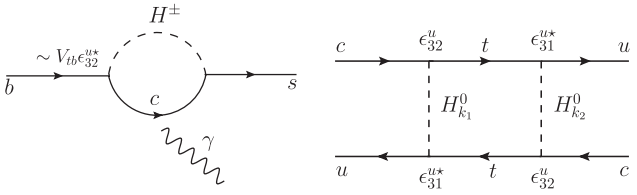

FIG. 16. Left: Feynman diagram contributing to $b \to s\gamma$ via a charm loop containing $\epsilon^{u\star}_{32}$. The contribution is suppressed, since the small charm mass enters either from the propagator or from the charged Higgs coupling to the charm and strange quark. Right: Feynman diagram showing a neutral Higgs box contribution to $D - \bar{D}$ mixing arising if ϵ^u_{31} and ϵ^u_{32} are simultaneously different from zero.

lies within this range. In this way, we obtain the constraints on our model parameters ϵ^u_{ij} as illustrated in Figs. 17 and 18.

The analysis for $b \to d\gamma$ is performed in an analogous way. In addition we use here the fact that most of the hadronic uncertainties cancel in the CP-averaged branching ratio for $B \to X_d\gamma$ [104,105]. The current experimental value of the *BABAR* collaboration [106,107] for the CP averaged branching ratio reads

$$\mathcal{B}[B \to X_d\gamma]|^{\rm exp}_{E_\gamma > 1.6\,{\rm GeV}} = (1.41 \pm 0.57) \times 10^{-5}. \quad (47)$$

Here we take into account a conservative estimate of the uncertainty coming from the extrapolation in the photon energy cut [108]. For the theory prediction we use the NLO SM predictions of the CP-averaged branching ratio $\mathcal{B}(B \to X_d\gamma)|_{E_\gamma > 1.6\,{\rm GeV}}$ of Refs. [109,110], which was recently updated in Ref. [108] and reads

$$\mathcal{B}[B \to X_d\gamma]|^{\rm SM}_{E_\gamma > 1.6\,{\rm GeV}} = (1.54^{+0.26}_{-0.31}) \times 10^{-5}. \quad (48)$$

After defining the ratios $R^{b\to d\gamma}_{\rm exp}$ and $R^{b\to d\gamma}_{\rm theory}$ we continue as in the case of $\mathcal{B}[B \to X_s\gamma]$ in order to constrain ϵ^u_{13}.

As can be seen from Figs. 17 and 18, the constraints that $B \to X_{s(d)}\gamma$ enforces on $\epsilon^u_{23(13)}$ are stronger than the ones from $B_{s(d)}$ mixing. Even ϵ^u_{33} can be restricted to a rather small range.

While in the 2HDM of type II $b \to s\gamma$ enforces a lower limit on the charged Higgs mass of 360 GeV [49] this constraint can get weakened in the 2HDM of type III: The off-diagonal element ϵ^u_{23} can lead to a destructive interference with the SM (depending on its phase) and thus reduce the 2HDM contribution. Lighter charged Higgs masses are also constrained from $b \to d\gamma$ but also this constraint can be avoided by ϵ^u_{13}.

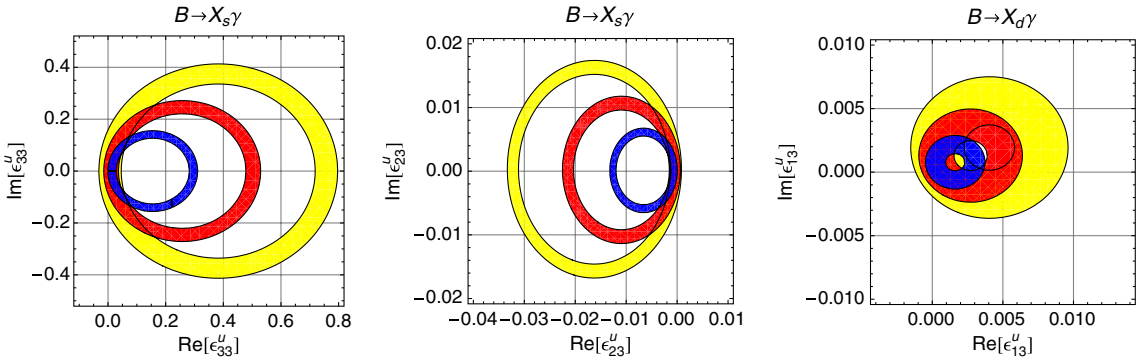

FIG. 17 (color online). Allowed regions for ϵ^u_{ij} from $B \to X_{s(d)}\gamma$, obtained by adding the 2σ experimental error and theoretical uncertainty linear for $\tan\beta = 50$ and $m_H = 700$ GeV (yellow), $m_H = 500$ GeV (red) and $m_H = 300$ GeV (blue).

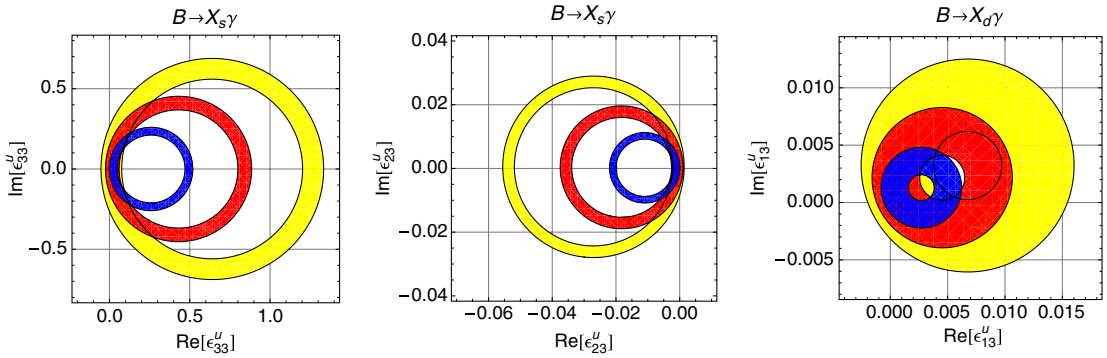

FIG. 18 (color online). Allowed regions for ϵ^u_{ij} from $B \to X_{s(d)}\gamma$, obtained by adding the 2σ experimental error and theoretical uncertainty linear for $\tan\beta = 30$ and $m_H = 700$ GeV (yellow), $m_H = 500$ GeV (red) and $m_H = 300$ GeV (blue).

C. Neutral Higgs box contributions to $D - \bar{D}$ mixing

Nearly all the loop-induced neutral Higgs contributions to FCNC processes can be neglected because the elements involved are already stringently constrained from tree-level processes. However, there is one exception: since the constraints on $\epsilon^u_{31,32}$ are particularly weak (because of the light charm or up quark entering the loop) this can give a sizable effect in $D - \bar{D}$ mixing via a neutral Higgs box[12] (see Fig. 16). As we will use ϵ^u_{31} and ϵ^u_{32} in Sec. VII for explaining the mentioned deviations from the SM prediction in $B \to \tau\nu$, $B \to D\tau\nu$ and $B \to D^*\tau\nu$ it is interesting to ask if all processes can be explained simultaneously without violating $D - \bar{D}$ mixing. In principle also charged Higgs contributions to $D - \bar{D}$ mixing arise but we find that they are very small compared to the H^0_k contributions. The explicit expression for the Wilson coefficients can be found in the Appendix.

Figure 19 shows the allowed regions in the complex $\epsilon^u_{32}\epsilon^{u\star}_{31}$ plane. The constraints are again obtained by using the recent UTfit [97] analysis for the $D - \bar{D}$ system.

D. Radiative lepton decays : $\mu \to e\gamma$, $\tau \to e\gamma$ and $\tau \to \mu\gamma$

The bounds on $\epsilon^\ell_{13,31}$ and $\epsilon^\ell_{23,32}$ from the radiative lepton decays $\tau \to e\gamma$ and $\tau \to \mu\gamma$ (using the experimental values given in Table II) turn out to be significantly weaker than the ones from $\tau^- \to \mu^-\mu^+\mu^-$ and $\tau^- \to e^-\mu^+\mu^-$. Concerning $\mu \to e\gamma$ we expect constraints which are at least comparable to the ones from $\mu^- \to e^-e^+e^-$ since $\mu \to e\gamma$ does not involve the small electron Yukawa coupling entering $\mu^- \to e^-e^+e^-$. In fact, using the new MEG results [113] the constraints from $\mu \to e\gamma$ turn out to be stronger than the ones from $\mu^- \to e^-e^+e^-$ (see Fig. 20). Note that the constraints from $\mu^- \to e^-e^+e^-$ can be avoided if $v_u\epsilon^\ell_{11} \approx m_e$ while the leading contribution to $\mu \to e\gamma$ vanishes for $v_u\epsilon^\ell_{22} \approx m_\mu$.

In principle, for $\mu \to e\gamma$ a simplified expression for the branching ratio in the large $\tan\beta$ limit and $v \ll m_H$ could also be given. However, due to the large logarithm with a relative big prefactor [last term of Eq. (A21)] this is only a good approximation for very heavy Higgses and we therefore use the full expression in our numerical analysis.

We will return to the radiative lepton decays in Sec. VIII and correlate them to the decays $\tau^- \to \mu^-\mu^+\mu^-$, $\tau^- \to e^-\mu^+\mu^-$ and $\mu^- \to e^-e^+e^-$.

E. $B_s \to \mu^+\mu^-$

Setting $\epsilon^q_{ij} = 0$ only the loop induced charged Higgs contribution to $B_s \to \mu^+\mu^-$ (and $B_d \to \mu^+\mu^-$) exists.

[12]In principle, one can also get contribution to $\bar{D}^0 \to \mu^+\mu^-$ through H^0_k box and penguin contributions if the elements ϵ^u_{32} and ϵ^u_{31} are simultaneously nonzero. However, we observe that they are negligible.

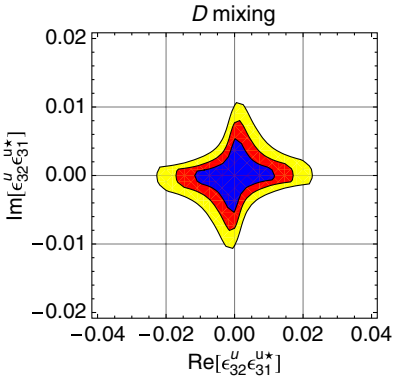

FIG. 19 (color online). Allowed region in the complex $\epsilon^u_{32}\epsilon^{u\star}_{31}$ plane obtained from neutral Higgs box contributions to $D - \bar{D}$ mixing for $\tan\beta = 50$ and $m_H = 700$ GeV (yellow), $m_H = 500$ GeV (red) and $m_H = 300$ GeV (blue).

This contribution [see Eq. (24)] gets altered in the presence of nonzero elements ϵ^ℓ_{ij}, e.g., ϵ^ℓ_{22}. In the large $\tan\beta$ limit, the loop induced result in Eq. (24) is modified to

$$C^{bs}_S = C^{bs}_P = -\frac{m_b V^\star_{tb} V_{ts}}{2}\frac{m_\mu - v_u\epsilon^\ell_{22}}{2M^2_W}\tan^2\beta\frac{\log(m^2_H/m^2_t)}{m^2_H/m^2_t - 1}. \quad (49)$$

The resulting constraints on ϵ^ℓ_{22} from $B_s \to \mu^+\mu^-$ are shown in Fig. 21 and the ones from $B_d \to \mu^+\mu^-$ are found to be weaker.

F. Electric dipole moments and anomalous magnetic moments

1. Charged leptons

The same diagrams which contribute to the radiative lepton decays for $\ell_i \neq \ell_f$ also affect the electric dipole moments and the anomalous magnetic moments of leptons for $\ell_i = \ell_f$ (see Fig. 22). For this reason we use the same conventions as in Eq. (A18) and express the EDMs of leptons in terms of the coefficients $c^{\ell_f\ell_i}_{L,R}$ of the magnetic dipole operators $O^{\ell_f\ell_i}_{L,R}$ in the following way (using that for flavor conserving transitions $c^{\ell_i\ell_i}_L = c^{\ell_i\ell_i\star}_R$):

$$d_{\ell_i} = 2m_{\ell_i}\mathrm{Im}[c^{\ell_i\ell_i}_R]. \quad (50)$$

In SM there is no contribution to the EDMs of leptons at the one-loop level. This is also true in the 2HDM of type II,

TABLE II. Experimental upper limits on the branching ratios of lepton-flavor violating decays.

Process	Experimental bounds
$\mathcal{B}[\tau \to \mu\gamma]$	$\leq 4.5 \times 10^{-8}$ [111,112]
$\mathcal{B}[\tau \to e\gamma]$	$\leq 1.1 \times 10^{-7}$ [111]
$\mathcal{B}[\mu \to e\gamma]$	$\leq 5.7 \times 10^{-13}$ [113]

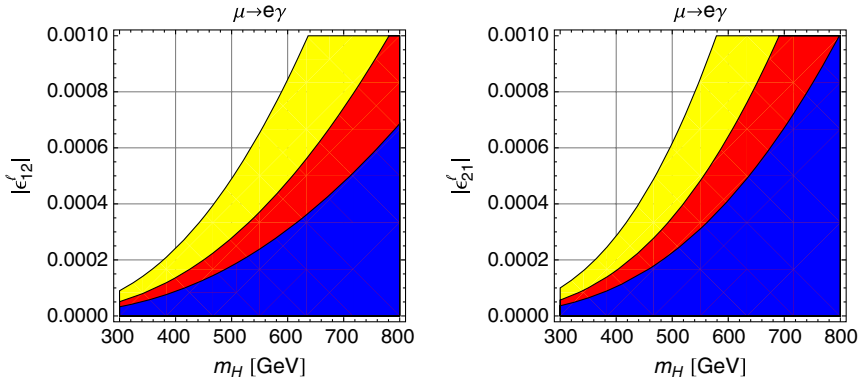

FIG. 20 (color online). Allowed region for ϵ^{ℓ}_{12} (left plot) and ϵ^{ℓ}_{21} (right plot) from $\mu \to e\gamma$ for $\tan\beta = 30$ (yellow), $\tan\beta = 40$ (red) and $\tan\beta = 50$ (blue).

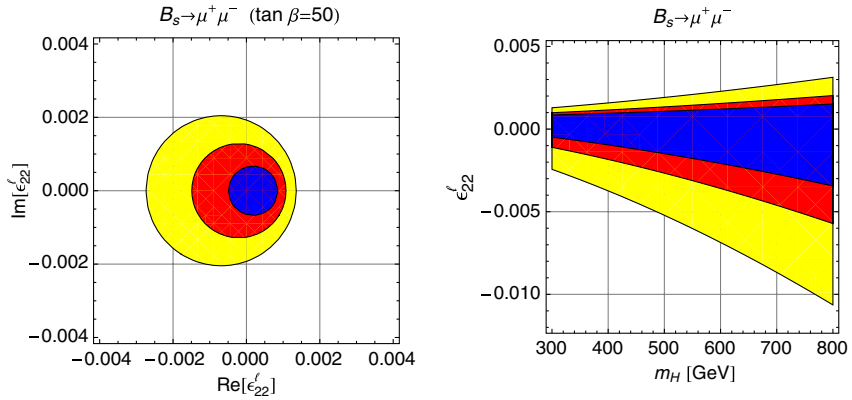

FIG. 21 (color online). Left: Allowed regions in the complex ϵ^{ℓ}_{22} plane from $B_s \to \mu^+\mu^-$ for $\tan\beta = 50$ and $m_H = 700$ GeV (yellow), $m_H = 500$ GeV (red) and $m_H = 300$ GeV (blue). Right: Allowed regions in the $\epsilon^{\ell}_{22} - m_H$ plane from $B_s \to \mu^+\mu^-$ for $\tan\beta = 30$ (yellow), $\tan\beta = 40$ (red), $\tan\beta = 50$ (blue) and real values of ϵ^{ℓ}_{22}.

because the Wilson coefficients are purely real since the phases of the Pontecorvo-Maki-Nakagawa-Sakata (PMNS) matrix drop out in the charged Higgs contributions after summing over the massless neutrinos. However, in a 2HDM of type III, one can have neutral Higgs mediated contributions to EDMs. Note that there is no charged Higgs contribution to the charged lepton EDMs also in the 2HDM of type III because the Wilson coefficients are purely real in this case. Comparing the expression for the EDMs in the 2HDM of type III with the experimental upper bounds on d_e, d_μ and d_τ (see Table III), one can constrain the parameters ϵ^{ℓ}_{ij} (or combination of them) if they are complex.

We observe that while d_e enforces strong constraints on the products $\mathrm{Im}[\epsilon^{\ell}_{13}\epsilon^{\ell}_{31}]$ and $\mathrm{Im}[\epsilon^{\ell}_{12}\epsilon^{\ell}_{21}]$ (see Fig. 23), d_μ and d_τ are not capable of placing good constraints on our model parameters.

Similarly, following the conventions in Eq. (A18), the anomalous magnetic moments (AMMs) can be written in terms of $c_R^{\ell_i\ell_i}$ as (e > 0)

$$a_{\ell_i} = -\frac{4m^2_{\ell_i}}{e}\,\mathrm{Re}[c_R^{\ell_i\ell_i}]. \tag{51}$$

The discrepancy between experiment and the SM prediction for the muon magnetic moment $a_\mu = (g-2)/2$ is [118–122]

$$\Delta a_\mu = a_\mu^{\mathrm{exp}} - a_\mu^{\mathrm{SM}} \approx (3 \pm 1) \times 10^{-9}. \tag{52}$$

In the 2HDM of type II, the sum of the neutral and charged Higgs mediated diagrams gives the following contribution to a_μ (for $\tan\beta = 50$ and $m_H = 500$ GeV):

$$a_\mu^{\mathrm{2HDM\,II}} \approx 2.7 \times 10^{-13}, \tag{53}$$

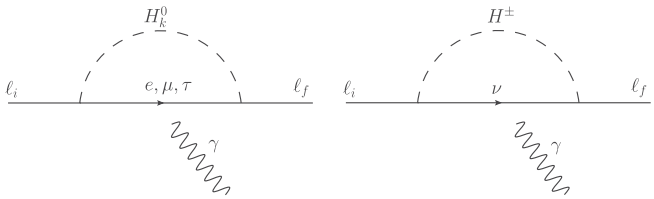

FIG. 22. Left: Feynman diagram contributing to EDMs (for $i = f$) or LFV decays (for $i \neq f$) involving a neutral-Higgs boson. Right: Feynman diagram contributing to EDMs (for $i = f$) or LFV decays (for $i \neq f$) involving a charged-Higgs boson.

TABLE III. Experimental (upper) bounds on electric dipole moments.

EDMs	$\lvert d_e\rvert$	$\lvert d_\mu\rvert$	d_τ	$\lvert d_n\rvert$
Bounds (e cm)	10.5×10^{-28} [114]	1.9×10^{-19} [115]	$\in [-2.5, 0.8] \times 10^{-17}$ [116]	2.9×10^{-26} [117]

which is interfering constructively with the SM. Anyway, it can be seen that the effect is orders of magnitude smaller than the actual sensitivity and it even gets smaller for higher Higgs masses.

Concerning the 2HDM of type III the discrepancy between experiment and the SM prediction given in Eq. (52) could be explained but only with severe fine-tuning. One would need to allow for very large values of ϵ^ℓ_{22} which would not only violate 't Hooft's naturalness criterion but also enhance $B_s \to \mu^+\mu^-$ by orders of magnitude above the experimental limit. If one would try to explain the anomaly using ϵ^ℓ_{23} and ϵ^ℓ_{32} (ϵ^ℓ_{12} and ϵ^ℓ_{21}) one would violate the bounds from $\tau^- \to \mu^-\mu^+\mu^-$ ($\mu^- \to e^-e^+e^-$ or $\mu \to e\gamma$) as illustrated in Fig. 24.

In conclusion, neither a type-II nor a type-III 2HDM can give a sizable effect in a_μ and both models are not capable of explaining the deviation from the SM.

2. Electric dipole moment of the neutron

The neutron electric dipole moment d_n can also provide constraints on the parameters ϵ^q_{ij}. In the SM, there is no contribution to d_n at the one-loop level since the coefficients are real. This is also true in the type-II 2HDM.

Using the theory estimate of Ref. [123], which is based on the QCD sum-rules calculations of Refs. [124–127], the neutron EDM can be written as

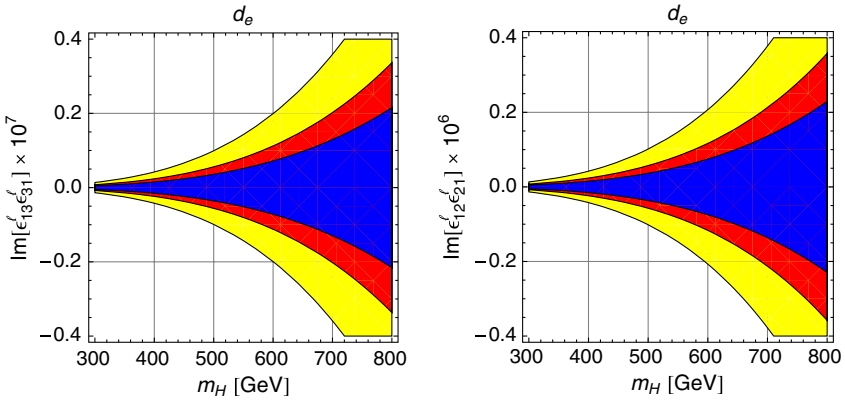

FIG. 23 (color online). Allowed regions in the $\mathrm{Im}[\epsilon^\ell_{13}\epsilon^\ell_{31}] - m_H$ and $\mathrm{Im}[\epsilon^\ell_{12}\epsilon^\ell_{21}] - m_H$ planes from neutral Higgs contribution to d_e for $\tan\beta = 50$ (blue), $\tan\beta = 40$ (red) and $\tan\beta = 30$ (yellow). The constraints on $\mathrm{Im}[\epsilon^\ell_{11}]$ are not sizable.

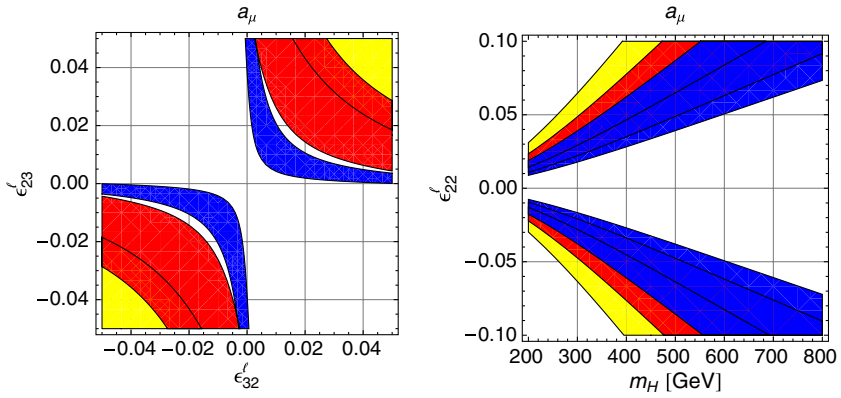

FIG. 24 (color online). Left: Allowed region in the $\epsilon^\ell_{23} - \epsilon^\ell_{32}$ plane from Δa_μ for real values of ϵ^ℓ_{23}, ϵ^ℓ_{32} and $\tan\beta = 50$, $m_H = 700$ GeV (yellow), $m_H = 500$ GeV (red) and $m_H = 300$ GeV (blue). Right: Allowed region in the $\epsilon^\ell_{22} - m_H$ plane from Δa_μ for real values of ϵ^ℓ_{22} and $\tan\beta = 50$ (blue), $\tan\beta = 40$ (red) and $\tan\beta = 30$ (yellow).

$$d_n = (1 \pm 0.5)[1.4(d_d - 0.25 d_u) + 1.1 e(d_d^g + 0.5 d_u^g)], \tag{54}$$

where d_u (d_d) is the EDM of the up (down) quark and $d^g_{u(d)}$ define the corresponding chromoelectric dipole moments which stem from the chromomagnetic dipole operator

$$O^{q_f q_i}_{R(L)} = m_{q_i} \bar{q}_f \sigma^{\mu\nu} T^a P_{R(L)} q_i G^a_{\mu\nu}. \tag{55}$$

Similar to EDMs, the (chromo)electric dipole moments of quarks are given as

$$d^{(g)}_{q_i} = 2 m_{q_i} \mathrm{Im}[c^{q_i q_i}_{R,(g)}]. \tag{56}$$

Using the upper limit on d_n (see Table III) we can constrain some of ϵ^u_{ij} (for $\epsilon^d_{ij} = 0$) as shown in Figs. 25 and 26. These constraints are obtained for the conservative case of assuming a prefactor of 0.5 in Eq. (54). The explicit expressions for $c^{q_i q_i}_{R,(g)}$ stemming from neutral and charged Higgs contributions to $d^{(g)}_{q_i}$ are relegated to the Appendix. Note that for the neutron EDM we did not include QCD corrections.

VII. TREE-LEVEL CHARGED CURRENT PROCESSES

In this section we study the constraints from processes which are mediated in the SM by a tree-level W exchange and which receive additional contributions from charged Higgs exchange in 2HDMs. We study purely leptonic meson decays, semileptonic meson decays and tau lepton decays. Concerning B meson decays we consider $B \to \tau\nu$, $B \to D\tau\nu$ and $B \to D^*\tau\nu$ which are, as outlined in the Introduction, very interesting in the light of the observed deviation from the SM. We consider in addition $D_{(s)} \to \tau\nu$, $D_{(s)} \to \mu\nu$, $K(\pi) \to e\nu$, $K(\pi) \to \mu\nu$ and $\tau \to K(\pi)\nu$ and look for violation of lepton flavor universality via $K(\pi) \to e\nu/K(\pi) \to \mu\nu$ and $\tau \to K(\pi)\nu/K(\pi) \to \mu\nu$. Even though no deviations from the SM have been observed in these channels, they put relevant constraints on the parameter space of the type-III 2HDM.

For purely leptonic decays of a pseudoscalar meson M (and also tau decays to mesons) to a lepton ℓ_j and a neutrino ν (which is not detected) the SM prediction is given by

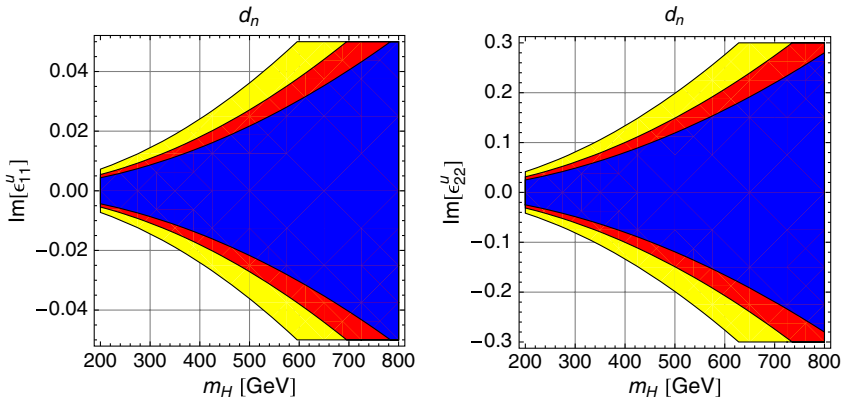

FIG. 25 (color online). Allowed regions in the $\mathrm{Im}[\epsilon^u_{11,22}] - m_H$ planes from the electric dipole moment of the neutron for $\tan\beta = 50$ (blue), $\tan\beta = 40$ (red) and $\tan\beta = 30$ (yellow). We observe that d_n can not provide good constraints on the real parts of $\epsilon^u_{11,22}$.

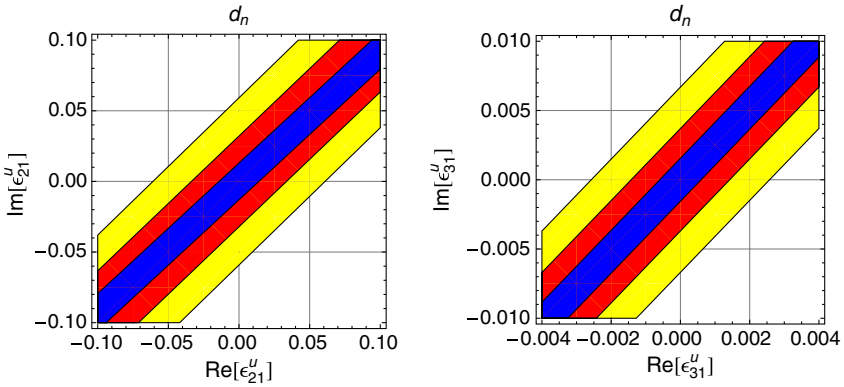

FIG. 26 (color online). Allowed regions in the complex $\epsilon^u_{21,31}$ planes from d_n for $\tan\beta = 50$ and $m_H = 700$ GeV (yellow), $m_H = 500$ GeV (red) and $m_H = 300$ GeV (blue). We see that the absolute value of ϵ^u_{31} can only be large if it is aligned to V_{ub}, i.e., $\mathrm{Arg}[V_{ub}] = \mathrm{Arg}[\epsilon^u_{31}] \pm \pi$ which is very important when we consider later $B \to \tau\nu$.

$$\mathcal{B}_{\rm SM}[M \to \ell_j \nu] = \frac{m_M}{8\pi} G_F^2 m_{\ell_j}^2 \tau_M f_M^2 |V_{u_f d_i}|^2 \left(1 - \frac{m_{\ell_j}^2}{m_M^2}\right)^2 (1 + \delta_{\rm EM}^{M\ell_j}), \quad (57)$$

where $\delta_{\rm EM}^{M\ell_j}$ stands for channel dependent electromagnetic corrections (see Table IV), m_M is the mass of the meson involved and m_{u_f} (m_{d_i}) refers to the mass of its constituent up (down) type quark. The expression for $\tau \to M\nu$ differs by the exchange of the meson masses (life time) with the tau masses (life time) and by a factor of $1/2$ stemming from spin averaging.

NP via scalar operators can be included very easily:

$$\mathcal{B}_{\rm NP} = \mathcal{B}_{\rm SM} \left| 1 + \frac{m_M^2}{(m_{u_f} + m_{d_i}) m_{\ell_j}} \frac{C_R^{u_f d_i, \ell_j} - C_L^{u_f d_i, \ell_j}}{C_{\rm SM}^{u_f d_i, \ell_j}} \right|^2 \quad (58)$$

with

$$C_{\rm SM}^{u_f d_i, \ell_j} = 4 G_F V_{u_f d_i} / \sqrt{2}. \quad (59)$$

All quantities in Eq. (58) are understood to be at the meson scale m_M. Like for $B_s \to \mu^+ \mu^-$, the SM Wilson coefficient is renormalization scale independent and the scalar Wilson coefficients evolve in the same way as the quark masses.

In the 2HDM III the Wilson coefficients $C_L^{u_f d_i, \ell_j}$ and $C_R^{u_f d_i, \ell_j}$ are given by (neglecting terms which are not $\tan\beta$ enhanced)

$$C_R^{u_f d_i, \ell_j} = -\frac{\tan^2\beta}{m_{H^\pm}^2} \left(V_{fi} \frac{m_{d_i}}{v} - \sum_{j=1}^{3} V_{fj} \epsilon_{ji}^{d} \right) \left(\frac{m_{\ell_j}}{v} - \sum_{k=1}^{3} \epsilon_{kj}^{\ell\star} \right),$$

$$C_L^{u_f d_i, \ell_j} = \frac{\tan\beta}{m_{H^\pm}^2} \sum_{j=1}^{3} V_{ji} \epsilon_{jf}^{\star u} \left(\frac{m_{\ell_j}}{v} - \sum_{k=1}^{3} \epsilon_{kj}^{\ell\star} \right). \quad (60)$$

Note that $C_L^{u_f d_i, \ell_j}$ is only proportional to one power of $\tan\beta$ while $C_R^{u_f d_i, \ell_j}$ is proportional to $\tan^2\beta$. The Hamiltonian governing $M \to \ell_j \nu$ ($\tau \to M\nu$) and the Wilson coefficients for general scalar interactions are given in the Appendix. It is important to keep in mind that, since we are dealing with lepton flavor-violating terms, we must sum over the neutrinos in the final state because the neutrino is not detected. Note that we did not include the PMNS matrix in both $C_{\rm SM}^{u_f d_i, \ell_j}$ and $C_{L,R}^{u_f d_i, \ell_j}$ for simplifying the expressions, since it cancels in the final expression after summing over the neutrinos.

For semileptonic meson decays $B \to D\tau\nu$ and $B \to D^*\tau\nu$, which have a three-body final state, both the SM prediction and the inclusion of NP are more complicated, as will be discussed in Sec. VII A 1.

A. Tauonic charged B meson decays: $B \to \tau\nu$, $B \to D\tau\nu$ and $B \to D^*\tau\nu$

As discussed in the Introduction the *BABAR* collaboration performed an analysis of the semileptonic B decays $B \to D\tau\nu$ and $B \to D^*\tau\nu$ using the full available data set [8,9]. They find for the ratios

$$\mathcal{R}(D^{(*)}) = \mathcal{B}(B \to D^{(*)}\tau\nu) / \mathcal{B}(B \to D^{(*)}\ell\nu), \quad (61)$$

(with $\ell = e, \mu$) the following results:

$$\mathcal{R}(D) = 0.440 \pm 0.058 \pm 0.042, \quad (62)$$

$$\mathcal{R}(D^*) = 0.332 \pm 0.024 \pm 0.018. \quad (63)$$

Here the first error is statistical and the second one is systematic. Comparing these measurements to the SM predictions

$$\mathcal{R}_{\rm SM}(D) = 0.297 \pm 0.017, \quad (64)$$

$$\mathcal{R}_{\rm SM}(D^*) = 0.252 \pm 0.003, \quad (65)$$

we see that there is a discrepancy of 2.0σ for $\mathcal{R}(D)$ and 2.7σ for $\mathcal{R}(D^*)$. For the theory predictions we used the updated results of [8], which rely on the calculations of Refs. [55,131] based on the results of Refs. [132–136]. The measurements of both ratios $\mathcal{R}(D)$ and $\mathcal{R}(D^*)$ exceed the

TABLE IV. Experimental values, SM predictions and electromagnetic corrections (in the SM) for the ratios of charged current processes. The experimental values are obtained by adding the errors of the individual branching ratios given in Ref. [70] in quadrature. The SM predictions include the uncertainties from $\delta_{\rm EM}^{M\ell_j}$ and (if involved) as well as the uncertainties due to CKM factors and decay constants. As always, we add the theory error linear to the experimental ones.

Ratio	Experimental value	SM prediction	$\delta_{\rm EM}^{M\ell_j}$
$\mathcal{B}[K \to e\nu]/\mathcal{B}[K \to \mu\nu]$	$(2.488 \pm 0.013) \times 10^{-5}$	$(2.472 \pm 0.001) \times 10^{-5}$	-0.0378 ± 0.0004 [61]
$\mathcal{B}[K \to \mu\nu]/\mathcal{B}[\pi \to \mu\nu]$	$(63.55 \pm 0.11) \times 10^{-2}$	$(63.48 \pm 1.37) \times 10^{-2}$	-0.0070 ± 0.0018 [128]
$\mathcal{B}[K \to e\nu]/\mathcal{B}[\pi \to e\nu]$	$(1.285 \pm 0.008) \times 10^{-1}$	$(1.270 \pm 0.027) \times 10^{-1}$	-0.0070 ± 0.0018 [128]
$\mathcal{B}[\pi \to e\nu]/\mathcal{B}[\pi \to \mu\nu]$	$(1.230 \pm 0.004) \times 10^{-4}$	1.234×10^{-4}	-3.85% [129]
$\mathcal{B}[\tau \to K\nu]/\mathcal{B}[\tau \to \pi\nu]$	$(6.46 \pm 0.10) \times 10^{-2}$	$(6.56 \pm 0.16) \times 10^{-2}$	0.0003 ± 0.0044 [130]
$\mathcal{B}[\tau \to \pi\nu]/\mathcal{B}[\pi \to \mu\nu]$	$(10.83 \pm 0.06) \times 10^{-2}$	10.87×10^{-2}	$+1.2\%$ [129]
$\mathcal{B}[\tau \to K\nu]/\mathcal{B}[K \to \mu\nu]$	$(1.102 \pm 0.016) \times 10^{-2}$	1.11×10^{-2}	$+2.0\%$ [129]

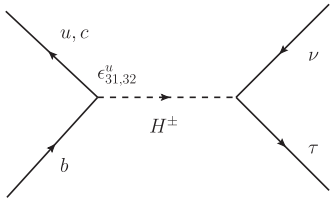

FIG. 27. Feynman diagram showing a charged Higgs contributing to $B \to \tau\nu$ and $B \to D^{(*)}\tau\nu$ involving the flavor changing parameters ϵ^u_{31} and ϵ^u_{32} which affect $B \to \tau\nu$ and $B \to D^{(*)}\tau\nu$, respectively.

SM prediction, and combining them gives a 3.4σ deviation from the SM [8,9] expectation.

This evidence for the violation of lepton flavor universality in $B \to D\tau\nu$ and $B \to D^*\tau\nu$ is further supported by the measurement of $B \to \tau\nu$ by *BABAR* [10,11] and BELLE [12]. Until recently, all measurements of $B \to \tau\nu$ (the hadronic tag and the leptonic tag both from *BABAR* and BELLE) were significantly above the SM prediction. However, the latest BELLE result for the hadronic tag [13] of $\mathcal{B}[B \to \tau\nu] = (0.72^{+0.27}_{-0.25} \pm 0.11) \times 10^{-4}$ is in agreement with the SM prediction [14]:

$$\mathcal{B}_{\rm SM}[B \to \tau\nu] = (0.796^{+0.088}_{-0.087}) \times 10^{-4}. \quad (66)$$

Averaging all measurements, one obtains the branching ratio

$$\mathcal{B}_{\rm exp}[B \to \tau\nu] = (1.15 \pm 0.23) \times 10^{-4}, \quad (67)$$

which now disagrees with the SM prediction by 1.6σ using V_{ub} from the global fit [14].

Combining $\mathcal{R}(D)$, $\mathcal{R}(D^*)$ and $B \to \tau\nu$, we have evidence for violation of lepton flavor universality. Assuming that these deviations from the SM are not statistical fluctuations or underestimated theoretical or systematic uncertainties, it is interesting to ask which model of new physics can explain the measured values [16,137–146].

1. $B \to D\tau\nu$ and $B \to D^*\tau\nu$

Let us first consider the semileptonic decays $B \to D\tau\nu$ and $B \to D^*\tau\nu$. Here the Wilson coefficients $C_R^{qb,\tau}$ and $C_L^{qb,\tau}$ affect $B \to D\tau\nu$ and $B \to D^*\tau\nu$ in the following way [54,55,147]:

$$\mathcal{R}(D) = \mathcal{R}_{\rm SM}(D)\left(1 + 1.5\,{\rm Re}\left[\frac{C_R^{cb,\tau} + C_L^{cb,\tau}}{C_{\rm SM}^{cb,\tau}}\right] + 1.0\left|\frac{C_R^{cb,\tau} + C_L^{cb,\tau}}{C_{\rm SM}^{cb,\tau}}\right|^2\right), \quad (68)$$

$$\mathcal{R}(D^*) = \mathcal{R}_{\rm SM}(D^*)\left(1 + 0.12\,{\rm Re}\left[\frac{C_R^{cb,\tau} - C_L^{cb,\tau}}{C_{\rm SM}^{cb,\tau}}\right] + 0.05\left|\frac{C_R^{cb,\tau} - C_L^{cb,\tau}}{C_{\rm SM}^{cb,\tau}}\right|^2\right). \quad (69)$$

For our analysis we add the experimental errors in quadrature and the theoretical uncertainty linear on top of this. There are also efficiency corrections to $\mathcal{R}(D)$ due to the *BABAR* detector [8] which are important in the case of large contributions from the scalar Wilson coefficients $C_{R,L}^{cb,\tau}$ [i.e., if one wants to explain $\mathcal{R}(D)$ with destructive interference with the SM contribution]. As shown in Ref. [137], these corrections can be effectively taken into account by multiplying the quadratic term in $C_{R,L}^{cb,\tau}$ of Eq. (68) by an approximate factor of 1.5 [not included in Eq. (68)].

Since ϵ^d_{33} contributes to $C_R^{cb,\tau}$ (the same Wilson coefficient generated in the type-II 2HDM) it cannot simultaneously explain $\mathcal{R}(D)$ and $\mathcal{R}(D^*)$. Therefore, we are left with ϵ^u_{32}, which contributes to $B \to D\tau\nu$ and $B \to D^*\tau\nu$ (as shown in Fig. 27). In the left frame of Fig. 28 we see the allowed region in the complex ϵ^u_{32}-plane, which gives the correct values for $\mathcal{R}(D)$ and $\mathcal{R}(D^*)$ within the 1σ uncertainties for $\tan\beta = 50$ and $m_H = 500$ GeV, and the middle and the right frames correspond to the allowed regions on ϵ^u_{31} from $B \to \tau\nu$.

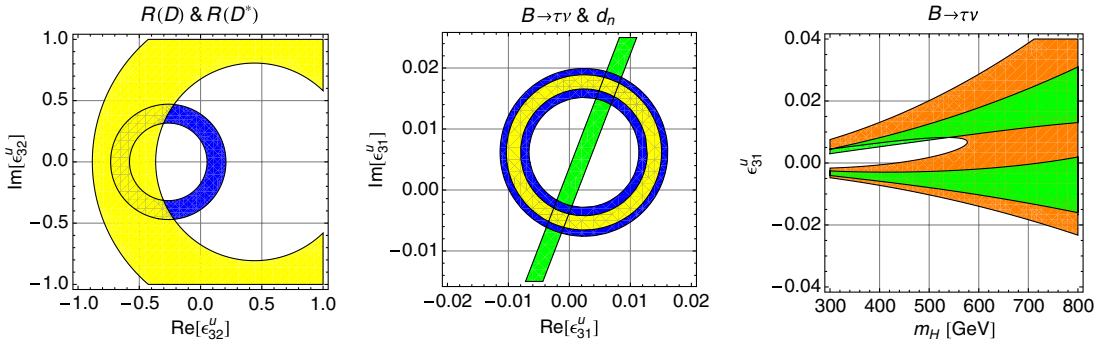

FIG. 28 (color online). Left: Allowed regions in the complex ϵ^u_{32} plane from $\mathcal{R}(D)$ (blue) and $\mathcal{R}(D^*)$ (yellow) for $\tan\beta = 50$ and $m_H = 500$ GeV. Middle: Allowed regions in the complex ϵ^u_{31} plane combining the constraints from $B \to \tau\nu$ [1σ (yellow) and 2σ (blue)] and neutron EDM (green) for $\tan\beta = 50$ and $m_H = 500$ GeV. Right: Allowed regions in the $m_H - \epsilon^u_{31}$ plane from $B \to \tau\nu$ for real values of ϵ^u_{31} and $\tan\beta = 50$ (green), $\tan\beta = 30$ (orange).

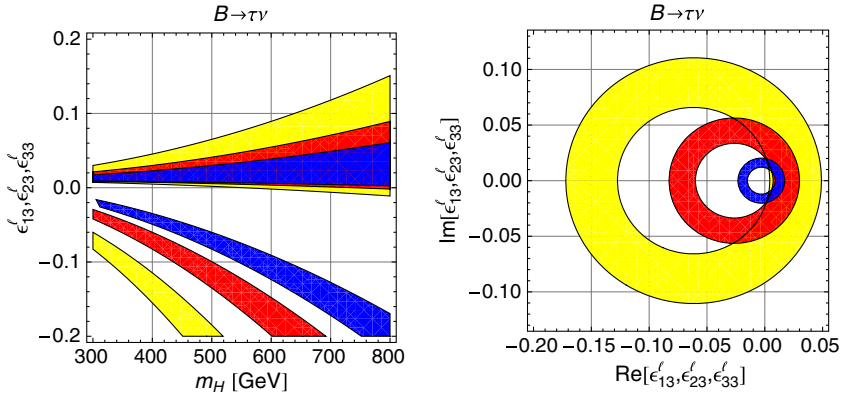

FIG. 29 (color online). Left: Allowed regions in the $m_H - \epsilon^{\ell}_{i3}$ plane from $B \to \tau\nu$ for real values of ϵ^{ℓ}_{i3} and $\tan\beta = 30$ (yellow), $\tan\beta = 40$ (red), $\tan\beta = 50$ (blue). Right: Allowed regions in the complex ϵ^{ℓ}_{13}, ϵ^{ℓ}_{23} and ϵ^{ℓ}_{33} planes from $B \to \tau\nu$ for $m_H = 700$ GeV (yellow), $m_H = 500$ GeV (red) and $m_H = 300$ GeV (blue).

2. $B \to \tau\nu$

In principle, $B \to \tau\nu$ can be explained either by using ϵ^{d}_{33} (as in 2HDMs with MFV) or by ϵ^{u}_{31} (or by a combination of both of them). However, ϵ^{d}_{33} alone cannot explain the deviation from the SM without fine-tuning, while ϵ^{u}_{31} is capable of doing this [16].

$B \to \tau\nu$ can also be used to constrain ϵ^{ℓ}_{13}, ϵ^{ℓ}_{23} and ϵ^{ℓ}_{33} as illustrated in Fig. 29. In order to obtain these constraints, we assumed that all other relevant elements (ϵ^{d}_{33} and ϵ^{u}_{31}) are zero.

B. $D_{(s)} \to \tau\nu$ and $D_{(s)} \to \mu\nu$

Previously, there were some indications for NP in $D_s \to \tau\nu$ [148–150]. However, using the new experimental values for $\mathcal{B}[D_s \to \tau\nu]$ (see Table V) and the improved lattice determination for the decay constant f_{D_s} [80,152] we find agreement between the SM predictions and experiment. Nevertheless, it is interesting to consider the constraints on the 2HDM of type-III parameter space. Charged Higgs contributions to $D_{(s)} \to \tau\nu$ and $D_{(s)} \to \mu\nu$ have been investigated in Refs. [58–60,153].

The most important constraints on the 2HDM of type-III parameter space are the ones on ϵ^{u}_{22} (shown in Fig. 30). $D_{(s)} \to \tau\nu$ and $D_{(s)} \to \mu\nu$ constrains $\mathrm{Re}[\epsilon^{u}_{22}]$ while the constraints on $\mathrm{Im}[\epsilon^{u}_{22}]$ are very weak. In principle, also the ratio $D_{(s)} \to \tau\nu/D_{(s)} \to \mu\nu$ could be used for constraining deviations from lepton flavor universality, but the constraints from $K(\pi) \to e\nu/K(\pi) \to \mu\nu$ and $\tau \to K(\pi)\nu/K(\pi) \to \mu\nu$ turn out to be stronger.

TABLE V. Experimental values (upper bounds) and SM predictions for $D_{(s)} \to \tau\nu$ and $D_{(s)} \to \mu\nu$ processes. The SM prediction for $D_s \to \mu\nu$ mode takes into account the EM correction effects of $+1.0\%$ [148,149,151].

Process	Experimental value (bound)	SM prediction
$\mathcal{B}[D_s \to \tau\nu]$	$(5.43 \pm 0.31) \times 10^{-2}$	$(5.36^{+0.54}_{-0.50}) \times 10^{-2}$
$\mathcal{B}[D_s \to \mu\nu]$	$(5.90 \pm 0.33) \times 10^{-3}$	$(5.50^{+0.55}_{-0.52}) \times 10^{-3}$
$\mathcal{B}[D \to \tau\nu]$	$\leq 1.2 \times 10^{-3}$	$(1.10 \pm 0.06) \times 10^{-3}$
$\mathcal{B}[D \to \mu\nu]$	$(3.82 \pm 0.33) \times 10^{-4}$	$(4.15^{+0.22}_{-0.21}) \times 10^{-4}$

C. $K \to \mu\nu/\pi \to \mu\nu$ and $K \to e\nu/\pi \to e\nu$

The ratio $R_{K_{\ell 2},\pi_{\ell 2}} = \mathcal{B}[K \to \ell\nu]/\mathcal{B}[\pi \to \ell\nu]$ ($\ell = e, \mu$) is useful for constraining ϵ^{d}_{22}, ϵ^{ℓ}_{i1} and ϵ^{ℓ}_{i2} because the ratio of the decay constants f_K/f_π is known more precisely than the single decay constants [61].

For obtaining the experimental values we add the errors of the individual branching ratios in quadrature and the SM values take into account the electromagnetic correction. The corresponding values are given in Table IV. The errors are due to the combined uncertainties in f_K/f_π, the CKM

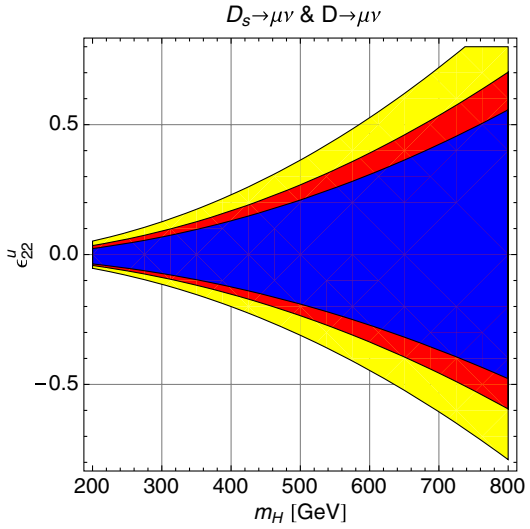

FIG. 30 (color online). Left: Allowed region in the $m_H - \epsilon^{u}_{22}$ plane (for real values of ϵ^{u}_{22}) obtained by combining the constraints from $D \to \mu\nu$ and $D_s \to \mu\nu$ for $\tan\beta = 30$ (yellow), $\tan\beta = 40$ (red) and $\tan\beta = 50$ (blue). While the upper bound on ϵ^{u}_{22} comes from $D_s \to \mu\nu$, $D \to \mu\nu$ is more constraining for negative values of ϵ^{u}_{22}. The bounds on the imaginary part of ϵ^{u}_{22} are very weak. The constraints from $D_s \to \tau\nu$ turn out to be comparable (but a bit weaker) while the ones from $D \to \tau\nu$ are weak.

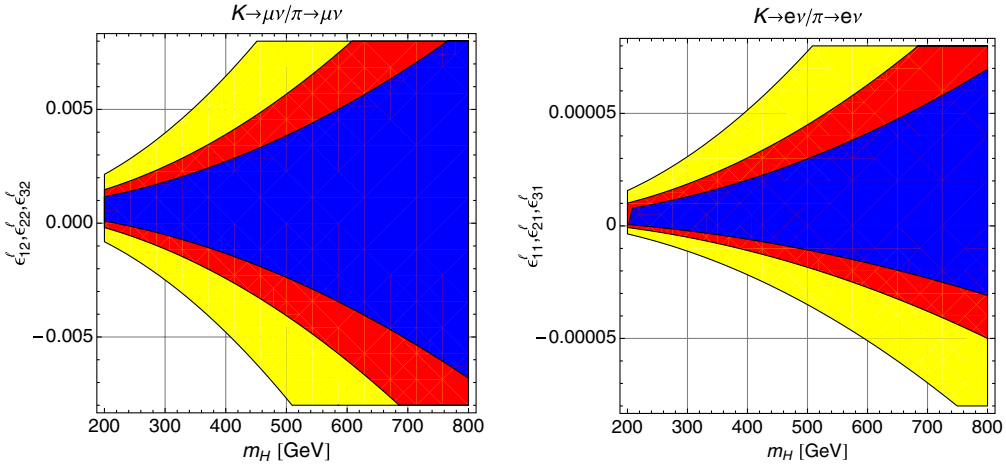

FIG. 31 (color online). Allowed regions in the $m_H - \epsilon^{\ell}_{i1,i2}$ plane from $K \to \mu\nu/\pi \to \mu\nu$ and $K \to e\nu/\pi \to e\nu$ for real values of $\epsilon^{\ell}_{i1,i2}$ and $\tan\beta = 30$ (yellow), $\tan\beta = 40$ (red) and $\tan\beta = 50$ (blue). The constraints are weaker than the ones from $K(\pi) \to e\nu/K(\pi) \to \mu\nu$ and $\tau \to K(\pi)\nu/K(\pi) \to \mu\nu$ but cannot be avoided assuming the MFV limit ($\frac{m_{\ell_i}}{m_{\ell_j}} = \frac{\epsilon^{\ell}_{ii}}{\epsilon^{\ell}_{jj}}$).

elements and the EM corrections. We obtained the value for V_{us} from $K \to \pi\ell\nu$ (which is much less sensitive to charged Higgs contributions than $K \to \mu\nu/\pi \to \mu\nu$) and V_{ud} by exploiting CKM unitarity.

Figure 32 illustrates the allowed regions for ϵ^{d}_{22} by combining the constraints from $K \to \mu\nu/\pi \to \mu\nu$ and $K \to e\nu/\pi \to e\nu$. Like in $D_{(s)} \to \tau\nu$ and $D_{(s)} \to \mu\nu$ the constraints are on the real part of ϵ^{d}_{22} while the constraints on the imaginary part are very weak. Concerning ϵ^{ℓ}_{i1} and ϵ^{ℓ}_{i2} the constraints from $K(\pi) \to e\nu/K(\pi) \to \mu\nu$ will turn out to be more stringent but the latter ones can be avoided in the limit $\frac{m_{\ell_i}}{m_{\ell_j}} = \frac{\epsilon^{\ell}_{ii}}{\epsilon^{\ell}_{jj}}$ (see Figs. 31 and 33).

D. $\tau \to K\nu/\tau \to \pi\nu$

The τ is the only lepton which is heavy enough to decay into hadrons. The ratio $\mathcal{B}[\tau \to K\nu]/\mathcal{B}[\tau \to \pi\nu]$ can be considered for putting constraints on ϵ^{u}_{21}, ϵ^{d}_{12} and ϵ^{ℓ}_{i3}.

The experimental and theoretical values for this ratio are given in Table IV. We observe that the constraints from $\bar{D}^0 \to \mu^+\mu^-$ and $D - \bar{D}$ mixing on ϵ^{u}_{21} and $K_L \to \mu^+\mu^-$ on ϵ^{d}_{12} are too stringent so that no sizable effects stemming from these elements are possible. Also concerning ϵ^{ℓ}_{i3}, as we will see in the following sections, the constraints from $\tau \to \pi\nu/\pi \to \mu\nu$ will be stronger but again the latter ones can be avoided in the MFV limit $\frac{m_{\ell_i}}{m_{\ell_j}} = \frac{\epsilon^{\ell}_{ii}}{\epsilon^{\ell}_{jj}}$ (see Fig. 32).

E. Tests for lepton flavor universality: $K(\pi) \to e\nu/K(\pi) \to \mu\nu$ and $\tau \to K(\pi)\nu/K(\pi) \to \mu\nu$

$K_{\ell 2}(K \to \ell\nu)$ decays ($\ell = e, \mu$) are helicity suppressed in the SM and suffer from large theoretical uncertainties due to the decay constants. However, considering the ratio $R_{K_{\ell 2}} = \mathcal{B}[K \to e\nu]/\mathcal{B}[K \to \mu\nu]$ the dependence on decay constants drops out.

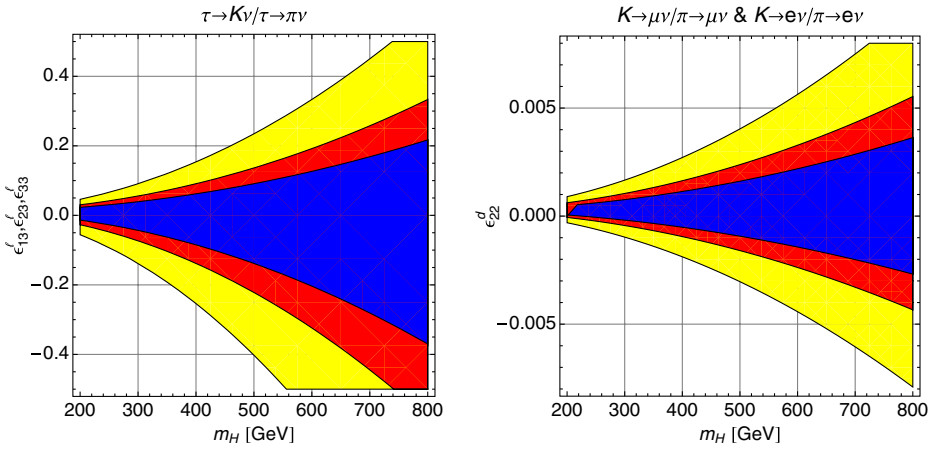

FIG. 32 (color online). Left: Allowed regions in the $m_H - \epsilon^{\ell}_{i3}$ plane from $\tau \to K\nu/\tau \to \pi\nu$. Right: Allowed regions in the $m_H - \epsilon^{d}_{22}$ plane obtained by combining the constraints from $K \to \mu\nu/\pi \to \mu\nu$ and $K \to e\nu/\pi \to e\nu$ for real values of ϵ^{d}_{22}. In both plots $\tan\beta = 30$ (yellow), $\tan\beta = 40$ (red) and $\tan\beta = 50$ (blue).

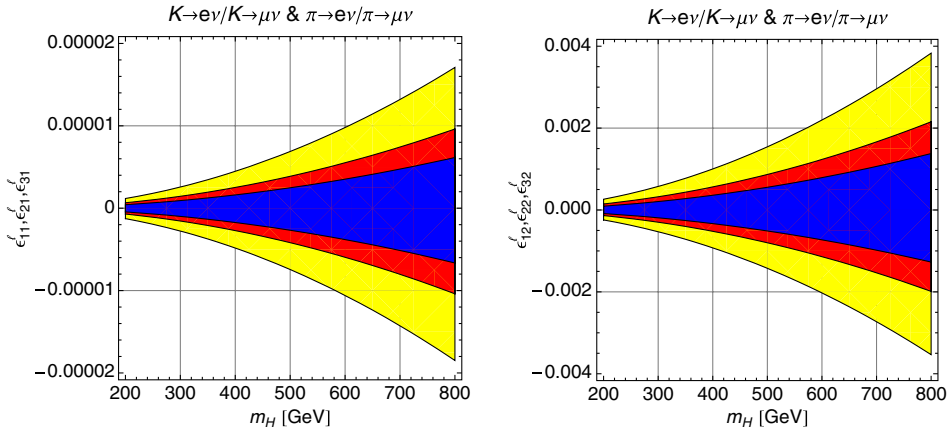

FIG. 33 (color online). Allowed regions in the $m_H - \epsilon^\ell_{ij}$ plane obtained by combining the constraints from $K \to e\nu/K \to \mu\nu$ and $\pi \to e\nu/\pi \to \mu\nu$ for real values of ϵ^ℓ_{ij} and $\tan\beta = 30$ (yellow), $\tan\beta = 40$ (red) and $\tan\beta = 50$ (blue). The constraints on ϵ^ℓ_{i1} (affecting the electron coupling) are more stringent than the constraints on ϵ^ℓ_{i2} (which affect the muon coupling).

In the 2HDM of type II the charged Higgs contributions to $K(\pi) \to e\nu/K(\pi) \to \mu\nu$ and $\tau \to K(\pi)\nu/K(\pi) \to \mu\nu$ drop out. This is also true in the 2HDM of type III (for $\epsilon^\ell_{ij} = 0$ with $i \neq j$) as long as the MFV-like relation $\epsilon^\ell_{22}/m_\mu = \epsilon^\ell_{11}/m_e$ is not violated.

1. $K \to e\nu/K \to \mu\nu$ and $\pi \to e\nu/\pi \to \mu\nu$

$K \to e\nu/K \to \mu\nu$ is a very precise test of lepton flavor universality [154] (see Table IV). Including NP entering via scalar operators modifies this ratio according to Eq. (58).

We find strong constraints on ϵ^ℓ_{i2} (which affect the coupling to the muon) and the constraints on ϵ^ℓ_{i1} (where the coupling of the electron is involved) are even more stringent. Like for $D_{(s)} \to \tau\nu$ and $D_{(s)} \to \mu\nu$ the constraints are much better for the real part of ϵ^ℓ_{ij} than the imaginary part. Note that these constraints are obtained assuming that only one element ϵ^ℓ_{ij} is nonzero. In the case $\epsilon^\ell_{22}/m_\mu = \epsilon^\ell_{11}/m_e$ where lepton flavor universality is restored no constraints can be obtained.

Alternatively, the ratio $\pi \to e\nu/\pi \to \mu\nu$ can test lepton flavor universality. We find that the constraints from $\pi \to e\nu/\pi \to \mu\nu$ are comparable with the ones from $K \to e\nu/K \to \mu\nu$. Our results are illustrated in Fig. 33.

2. $\tau \to K\nu/K \to \mu\nu$ and $\tau \to \pi\nu/\pi \to \mu\nu$

The ratios $\tau \to K\nu/K \to \mu\nu$ and $\tau \to \pi\nu/\pi \to \mu\nu$ are very similar to $K(\pi) \to e\nu/K(\pi) \to \mu\nu$: all dependencies on decay constants and CKM elements drop out and they are only sensitive to NP which violates lepton-flavor universality. The corresponding experimental and the theoretical values for these ratios are given in Table IV.

We find that the constraints on ϵ^ℓ_{i3} from $\tau \to \pi\nu/\pi \to \mu\nu$ are stronger than the ones from $\tau \to K\nu/K \to \mu\nu$ and they are shown in Fig. 34.

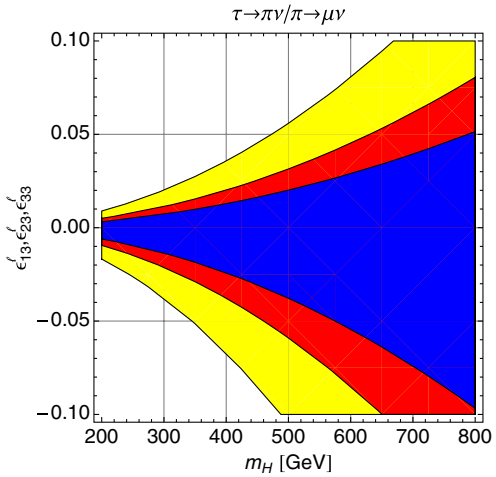

FIG. 34 (color online). Allowed regions in the $m_H - \epsilon^\ell_{i3}$ plane from $\tau \to \pi\nu/\pi \to \mu\nu$ for real values of ϵ^ℓ_{i3} and $\tan\beta = 30$ (yellow), $\tan\beta = 40$ (red), and $\tan\beta = 50$ (blue). The bounds on the imaginary parts are very weak.

VIII. UPPER LIMITS AND CORRELATION FOR LFV PROCESSES

In Sec. V we found that the neutral current lepton decays $\tau^- \to \mu^-\mu^+\mu^-$ and $\tau^- \to e^-\mu^+\mu^-$ give more stringent bounds on the elements $\epsilon^\ell_{32,23}$ and $\epsilon^\ell_{31,13}$ than the radiative decays $\tau \to \mu\gamma$ and $\tau \to e\gamma$. Also the LFV neutral meson decays $B_{s,d} \to \tau\mu$, $B_{s,d} \to \tau e$, $B_{s,d} \to \mu e$ cannot be arbitrarily large in the type-III 2HDM due to the constraints from $B_{s,d} \to \mu^+\mu^-$ and $\tau^- \to \mu^-\mu^+\mu^-$, $\tau^- \to e^-\mu^+\mu^-$, $\mu^- \to e^-e^+e^-$ (assuming again the absence of large cancellations).[13]

[13]See, e.g., Refs. [155–157] for an analysis of NP in $B_{s,d} \to \tau\mu$.

TABLE VI. Upper limits (90% C.L.) on the branching ratios of the lepton flavor-violating B meson decays.

Observables	$\mathcal{B}(B_s \to \mu e)$	$\mathcal{B}(B_d \to \mu e)$	$\mathcal{B}(B_d \to \tau\mu)$	$\mathcal{B}(B_d \to \tau e)$
Upper bounds	2.0×10^{-7} [161]	6.4×10^{-8} [161]	2.2×10^{-5} [162]	2.8×10^{-5} [162]

Therefore, in this section we study the upper limits on $B_{s,d} \to \tau\mu$, $B_{s,d} \to \tau e$, $B_{s,d} \to \mu e$ and the correlation among $\tau^- \to \mu^-\mu^+\mu^-$, $\tau^- \to e^-\mu^+\mu^-$, $\mu^- \to e^-e^+e^-$ and $\tau \to \mu\gamma$, $\tau \to e\gamma$, $\mu \to e\gamma$ in the type-III 2HDM.

A. Neutral meson decays: $B_{s,d} \to \tau\mu$, $B_{s,d} \to \tau e$ and $B_{s,d} \to \mu e$

In the SM (with massless neutrinos) the branching ratios for these decays vanish. Also in the 2HDM of type II these decays are not possible (even beyond tree level). In the type-III 2HDM, these decay modes are generated in the presence of flavor-violating terms ϵ^ℓ_{ij} and there exists even a tree-level neutral Higgs contribution to $B_s \to \ell_i^+\ell_j^-$ ($B_d \to \ell_i^+\ell_j^-$) if also $\epsilon^d_{23,32} \neq 0$ ($\epsilon^d_{13,31} \neq 0$).

In the large $\tan\beta$ limit, $v \ll m_H$ and neglecting the smaller lepton mass, the corresponding expressions for these branching ratios take the simple form

$$\mathcal{B}[B_q \to \ell_i^+\ell_j^-] \approx N^q_{ij}\left(\frac{\tan\beta/50}{m_H/500\ \text{GeV}}\right)^4 2[|\epsilon^\ell_{ji}|^2|\epsilon^d_{q3}|^2 + |\epsilon^\ell_{ij}|^2|\epsilon^d_{3q}|^2], \tag{70}$$

with $q = d, s$, $N^q_{ji} = N^q_{ij}$ and

$$\begin{aligned} N^s_{21} &\approx 2.1 \times 10^7 \frac{f_{B_s}}{0.229\ \text{GeV}}, \\ N^d_{21} &\approx 1.6 \times 10^7 \frac{f_{B_d}}{0.196\ \text{GeV}}, \\ N^s_{31,32} &\approx 1.7 \times 10^7 \frac{f_{B_s}}{0.229\ \text{GeV}}, \\ N^d_{31,32} &\approx 1.2 \times 10^7 \frac{f_{B_d}}{0.196\ \text{GeV}}. \end{aligned} \tag{71}$$

Note that the expressions for the branching ratios are not symmetric in ϵ^ℓ_{ij} and ϵ^ℓ_{ji}. Since experimentally both $B_q \to \ell_i^+\ell_j^-$ and $B_q \to \ell_i^-\ell_j^+$ are combined we compute the average

$$\mathcal{B}[B_q \to \ell_i\ell_j] = (\mathcal{B}[B_q \to \ell_i^+\ell_j^-] + \mathcal{B}[B_q \to \ell_j^+\ell_i^-])/2.$$

In order to obtain the upper limits we insert the biggest allowed values for Abs $[\epsilon^{d,\ell}_{ij}]$. For $\epsilon^d_{23,32}$ ($\epsilon^d_{13,31}$) we use the biggest allowed absolute value compatible with the bounds from $B_s \to \mu^+\mu^-$ ($B_d \to \mu^+\mu^-$). As we can see from Fig. 4 (Fig. 5) the absolute value for ϵ^d_{32} (ϵ^d_{31}) can be bigger than ϵ^d_{23} (ϵ^d_{13}). For the leptonic parameters $\epsilon^\ell_{13,31}$ and $\epsilon^\ell_{23,32}$ we use the constraints obtained from $\tau^- \to \mu^-\mu^+\mu^-$, $\tau^- \to e^-\mu^+\mu^-$ (see Sec. V C),

$$\begin{aligned} |\epsilon^\ell_{31,13}| &\leq 4.2 \times 10^{-3}\left(\frac{m_H/500\ \text{GeV}}{\tan\beta/50}\right)^2, \\ |\epsilon^\ell_{32,23}| &\leq 3.7 \times 10^{-3}\left(\frac{m_H/500\ \text{GeV}}{\tan\beta/50}\right)^2, \end{aligned} \tag{72}$$

while for $\epsilon^\ell_{12,21}$ we use the combined constraints from $\mu^- \to e^-e^+e^-$ and from $\mu \to e\gamma$ (see Sec. VI D).

Our results are shown in Fig. 35 (see Table VI for the current experimental limits). We see that for bigger Higgs masses larger values for the branching ratios are possible.

B. Radiative lepton decays: $\tau \to \mu\gamma$, $\tau \to e\gamma$ and $\mu \to e\gamma$

In Secs. V C and VI D we found that the radiative lepton decays $\tau \to \mu\gamma$ and $\tau \to e\gamma$ give less stringent bounds on the parameters $\epsilon^\ell_{23,32}$ and $\epsilon^\ell_{13,31}$ than the processes $\tau^- \to \mu^-\mu^+\mu^-$ and $\tau^- \to e^-\mu^+\mu^-$ while the constraints on $\epsilon^\ell_{12,21}$ from $\mu \to e\gamma$ are stronger than the ones from $\mu^- \to e^-e^+e^-$.

There are however interesting correlations between these decays in the type-III 2HDM. In the large $\tan\beta$ limit and for $v \ll m_H$ we obtain the following relation:

$$\frac{\mathcal{B}[\ell_i \to \ell_f\gamma]}{\mathcal{B}[\ell_i^- \to \ell_f^-\ell_j^+\ell_j^-]} = \frac{\alpha_{\text{em}}}{24\pi}\frac{|m_{\ell_i}/v - \epsilon^\ell_{ii}|^2}{|m_{\ell_j}/v - \epsilon^\ell_{jj}|^2}\frac{(|\epsilon^\ell_{if}|^2 + 4|\epsilon^\ell_{fi}|^2)}{(|\epsilon^\ell_{if}|^2 + |\epsilon^\ell_{fi}|^2)}. \tag{73}$$

As already noted in Sec. VI D, we stress that this formula is only a good approximation for very heavy Higgs due to the large logarithmic term in the expression for $\ell_i \to \ell_f\gamma$ [see Eq. (A21)]. Therefore, the relation in Eq. (73) gets modified for lighter Higgs masses as shown in Fig. 36. We see that, as expected, for very large Higgs masses the ratios approach

$$\begin{aligned} \frac{\mathcal{B}[\ell_i \to \ell_f\gamma]}{\mathcal{B}[\ell_i^- \to \ell_f^-\ell_j^+\ell_j^-]} &= \frac{\alpha_{\text{em}}}{24\pi}\frac{m^2_{\ell_i}}{m^2_{\ell_j}} \quad \text{for } \epsilon^\ell_{if} \neq 0, \\ \frac{\mathcal{B}[\ell_i \to \ell_f\gamma]}{\mathcal{B}[\ell_i^- \to \ell_f^-\ell_j^+\ell_j^-]} &= \frac{\alpha_{\text{em}}}{6\pi}\frac{m^2_{\ell_i}}{m^2_{\ell_j}} \quad \text{for } \epsilon^\ell_{fi} \neq 0, \end{aligned} \tag{74}$$

where, we assumed that $\epsilon^\ell_{jj}/\epsilon^\ell_{ii} = m_{\ell_j}/m_{\ell_i}$ and that only one flavor changing element ϵ^ℓ_{fi}, ϵ^ℓ_{if} is different from zero.

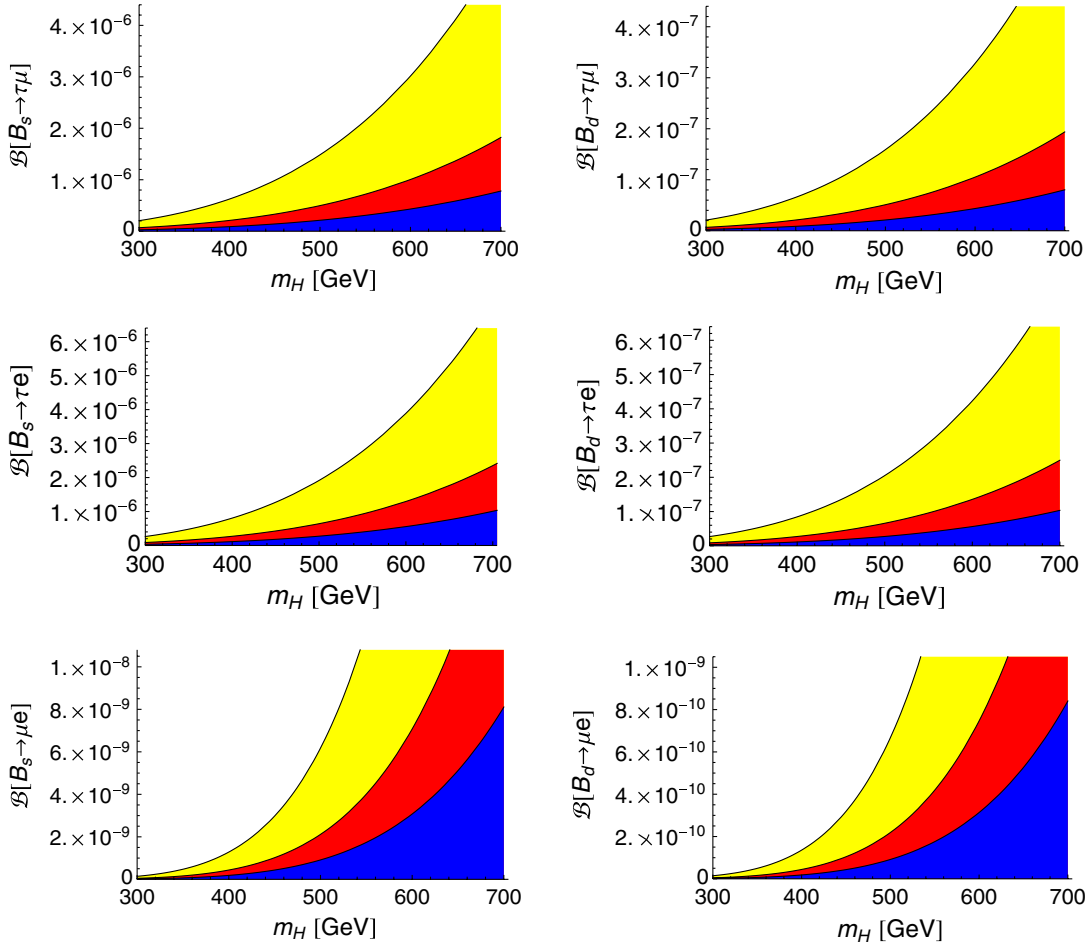

FIG. 35 (color online). Upper limits on the branching ratios of the lepton flavor violating B meson decays as a function of m_H for $\tan\beta = 30$ (yellow), $\tan\beta = 40$ (red) and $\tan\beta = 50$ (blue).

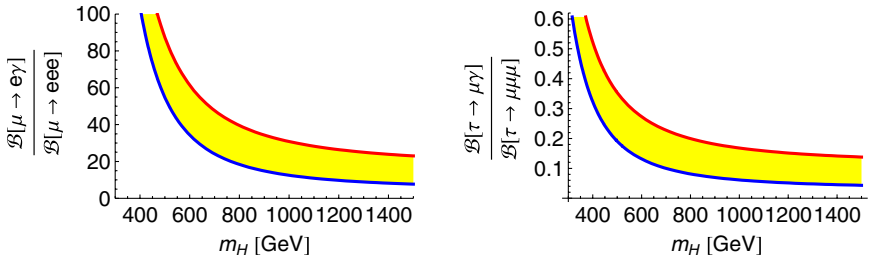

FIG. 36 (color online). Left: $\frac{\mathcal{B}[\mu\to e\gamma]}{\mathcal{B}[\mu^-\to e^-e^+e^-]}$ as a function of m_H assuming that only ϵ^ℓ_{12} (red) or ϵ^ℓ_{21} (blue) is different from zero for $\tan\beta = 50$. Right: $\frac{\mathcal{B}[\tau\to\mu\gamma]}{\mathcal{B}[\tau^-\to\mu^-\mu^+\mu^-]}$ as a function of m_H assuming that only ϵ^ℓ_{23} (red) or ϵ^ℓ_{32} (blue) is different from zero for $\tan\beta = 50$. For scenarios in which both ϵ^ℓ_{23} and ϵ^ℓ_{32} (ϵ^ℓ_{12} and ϵ^ℓ_{21}) are different from zero the 2HDM of type III predicts the ratio $\frac{\mathcal{B}[\tau\to\mu\gamma]}{\mathcal{B}[\tau^-\to\mu^-\mu^+\mu^-]}$ ($\frac{\mathcal{B}[\mu\to e\gamma]}{\mathcal{B}[\mu^-\to e^-e^+e^-]}$) to be within the yellow region. These ratios are to a good approximation independent of $\tan\beta$ for $\tan\beta \gtrsim 20$. The behavior of $\frac{\mathcal{B}[\tau\to e\gamma]}{\mathcal{B}[\tau^-\to e^-\mu^+\mu^-]}$ (not shown here) is very similar to the case of $3 \to 2$ transitions.

IX. CONCLUSIONS

In this article we studied in detail the flavor phenomenology of a 2HDM with general Yukawa couplings. Motivated by the fact that the 2HDM of type III is the decoupling limit of the MSSM we assumed a MSSM-like Higgs potential. In our analysis we proceeded in several steps:

(1) We gave order of magnitude constraints on the parameters $\epsilon^{q,\ell}_{ij}$ from 't Hooft's naturalness criterion and found that all couplings except $\epsilon^u_{i3,3i}$ and $\epsilon^u_{21,22}$ should be much smaller than one.

(2) Considering tree-level FCNC processes we constrained the elements ϵ^d_{ij} $(i \neq j)$ and $\epsilon^u_{12,21}$ from

neutral meson decays to muons and from $\Delta F = 2$ processes, finding that they are tiny for the values of m_H and $\tan\beta$ under investigation (assuming $\epsilon^{\ell}_{ij} = 0$). In the lepton sector the absolute values of all flavor off-diagonal elements ϵ^{ℓ}_{ij} were constrained from $\tau^- \to \mu^-\mu^+\mu^-$, $\tau^- \to e^-\mu^+\mu^-$ and $\mu^- \to e^-e^+e^-$ to be very small.

(3) After having found that the off-diagonal elements ϵ^{d}_{ij} must be very small due to constraints from tree-level contributions to FCNC processes we considered charged Higgs contributions to $K - \bar{K}$, $B_s - \bar{B}_s$, $B_d - \bar{B}_d$ mixing and $b \to s(d)\gamma$ arising at the one-loop level. In these contributions the so far unconstrained elements $\epsilon^{u}_{i3,3i}$ (and also ϵ^{u}_{22}) enter for the first time and we found that, setting $\epsilon^{d}_{ij} = 0$ (with $i \neq j$), $\epsilon^{u}_{13,23}$ should be rather small. Furthermore, the electric dipole moment of the neutron and of the charged leptons constrain ϵ^{u}_{11}, ϵ^{u}_{22}, ϵ^{u}_{21}, ϵ^{u}_{31} and ϵ^{ℓ}_{ij}, respectively. Respecting all other constraints, no sizable effect in a_μ is possible.

(4) Keeping in mind the constraints from the previous steps, we considered the possible effects in charged current processes. Here we found that tests for lepton flavor universality constrain the differences $\epsilon^{\ell}_{ii}/m_{\ell_i} - \epsilon^{\ell}_{jj}/m_{\ell_j}$. Most importantly, the unconstrained elements ϵ^{u}_{31} and ϵ^{u}_{32} enter the processes $B \to \tau\nu$ and $B \to D^{(*)}\tau\nu$ directly (without CKM suppression) and can remove the tension between experiment and theory prediction observed in the SM simultaneously.

(5) Finally we gave upper limits on the lepton flavor violating neutral B meson decays in the 2HDM of type III and correlated the radiative lepton decays to $\tau^- \to \mu^-\mu^+\mu^-$, $\tau^- \to e^-\mu^+\mu^-$ and $\mu^- \to e^-e^+e^-$.

In Tables VII and VIII we list all processes which have been under consideration and quote the constraints placed on the parameters $\epsilon^{q,\ell}_{ij}$ for our benchmark point $m_H = 500$ GeV and $\tan\beta = 50$.

In summary, combining the constraints from Tables VII and VIII the following bounds on the absolute values of the parameters ϵ^{q}_{ij} and ϵ^{ℓ}_{ij} (for our benchmark point with $m_H = 500$ GeV and $\tan\beta = 50$) are obtained:

TABLE VII. Results obtained in the type-III 2HDM from various processes for $\tan\beta = 50$ and $m_H = 500$ GeV.

Observable	Results
Neutral meson decays to muons	
$B_s \to \mu^+\mu^-$	$\lvert\epsilon^{d}_{32}\rvert \le 3.0 \times 10^{-5}$, $\lvert\epsilon^{d}_{23}\rvert \le 1.9 \times 10^{-5}$, $\lvert\epsilon^{\ell}_{22}\rvert \le 2.0 \times 10^{-3}$
$B_d \to \mu^+\mu^-$	$\lvert\epsilon^{d}_{31}\rvert \le 1.1 \times 10^{-5}$, $\lvert\epsilon^{d}_{13}\rvert \le 9.4 \times 10^{-6}$
$K_L \to \mu^+\mu^-$	$\lvert\epsilon^{d}_{21}\rvert \le 1.6 \times 10^{-6}$, $\lvert\epsilon^{d}_{12}\rvert \le 1.6 \times 10^{-6}$
$\bar{D}^0 \to \mu^+\mu^-$	$\lvert\epsilon^{u}_{21}\rvert \le 3.0 \times 10^{-2}$, $\lvert\epsilon^{u}_{12}\rvert \le 3.0 \times 10^{-2}$
$\Delta F = 2$ processes	
$B_s - \bar{B}_s$ mixing	$\lvert\epsilon^{d}_{23}\epsilon^{d\star}_{32}\rvert \le 9.2 \times 10^{-10}$, $\lvert\epsilon^{u}_{23}\rvert \le 0.18$, $\lvert\epsilon^{u}_{32}\rvert \le 1.7$, $\lvert\epsilon^{u}_{33}\rvert \le 0.7$
$B_d - \bar{B}_d$ mixing	$\lvert\epsilon^{d}_{13}\epsilon^{d\star}_{31}\rvert \le 3.9 \times 10^{-11}$, $\lvert\epsilon^{u}_{23}\rvert \le 0.2$, $\lvert\epsilon^{u}_{13}\rvert \le 0.04$, $\lvert\epsilon^{u}_{31}\rvert \le 1.9$
$K - \bar{K}$ mixing	$\lvert\epsilon^{d}_{12}\epsilon^{d\star}_{21}\rvert \le 1.0 \times 10^{-12}$, $\lvert\epsilon^{u}_{22}\rvert \le 0.25$, $\lvert\epsilon^{u}_{23}\rvert \le 0.14$
$D - \bar{D}$ mixing	$\lvert\epsilon^{u}_{12}\epsilon^{u\star}_{21}\rvert \le 2.0 \times 10^{-8}$, $\lvert\epsilon^{u}_{32}\epsilon^{u\star}_{31}\rvert \le 0.02$
Radiative B decays	
$b \to s\gamma$	$\lvert\epsilon^{u}_{23}\rvert \le 0.024$, $\lvert\epsilon^{u}_{33}\rvert \le 0.55$
$b \to d\gamma$	$\lvert\epsilon^{u}_{13}\rvert \le 7.0 \times 10^{-3}$
Radiative lepton decays	
$\mu \to e\gamma$	$\lvert\epsilon^{\ell}_{12}\rvert \le 1.7 \times 10^{-4}$, $\lvert\epsilon^{\ell}_{21}\rvert \le 2.2 \times 10^{-4}$, $55 \le \frac{\mathcal{B}[\mu\to e\gamma]}{\mathcal{B}[\mu^-\to e^-e^+e^-]} \le 86$
$\tau \to e\gamma$	$0.19 \le \frac{\mathcal{B}[\tau\to e\gamma]}{\mathcal{B}[\tau^-\to e^-\mu^+\mu^-]} \le 0.35$
$\tau \to \mu\gamma$	$0.19 \le \frac{\mathcal{B}[\tau\to \mu\gamma]}{\mathcal{B}[\tau^-\to \mu^-\mu^+\mu^-]} \le 0.35$
Neural current lepton decays	
$\mu^- \to e^-e^+e^-$	$\lvert\epsilon^{\ell}_{12,21}\rvert \le 2.3 \times 10^{-3}$
$\tau^- \to e^-\mu^+\mu^-$	$\lvert\epsilon^{\ell}_{13,31}\rvert \le 4.2 \times 10^{-3}$
$\tau^- \to \mu^-\mu^+\mu^-$	$\lvert\epsilon^{\ell}_{23,32}\rvert \le 3.7 \times 10^{-3}$

TABLE VIII. Results obtained in the type-III 2HDM from various processes for $\tan\beta = 50$ and $m_H = 500$ GeV.

Observable	Results
Charged current processes	
$B \to \tau\nu$	$2.7 \times 10^{-3} \le \lvert\epsilon^{u}_{31}\rvert \le 2.0 \times 10^{-2}$, $\lvert\epsilon^{\ell}_{i3}\rvert \le 6.0 \times 10^{-2}$
$B \to D\tau\nu$ & $B \to D^\star\tau\nu$	$0.43 \le \lvert\epsilon^{u}_{32}\rvert \le 0.74$
$D_s \to \tau\nu$ & $D_{(s)} \to \mu\nu$	$\lvert\mathrm{Re}[\epsilon^{u}_{22}]\rvert \le 0.2$
$D \to \tau\nu$	…
$K \to \mu(e)\nu/\pi \to \mu(e)\nu$	$\lvert\mathrm{Re}[\epsilon^{d}_{22}]\rvert \le 1.0 \times 10^{-3}$
$K(\pi) \to e\nu/K(\pi) \to \mu\nu$	$\lvert\mathrm{Re}[\epsilon^{\ell}_{i1}]\rvert \le 2.0 \times 10^{-6}$, $\lvert\mathrm{Re}[\epsilon^{\ell}_{i2}]\rvert \le 5.0 \times 10^{-4}$
$\tau \to K(\pi)\nu/K(\pi) \to \mu\nu$	$-4.0 \times 10^{-2} \le \mathrm{Re}[\epsilon^{\ell}_{i3}] \le 2.0 \times 10^{-2}$
$\tau \to K\nu/\tau \to \pi\nu$	$\lvert\epsilon^{\ell}_{i3}\rvert \le 0.14$
EDMs and anomalous magnetic moments	
d_e	$\lvert\mathrm{Im}[\epsilon^{\ell}_{12}\epsilon^{\ell}_{21}]\rvert \le 2.5 \times 10^{-8}$, $\lvert\mathrm{Im}[\epsilon^{\ell}_{13}\epsilon^{\ell}_{31}]\rvert \le 2.5 \times 10^{-9}$
d_μ	…
d_τ	…
d_n	$\lvert\mathrm{Im}[\epsilon^{u}_{11}]\rvert \le 2.2 \times 10^{-2}$, $\lvert\mathrm{Im}[\epsilon^{u}_{22}]\rvert \le 1.1 \times 10^{-1}$, $\mathrm{Arg}[\epsilon^{u}_{31}] = \mathrm{Arg}[V_{ub}] \pm \pi$
a_μ	Deviation from the SM cannot be explained
LVF B meson decays	
$B_s \to \tau\mu$	$\mathcal{B}[B_s \to \tau\mu] \le 2.0 \times 10^{-7}$
$B_s \to \mu e$	$\mathcal{B}[B_s \to \mu e] \le 9.2 \times 10^{-10}$
$B_s \to \tau e$	$\mathcal{B}[B_s \to \tau e] \le 2.8 \times 10^{-7}$
$B_d \to \tau\mu$	$\mathcal{B}[B_d \to \tau\mu] \le 2.1 \times 10^{-8}$
$B_d \to \mu e$	$\mathcal{B}[B_d \to \mu e] \le 9.2 \times 10^{-11}$
$B_d \to \tau e$	$\mathcal{B}[B_d \to \tau e] \le 2.8 \times 10^{-8}$

$$|\epsilon^u_{ij}| \leq \begin{pmatrix} 3.4\times10^{-4} & 3.0\times10^{-2} & 7.0\times10^{-3} \\ 3.0\times10^{-2} & 1.4\times10^{-1} & 2.4\times10^{-2} \\ 2.0\times10^{-2} & 7.4\times10^{-1} & 5.5\times10^{-1} \end{pmatrix}_{ij}$$
$$|\epsilon^d_{ij}| \leq \begin{pmatrix} 1.3\times10^{-4} & 1.6\times10^{-6} & 9.4\times10^{-6} \\ 1.6\times10^{-6} & 2.6\times10^{-4} & 2.0\times10^{-5} \\ 1.1\times10^{-5} & 3.0\times10^{-5} & 1.4\times10^{-2} \end{pmatrix}_{ij}$$
$$|\epsilon^\ell_{ij}| \leq \begin{pmatrix} 2.9\times10^{-6} & 1.7\times10^{-4} & 4.2\times10^{-3} \\ 2.2\times10^{-4} & 6.1\times10^{-4} & 3.7\times10^{-3} \\ 4.2\times10^{-3} & 3.7\times10^{-3} & 1.0\times10^{-2} \end{pmatrix}_{ij}. \quad (75)$$

These bounds hold in the absence of large cancellations between different contributions. Note that in Eq. (75) we applied the naturalness bounds in case they were stronger than the experimental limits.

It is interesting that $B \to \tau\nu$, $B \to D\tau\nu$ and $B \to D^*\tau\nu$ can be explained simultaneously in the 2HDM of type III without violating bounds from other observables and without significant fine-tuning. It remains to be seen if these tensions with the SM remain when updated experimental results and improved theory predictions will be available in the future. In order to further test the model and constrain the parameters ϵ^u_{32} (ϵ^u_{31}) we propose to study $H^0, A^0 \to \bar{t}c$ ($H^0, A^0 \to \bar{t}u$) at the LHC.

ACKNOWLEDGMENTS

This work is supported by the Swiss National Science Foundation. We thank Jernej Kamenik and Ulrich Nierste for collaboration in the early stages of this work. A. C. also thanks Jernej Kamenik for useful comments on the manuscript.

APPENDIX

In this Appendix, we collect the Wilson coefficients (to the relevant precision at the matching scale) which are needed for the calculation of $b \to s(d)\gamma$, $\Delta F = 2$ processes (i.e., neutral meson mixing), leptonic neutral meson decays ($\Delta F = 1$ processes), $B \to \tau\nu$, $B \to D\tau\nu$, $B \to D^*\tau\nu$, $D_{(s)} \to \ell\nu_\ell$, $K(\pi) \to \ell\nu_\ell$, $\tau \to K(\pi)\nu$, LFV radiative lepton transitions, EDMs of charged leptons and neutron, as well as the AMM of the muon. In addition, we give general expressions for some branching ratios, the explicit form of the loop functions entering our results and summarize the input parameters used in our analysis in tabular form.

1. Loop functions

We give the explicit form of the loop functions entering our results. In the limit of vanishing external momentum the one- and two-point Passarino Veltman functions [158] are defined as

$$A_0(m^2) = \frac{16\pi^2}{i}\mu^{4-d}\int\frac{d^dk}{(2\pi)^d}\frac{1}{(k^2-m^2)},$$
$$B_0(m_1^2,m_2^2) = \frac{16\pi^2}{i}\mu^{4-d}\int\frac{d^dk}{(2\pi)^d}\frac{1}{(k^2-m_1^2)(k^2-m_2^2)}, \quad (A1)$$

where μ is the renormalization scale.

The loop functions C_0 (three-point) and D_0 (four-point) are defined in analogy to B_0, but with three and four propagators, respectively. Evaluating these loop functions yields (with $d = 4 - 2\varepsilon$)

$$A_0(m^2) = m^2\left[1 + \frac{1}{\varepsilon} - \gamma_E + \ln(4\pi) + \ln\left(\frac{\mu^2}{m^2}\right)\right] + O(\varepsilon),$$
$$B_0(m_1^2,m_2^2) = 1 + \frac{1}{\varepsilon} - \gamma_E + \ln(4\pi) + \frac{m_1^2\ln(\frac{\mu^2}{m_1^2}) - m_2^2\ln(\frac{\mu^2}{m_2^2})}{m_1^2-m_2^2} + O(\varepsilon), \quad (A2)$$

$$C_0(m_1^2,m_2^2,m_3^2) = \frac{B_0(m_1^2,m_2^2)-B_0(m_1^2,m_3^2)}{m_2^2-m_3^2} = \frac{m_1^2m_2^2\ln(\frac{m_1^2}{m_2^2}) + m_3^2m_2^2\ln(\frac{m_2^2}{m_3^2}) + m_3^2m_1^2\ln(\frac{m_3^2}{m_1^2})}{(m_1^2-m_2^2)(m_3^2-m_1^2)(m_2^2-m_3^2)},$$
$$D_0(m_1^2,m_2^2,m_3^2,m_4^2) = \frac{C_0(m_1^2,m_2^2,m_3^2)-C_0(m_1^2,m_2^2,m_4^2)}{m_3^2-m_4^2}. \quad (A3)$$

Here, the one- and the two-point loop functions A_0, B_0 are UV divergent and ε is the UV regulator.

At various places also the functions C_2 and D_2 appear, which have, compared to C_0 and D_0, an additional factor k^2 in the numerator of the integrand. These functions read

$$C_2(m_1^2,m_2^2,m_3^2) = B_0(m_1^2,m_2^2) + m_3^2C_0(m_1^2,m_2^2,m_3^2),$$
$$D_2(m_1^2,m_2^2,m_3^2,m_4^2) = C_0(m_1^2,m_2^2,m_3^2) + m_4^2D_0(m_1^2,m_2^2,m_3^2,m_4^2). \quad (A4)$$

2. Radiative $b \to s(d)\gamma$ decays

Concerning new physics contributions to $b \to s(d)\gamma$, we work in leading logarithmic precision in this paper. As mentioned before, we use these processes to constrain certain elements ϵ^u_{ij}. For this purpose, we put the ϵ^d_{ij} couplings (which are already constrained to be very small) to zero. When also neglecting the mass of the strange quark and further neglecting operators with mass dimension higher than six, we obtain the same effective Hamiltonian as in the SM, reading for $b \to s\gamma$ (see, e.g., Ref. [47]):

$$\mathcal{H}_{\rm eff}^{b\to s\gamma} = -\frac{4G_F}{\sqrt{2}} V_{tb}V_{ts}^\star \sum_i C_i O_i. \tag{A5}$$

For $b \to d\gamma$ the CKM structure is slightly more complicated (see, e.g., Ref. [109]). In our approximation only the Wilson coefficients C_7 and C_8 of the operators

$$\begin{aligned} O_7 &= \frac{e}{16\pi^2} m_b \bar{s}\sigma^{\mu\nu} P_R b F_{\mu\nu}; \\ O_8 &= \frac{g_s}{16\pi^2} m_b \bar{s}\sigma^{\mu\nu} T^a P_R b G^a_{\mu\nu} \end{aligned} \tag{A6}$$

get new physics contributions. They are induced through charged Higgs bosons propagating in the loop (neutral Higgs boson exchange leads to power suppressed contributions which we neglect). For $b \to s\gamma$ the new physics contributions read (with $y_j = m^2_{u_j}/m^2_{H^+}$ and $\lambda_t = V_{tb}V_{ts}^\star$)

$$\begin{aligned} C_7^{\rm NP} &= \frac{v^2}{\lambda_t}\frac{1}{m_b}\sum_{j=1}^3 \Gamma^{RLH^\pm}_{u_j d_2} \star \Gamma^{LRH^\pm}_{u_j d_3} \frac{C^0_{7,XY}(y_j)}{m_{u_j}} \\ &\quad + \frac{v^2}{\lambda_t}\sum_{j=1}^3 \Gamma^{RLH^\pm}_{u_j d_2} \star \Gamma^{RLH^\pm}_{u_j d_3} \frac{C^0_{7,YY}(y_j)}{m^2_{u_j}}, \\ C_8^{\rm NP} &= \frac{v^2}{\lambda_t}\frac{1}{m_b}\sum_{j=1}^3 \Gamma^{RLH^\pm}_{u_j d_2} \star \Gamma^{LRH^\pm}_{u_j d_3} \frac{C^0_{8,XY}(y_j)}{m_{u_j}} \\ &\quad + \frac{v^2}{\lambda_t}\sum_{j=1}^3 \Gamma^{RLH^\pm}_{u_j d_2} \star \Gamma^{RLH^\pm}_{u_j d_3} \frac{C^0_{8,YY}(y_j)}{m^2_{u_j}}, \end{aligned} \tag{A7}$$

while for $b \to d\gamma$ the label d_2 and $\lambda_t = V_{tb}V_{ts}^\star$ have to be replaced by d_1 and $\lambda_t = V_{tb}V_{td}^\star$, respectively. The functions $C^0_{7,XY}$, $C^0_{7,YY}$, $C^0_{8,XY}$ and $C^0_{8,YY}$ were introduced in Ref. [47]; their explicit form reads

$$\begin{aligned} C^0_{7,XY}(y_j) &= \frac{y_j}{12}\left[\frac{-5y_j^2 + 8y_j - 3 + (6y_j - 4)\ln y_j}{(y_j-1)^3}\right], \\ C^0_{8,XY}(y_j) &= \frac{y_j}{4}\left[\frac{-y_j^2 + 4y_j - 3 - 2\ln y_j}{(y_j-1)^3}\right], \\ C^0_{7,YY}(y_j) &= \frac{y_j}{72}\left[\frac{-8y_j^3 + 3y_j^2 + 12y_j - 7 + (18y_j^2 - 12y_j)\ln y_j}{(y_j-1)^4}\right], \\ C^0_{8,YY}(y_j) &= \frac{y_j}{24}\left[\frac{-y_j^3 + 6y_j^2 - 3y_j - 2 - 6y_j \ln y_j}{(y_j-1)^4}\right]. \end{aligned} \tag{A8}$$

In Eq. (A7) we retained the contributions from internal up- and charm-quarks, although these contributions are subleading.

3. Wilson coefficients for $\Delta F = 2$ processes

The extended Higgs sector of our 2HDM of type-III also leads to extra contributions to $\Delta F = 2$ processes (B_s, B_d, Kaon and D mixing) which can be matched onto the effective Hamiltonian

$$\mathcal{H}_{\rm eff}^{\Delta F=2} = \sum_{j=1}^5 C_j O_j + \sum_{j=1}^3 C'_j O'_j + \text{H.c.}, \tag{A9}$$

where the operators read in the case of B_s mixing

$$\begin{aligned} &O_1 = (\bar{s}_\alpha \gamma^\mu P_L b_\alpha)(\bar{s}_\beta \gamma^\mu P_L b_\beta), \quad O_2 = (\bar{s}_\alpha P_L b_\alpha)(\bar{s}_\beta P_L b_\beta), \\ &O_3 = (\bar{s}_\alpha P_L b_\beta)(\bar{s}_\beta P_L b_\alpha), \quad O_4 = (\bar{s}_\alpha P_L b_\alpha)(\bar{s}_\beta P_R b_\beta), \\ &O_5 = (\bar{s}_\alpha P_L b_\beta)(\bar{s}_\beta P_R b_\alpha). \end{aligned} \tag{A10}$$

α and β are color indices and the primed operators can be obtained from $O_{1,2,3}$ by interchanging L and R. Similarly, the corresponding operator bases for B_d, Kaon and D mixing follow from Eq. (A10) through simple adjustment of the indices.

In the following subsections we present the contributions to these Wilson coefficients arising from: (1) one-loop box diagrams with charged Higgs boson exchange; (2) tree-level contributions induced by neutral Higgs boson exchange; and (3) box diagrams involving neutral Higgs bosons, relevant in the case of D mixing.

a. Charged Higgs box contributions

For definiteness, let us consider B_s mixing. The corresponding Wilson coefficients for B_d and Kaon mixing follow by a simple adjustment of the indices. We have performed our calculation in a general R_ξ gauge. The nonvanishing Wilson coefficients from pure charged Higgs boxes are given by

$$
\begin{aligned}
C_1 &= \frac{-1}{128\pi^2}\sum_{j,k=1}^{3}\Gamma^{RL\,H^\pm}_{u_j d_2}{}^{\star}\Gamma^{RL\,H^\pm}_{u_j d_3}\Gamma^{RL\,H^\pm}_{u_k d_2}{}^{\star}\Gamma^{RL\,H^\pm}_{u_k d_3} D_2(m^2_{u_j}, m^2_{u_k}, m^2_{H^\pm}, m^2_{H^\pm}),\\
C_2 &= \frac{-1}{32\pi^2}\sum_{j,k=1}^{3} m_{u_j} m_{u_k}\Gamma^{LR\,H^\pm}_{u_j d_2}{}^{\star}\Gamma^{RL\,H^\pm}_{u_j d_3}\Gamma^{LR\,H^\pm}_{u_k d_2}{}^{\star}\Gamma^{RL\,H^\pm}_{u_k d_3} D_0(m^2_{u_j}, m^2_{u_k}, m^2_{H^\pm}, m^2_{H^\pm}),\\
C_4 &= \frac{-1}{16\pi^2}\sum_{j,k=1}^{3} m_{u_j} m_{u_k}\Gamma^{LR\,H^\pm}_{u_j d_2}{}^{\star}\Gamma^{RL\,H^\pm}_{u_j d_3}\Gamma^{RL\,H^\pm}_{u_k d_2}{}^{\star}\Gamma^{LR\,H^\pm}_{u_k d_3} D_0(m^2_{u_j}, m^2_{u_k}, m^2_{H^\pm}, m^2_{H^\pm}),\\
C_5 &= \frac{1}{32\pi^2}\sum_{j,k=1}^{3}\Gamma^{LR\,H^\pm}_{u_j d_2}{}^{\star}\Gamma^{LR\,H^\pm}_{u_j d_3}\Gamma^{RL\,H^\pm}_{u_k d_2}{}^{\star}\Gamma^{RL\,H^\pm}_{u_k d_3} D_2(m^2_{u_j}, m^2_{u_k}, m^2_{H^\pm}, m^2_{H^\pm}).
\end{aligned}
\tag{A11}
$$

The sum of the charged Higgs-$W^\pm$ and charged Higgs-Goldstone-boson boxes is given by

$$
\begin{aligned}
C_1 &= \frac{g_2^2}{32\pi^2}\sum_{j,k=1}^{3}\left(m_{u_j} m_{u_k} V^{\star}_{j2} V_{k3}\Gamma^{RL\,H^\pm}_{u_j d_3}\Gamma^{RL\,H^\pm}_{u_k d_2}{}^{\star}\frac{4M_W^2 D_0(M_W^2, m^2_{H^\pm}, m^2_{u_j}, m^2_{u_k}) - D_2(M_W^2, m^2_{H^\pm}, m^2_{u_j}, m^2_{u_k})}{4M_W^2}\right),\\
C_4 &= \frac{1}{16\pi^2}\frac{g_2^2}{2}\sum_{j,k=1}^{3}\left(V_{j3} V^{\star}_{k2}\Gamma^{LR\,H^\pm}_{u_j d_2}{}^{\star}\Gamma^{LR\,H^\pm}_{u_k d_3}\frac{C_2(\xi M_W^2, m^2_{H^+}, m^2_{u_j}) - C_2(m^2_{H^+}, m^2_{u_j}, m^2_{u_k}) + m^2_{u_k} C_0(\xi M_W^2, m^2_{H^\pm}, m^2_{u_k})}{M_W^2}\right).
\end{aligned}
\tag{A12}
$$

We stress here that we want to use B_s mixing only to constrain certain ϵ^u_{ij} couplings, because the ϵ^d_{ij} quantities are already constrained to be very small. We therefore only took systematically into account those contributions to the Wilson coefficients which stay different from zero in the limit $\epsilon^d_{ij} \to 0$. At first sight, the Wilson coefficient C_4 seems to be gauge dependent. However, when using the unitarity of the CKM matrix (entering the expression for C_4 both, explicitly and implicitly through the Γ quantities), we find that the ξ-dependent terms are always proportional to an element ϵ^d_{ij}, which we put to zero in our analysis. Also note that our result agrees with the one of Ref. [159]. The only difference is that we neglected gauge dependent terms corresponding to higher dimensional operators. The Wilson coefficients of the primed operators can be obtained by interchanging L and R in the corresponding unprimed ones.

b. Tree-level H^0_k contribution

The Wilson coefficients from neutral Higgs mediated tree-level contributions to B_s mixing read

$$
C_2^{H^0_k} = \sum_{k=1}^{3}\frac{-1}{2m^2_{H^0_k}}(\Gamma^{LR\,H^0_k}_{d_3 d_2}{}^{\star})^2, \qquad C_2^{\prime H^0_k} = \sum_{k=1}^{3}\frac{-1}{2m^2_{H^0_k}}(\Gamma^{LR\,H^0_k}_{d_2 d_3})^2, \qquad C_4^{H^0_k} = \sum_{k=1}^{3}\frac{-1}{m^2_{H^0_k}}\Gamma^{LR\,H^0_k}_{d_2 d_3}\Gamma^{LR\,H^0_k}_{d_3 d_2}{}^{\star}.
\tag{A13}
$$

The corresponding coefficients for B_d, Kaon and D mixing follow by a careful adjustment of the indices.

Note that in the limit of large $\tan\beta$ and $m_A \gg v$, $C_2^{H^0_k}$ and $C_2^{\prime H^0_k}$ vanish and we only get a contribution to $C_4^{H^0_k}$.

c. Neutral Higgs box contribution to D mixing

The Wilson coefficients resulting from the neutral Higgs box contribution to D mixing are given as

$$
\begin{aligned}
C_1 &= \frac{-1}{128\pi^2}\sum_{j_1,j_2=1}^{3}\sum_{k_1,k_2=1}^{3}\Gamma^{LR\,H^0_{k_1}}_{u_2 u_{j_1}}{}^{\star}\Gamma^{LR\,H^0_{k_2}}_{u_1 u_{j_1}}\Gamma^{LR\,H^0_{k_2}}_{u_2 u_{j_2}}{}^{\star}\Gamma^{LR\,H^0_{k_1}}_{u_1 u_{j_2}} D_2(m^2_{u_{j_1}}, m^2_{u_{j_2}}, m^2_{H^0_{k_1}}, m^2_{H^0_{k_2}}),\\
C_2 &= \frac{-1}{32\pi^2}\sum_{j_1,j_2=1}^{3}\sum_{k_1,k_2=1}^{3} m_{u_{j_1}} m_{u_{j_2}}\Gamma^{LR\,H^0_{k_1}}_{u_{j_1} u_1}{}^{\star}\Gamma^{LR\,H^0_{k_2}}_{u_2 u_{j_1}}{}^{\star}\Gamma^{LR\,H^0_{k_1}}_{u_{j_2} u_1}{}^{\star}\Gamma^{LR\,H^0_{k_2}}_{u_2 u_{j_2}}{}^{\star} D_0(m^2_{u_{j_1}}, m^2_{u_{j_2}}, m^2_{H^0_{k_1}}, m^2_{H^0_{k_2}}),\\
C_3 &= 0,\\
C_4 &= \frac{-1}{16\pi^2}\sum_{j_1,j_2=1}^{3}\sum_{k_1,k_2=1}^{3} m_{u_{j_1}} m_{u_{j_2}}\Gamma^{LR\,H^0_{k_1}}_{u_{j_1} u_1}{}^{\star}\Gamma^{LR\,H^0_{k_2}}_{u_2 u_{j_1}}{}^{\star}\Gamma^{LR\,H^0_{k_2}}_{u_{j_2} u_2}\Gamma^{LR\,H^0_{k_1}}_{u_1 u_{j_2}} D_0(m^2_{u_{j_1}}, m^2_{u_{j_2}}, m^2_{H^0_{k_1}}, m^2_{H^0_{k_2}}),\\
C_5 &= \frac{-1}{128\pi^2}\sum_{j_1,j_2=1}^{3}\sum_{k_1,k_2=1}^{3}\Gamma^{LR\,H^0_{k_1}}_{u_{j_1} u_1}{}^{\star}\Gamma^{LR\,H^0_{k_2}}_{u_{j_1} u_2}\Gamma^{LR\,H^0_{k_1}}_{u_1 u_{j_2}}\Gamma^{LR\,H^0_{k_2}}_{u_2 u_{j_2}}{}^{\star} D_2(m^2_{u_{j_1}}, m^2_{u_{j_2}}, m^2_{H^0_{k_1}}, m^2_{H^0_{k_2}}).
\end{aligned}
\tag{A14}
$$

The indices j_1, j_2 describe the internal up-type quarks while k_1, k_2 stand for neutral Higgs indices (H^0, h^0, A^0). Moreover, the primed Wilson coefficients can be obtained from above by the replacement $L \leftrightarrow R$ in the couplings.

4. Semileptonic and leptonic meson decays and tau decays: $B \to (D^{(*)})\tau\nu$, $D_{(s)} \to \ell\nu_\ell$, $K(\pi) \to \ell\nu_\ell$ and $\tau \to K(\pi)\nu$ processes

These processes are governed by the effective Hamiltonian

$$\mathcal{H}_{\text{eff}} = C_{\text{SM}}^{u_f d_i,\ell_j} O_{\text{SM}}^{u_f d_i,\ell_j} + C_L^{u_f d_i,\ell_j} O_L^{u_f d_i,\ell_j} + C_R^{u_f d_i,\ell_j} O_R^{u_f d_i,\ell_j} + \text{H.c.}, \tag{A15}$$

with the operators defined as

$$\begin{aligned} O_{\text{SM}}^{u_f d_i,\ell_j} &= \bar{u}_f \gamma_\mu P_L d_i \bar{\ell}_j \gamma_\mu P_L \nu, \\ O_R^{u_f d_i,\ell_j} &= \bar{u}_f P_R d_i \bar{\ell}_j P_L \nu, \\ O_L^{u_f d_i,\ell_j} &= \bar{u}_f P_L d_i \bar{\ell}_j P_L \nu. \end{aligned} \tag{A16}$$

Here, for tauonic B meson decays $\ell_j = \tau$, $d_i = b$ and $u_f = u$ ($u_f = c$) for $B \to \tau\nu$ ($B \to D\tau\nu$ and $B \to D^*\tau\nu$). For $D_s \to \ell_j\nu$ ($D \to \ell_j\nu$), $u_f = c$ and $d_i = s$ (d), for $\tau \to K(\pi)\nu$, $\ell_j = \tau$, $u_f = u$ and $d_i = s$ (d) and for $K(\pi) \to \ell_j\nu$ we have $\ell_j = \mu$, e, $u_f = u$ and $d_i = s$ (d). The Wilson coefficients in 2HDM of type III at the matching scale read

$$C_{\text{SM}}^{u_f d_i,\ell_j} = \frac{4G_F}{\sqrt{2}} V_{u_f d_i}, \qquad C_R^{u_f d_i,\ell_j} = \frac{-1}{m_{H^\pm}^2} \Gamma_{u_f d_i}^{LRH^\pm} \Gamma_{\nu\ell_j}^{LR\,H^\pm\star},$$
$$C_L^{u_f d_i,\ell_j} = \frac{-1}{m_{H^\pm}^2} \Gamma_{u_f d_i}^{RL\,H^\pm} \Gamma_{\nu\ell_j}^{LR\,H^\pm\star}. \tag{A17}$$

5. Lepton flavor violation (LFV): $\ell_i \to \ell_f\gamma$ processes

The radiative lepton decays $\ell_i \to \ell_f\gamma$ ($\ell = e$, μ or τ) are induced by one-loop penguin diagrams with internal neutral or charged Higgs bosons. The result for the one-loop decay amplitude can be written as a tree-level matrix element of the effective Hamiltonian

$$\mathcal{H}_{\text{eff}} = c_R^{\ell_f\ell_i} O_R^{\ell_f\ell_i} + c_L^{\ell_f\ell_i} O_L^{\ell_f\ell_i}, \tag{A18}$$

where $c_R^{\ell_f\ell_i}$ and $c_L^{\ell_f\ell_i}$ are the effective Wilson coefficients of the magnetic dipole operators

$$O_{R(L)}^{\ell_f\ell_i} = m_{\ell_i} \bar{\ell}_f \sigma_{\mu\nu} P_{R(L)} \ell_i F^{\mu\nu}. \tag{A19}$$

With these conventions, the branching ratio for the radiative lepton decays $\ell_i \to \ell_f\gamma$ reads

$$\mathcal{B}[\ell_i \to \ell_f\gamma] = \frac{m_{\ell_i}^5}{4\pi\Gamma_{\ell_i}} (|c_R^{\ell_f\ell_i}|^2 + |c_L^{\ell_f\ell_i}|^2). \tag{A20}$$

The neutral Higgs ($H_k^0 = H^0, h^0, A^0$) penguin contribution to $c_R^{\ell_f\ell_i}$ is given by

$$c_{RH_k^0}^{\ell_f\ell_i} = \sum_{k,j=1}^{3} \frac{-e}{192\pi^2 m_{H_k^0}^2} \Big[\Gamma_{\ell_f\ell_j}^{LR\,H_k^0} \Gamma_{\ell_i\ell_j}^{LR\,H_k^0\star} + \frac{m_{\ell_f}}{m_{\ell_i}} \Gamma_{\ell_j\ell_f}^{LR\,H_k^0\star} \Gamma_{\ell_j\ell_i}^{LR\,H_k^0} - \frac{m_{\ell_j}}{m_{\ell_i}} \Gamma_{\ell_f\ell_j}^{LR\,H_k^0} \Gamma_{\ell_j\ell_i}^{LR\,H_k^0} \left(9 + 6\ln\left(\frac{m_{\ell_j}^2}{m_{H_k^0}^2}\right)\right) \Big], \tag{A21}$$

and $c_L^{\ell_f\ell_i}$ can be obtained from $c_R^{\ell_f\ell_i}$ by interchanging L and R. Similarly, for the charged Higgs penguin contributions we find

$$\begin{aligned} c_{L\;H^\pm}^{\ell_f\ell_i} &= \frac{e}{384\pi^2 m_{H^\pm}^2} \sum_{j=1}^{3} \Gamma_{\nu_j\ell_i}^{LR\,H^\pm} \Gamma_{\nu_j\ell_f}^{LR\,H^\pm\star}, \\ c_{R\;H^\pm}^{\ell_f\ell_i} &= \frac{m_{\ell_f}}{m_{\ell_i}} \frac{e}{384\pi^2 m_{H^\pm}^2} \sum_{j=1}^{3} \Gamma_{\nu_j\ell_i}^{LR\,H^\pm} \Gamma_{\nu_j\ell_f}^{LR\,H^\pm\star}. \end{aligned} \tag{A22}$$

6. Wilson coefficients for EDMs and the anomalous magnetic moment of the muon

a. Wilson coefficients for EDMs of charged leptons and the anomalous magnetic moment of the muon

As in the case of the LFV processes discussed in the previous section, we again have both neutral and charged Higgs penguin contributions to the flavor conserving radiative transitions $\ell_i \to \ell_i\gamma$. The corresponding effective Hamiltonian is obtained from Eqs. (A18) and (A19) by identifying ℓ_f with ℓ_i. The contribution to the effective Wilson coefficients related to neutral Higgs bosons (propagating in the loop) reads

$$c_{R\;H_k^0}^{\ell_i\ell_i} = \sum_{k,j=1}^{3} \frac{-e}{192\pi^2 m_{H_k^0}^2} \Big[\Gamma_{\ell_i\ell_j}^{LR\,H_k^0\star} \Gamma_{\ell_i\ell_j}^{LR\,H_k^0} + \Gamma_{\ell_j\ell_i}^{LR\,H_k^0\star} \Gamma_{\ell_j\ell_i}^{LR\,H_k^0} - \frac{m_{\ell_j}}{m_{\ell_i}} \Gamma_{\ell_i\ell_j}^{LR\,H_k^0} \Gamma_{\ell_j\ell_i}^{LR\,H_k^0} \left(9 + 6\ln\left(\frac{m_{\ell_j}^2}{m_{H_k^0}^2}\right)\right) \Big], \tag{A23}$$

$$c_{L\;H_k^0}^{\ell_i\ell_i} = c_{R\;H_k^0}^{\ell_i\ell_i\star}, \tag{A24}$$

while the charged Higgs penguin contribution leads to the (real) coefficients

$$c_{L\;H^\pm}^{\ell_i\ell_i} = c_{R\;H^\pm}^{\ell_i\ell_i} = \frac{e}{384\pi^2 m_{H^\pm}^2} \sum_{j=1}^{3} \Gamma_{\nu_j\ell_i}^{LR\,H^\pm} \Gamma_{\nu_j\ell_i}^{LR\,H^\pm\star}. \tag{A25}$$

b. Wilson coefficients for neutron EDM

In this section we consider the transitions $d \to d\gamma(g)$ and $u \to u\gamma(g)$ (denoted by $d_d^{(g)}$ and $d_u^{(g)}$) which are the building blocks for the electric dipole moment d_n of the neutron. As we are only interested in a rough estimate of

d_n, we do not include QCD corrections to these building blocks. In this approximation the latter can be described by the effective Hamiltonian

$$\begin{aligned}\mathcal{H}_{\text{eff}}^{dd,uu} &= c_R^{dd} m_d \bar{d}\sigma_{\mu\nu} P_R d F^{\mu\nu} + c_L^{dd} m_d \bar{d}\sigma_{\mu\nu} P_L d F^{\mu\nu} \\ &+ c_{R,g}^{dd} m_d \bar{d}\sigma_{\mu\nu} P_R T^a d G^{a,\mu\nu} \\ &+ c_{L,g}^{dd} m_d \bar{d}\sigma_{\mu\nu} P_L T^a d G^{a,\mu\nu} + (d \to u). \end{aligned} \tag{A26}$$

The effective Wilson coefficients $c_{R,L}^{dd,uu}$ and $c_{R,L,g}^{dd,uu}$ again receive neutral and charged Higgs contributions. The neutral contributions of the Wilson coefficients (involved in $d_d^{(g)}$) read

$$\begin{aligned} c_R^{dd,H_k^0} = \sum_{k,j=1}^{3} \frac{eQ_d}{192\pi^2 m_{H_k^0}^2} \Bigg[& \Gamma_{dd_j}^{LR\,H_k^0 \star} \Gamma_{dd_j}^{LR\,H_k^0} + \Gamma_{d_j d}^{LR\,H_k^0 \star} \Gamma_{d_j d}^{LR\,H_k^0} \\ & - \frac{m_{d_j}}{m_d} \Gamma_{dd_j}^{LR\,H_k^0} \Gamma_{d_j d}^{LR\,H_k^0} \left(9 + 6 \ln\left(\frac{m_{d_j}^2}{m_{H_k^0}^2} \right) \right) \Bigg], \end{aligned} \tag{A27}$$

$$\begin{aligned} c_{R,g}^{dd,H_k^0} = \sum_{k,j=1}^{3} \frac{g_s}{192\pi^2 m_{H_k^0}^2} \Bigg[& \Gamma_{dd_j}^{LR\,H_k^0 \star} \Gamma_{dd_j}^{LR\,H_k^0} + \Gamma_{d_j d}^{LR\,H_k^0 \star} \Gamma_{d_j d}^{LR\,H_k^0} \\ & - \frac{m_{d_j}}{m_d} \Gamma_{dd_j}^{LR\,H_k^0} \Gamma_{d_j d}^{LR\,H_k^0} \left(9 + 6 \ln\left(\frac{m_{d_j}^2}{m_{H_k^0}^2} \right) \right) \Bigg], \end{aligned} \tag{A28}$$

and $c_{L,(g)}^{dd,H_k^0} = c_{R,(g)}^{dd,H_k^0 \star}$. The charged Higgs penguin contributions to the Wilson coefficients (involved in $d_d^{(g)}$) read

$$\begin{aligned} c_R^{dd,H^\pm} = \sum_{j=1}^{3} \frac{-e}{16\pi^2 m_{u_j}^2} \Bigg[& \Gamma_{du_j}^{LR\,H^\pm \star} \Gamma_{du_j}^{LR\,H^\pm} C_{7,YY}^0 \left(\frac{m_{u_j}^2}{m_{H^+}^2} \right) \\ & + \Gamma_{u_j d}^{LR\,H^\pm \star} \Gamma_{u_j d}^{LR\,H^\pm} C_{7,YY}^0 \left(\frac{m_{u_j}^2}{m_{H^+}^2} \right) \\ & + \Gamma_{du_j}^{LR\,H^\pm} \Gamma_{u_j d}^{LR\,H^\pm} \frac{m_{u_j}}{m_d} C_{7,XY}^0 \left(\frac{m_{u_j}^2}{m_{H^+}^2} \right) \Bigg], \end{aligned} \tag{A29}$$

$$\begin{aligned} c_{R,g}^{dd,H^\pm} = \sum_{j=1}^{3} \frac{-g_s}{16\pi^2 m_{u_j}^2} \Bigg[& \Gamma_{du_j}^{LR\,H^\pm \star} \Gamma_{du_j}^{LR\,H^\pm} C_{8,YY}^0 \left(\frac{m_{u_j}^2}{m_{H^+}^2} \right) \\ & + \Gamma_{u_j d}^{LR\,H^\pm \star} \Gamma_{u_j d}^{LR\,H^\pm} C_{8,YY}^0 \left(\frac{m_{u_j}^2}{m_{H^+}^2} \right) \\ & + \Gamma_{du_j}^{LR\,H^\pm} \Gamma_{u_j d}^{LR\,H^\pm} \frac{m_{u_j}}{m_d} C_{8,XY}^0 \left(\frac{m_{u_j}^2}{m_{H^+}^2} \right) \Bigg], \end{aligned} \tag{A30}$$

and $c_{L,(g)}^{dd,H^\pm} = c_{R,(g)}^{dd,H^\pm \star}$.

The analogous expressions for $c_{R,(g)}^{uu,H^\pm,H_k^0}$, which are involved in the expressions of $d_u^{(g)}$ are given as

$$\begin{aligned} c_R^{uu,H_k^0} = \sum_{j,k=1}^{3} \frac{-eQ_u}{16\pi^2 m_{u_j}^2} \Bigg[& \Gamma_{uu_j}^{LR\,H_k^0 \star} \Gamma_{uu_j}^{LR\,H_k^0} C_{8,YY}^0 \left(\frac{m_{u_j}^2}{m_{H_k^0}^2} \right) \\ & + \Gamma_{u_j u}^{LR\,H_k^0 \star} \Gamma_{u_j u}^{LR\,H_k^0} C_{8,YY}^0 \left(\frac{m_{u_j}^2}{m_{H_k^0}^2} \right) \\ & + \Gamma_{uu_j}^{LR\,H_k^0} \Gamma_{u_j u}^{LR\,H_k^0} \frac{m_{u_j}}{m_u} C_{8,XY}^0 \left(\frac{m_{u_j}^2}{m_{H_k^0}^2} \right) \Bigg], \end{aligned} \tag{A31}$$

$$\begin{aligned} c_{R,g}^{uu,H_k^0} = \sum_{j,k=1}^{3} \frac{-g_s}{16\pi^2 m_{u_j}^2} \Bigg[& \Gamma_{uu_j}^{LR\,H_k^0 \star} \Gamma_{uu_j}^{LR\,H_k^0} C_{8,YY}^0 \left(\frac{m_{u_j}^2}{m_{H_k^0}^2} \right) \\ & + \Gamma_{u_j u}^{LR\,H_k^0 \star} \Gamma_{u_j u}^{LR\,H_k^0} C_{8,YY}^0 \left(\frac{m_{u_j}^2}{m_{H_k^0}^2} \right) \\ & + \Gamma_{uu_j}^{LR\,H_k^0} \Gamma_{u_j u}^{LR\,H_k^0} \frac{m_{u_j}}{m_u} C_{8,XY}^0 \left(\frac{m_{u_j}^2}{m_{H_k^0}^2} \right) \Bigg], \end{aligned} \tag{A32}$$

$$\begin{aligned} c_R^{uu,H^\pm} = \sum_{j=1}^{3} \frac{-e}{1152\pi^2 m_{H^+}^2} \Bigg[& 5\Gamma_{ud_j}^{LR\,H^\pm \star} \Gamma_{ud_j}^{LR\,H^\pm} \\ & + 5\Gamma_{d_j u}^{LR\,H^\pm \star} \Gamma_{d_j u}^{LR\,H^\pm} - \Gamma_{ud_j}^{LR\,H^\pm} \Gamma_{d_j u}^{LR\,H^\pm} \\ & \times \frac{m_{d_j}}{m_u} 12 \ln\left(\frac{m_{d_j}^2}{m_{H^+}^2} \right) \Bigg], \end{aligned} \tag{A33}$$

$$\begin{aligned} c_{R,g}^{uu,H^\pm} = \sum_{j=1}^{3} \frac{g_s}{192\pi^2 m_{H^+}^2} \Bigg[& \Gamma_{ud_j}^{LR\,H^\pm \star} \Gamma_{ud_j}^{LR\,H^\pm} \\ & + \Gamma_{d_j u}^{LR\,H^\pm \star} \Gamma_{d_j u}^{LR\,H^\pm} - \Gamma_{ud_j}^{LR\,H^\pm} \Gamma_{d_j u}^{LR\,H^\pm} \\ & \times \frac{m_{d_j}}{m_u} \left(9 + 6 \ln\left(\frac{m_{d_j}^2}{m_{H^+}^2} \right) \right) \Bigg]. \end{aligned} \tag{A34}$$

Again, we have $c_{L,(g)}^{uu,H_k^0} = c_{R,(g)}^{uu,H_k^0 \star}$ and $c_{L,(g)}^{uu,H^\pm} = c_{R,(g)}^{uu,H^\pm \star}$. The loop functions $C_{7,8,XY,YY}^0(y_j)$ are given in Eq. (A8).

7. Leptonic decays of neutral mesons

The effective Hamiltonian $\mathcal{H}_{\text{eff}}$ which includes the full set of operators for the general decays $PS(\bar{q}_f q_i) \to \ell_A^+ \ell_B^-$ (PS refers to the pseudoscalar meson) reads

$$\mathcal{H}_{\text{eff}}^{\Delta F=1} = -\frac{G_F^2 M_W^2}{\pi^2} [C_V^{q_f q_i} O_V^{q_f q_i} + C_A^{q_f q_i} O_A^{q_f q_i} + C_S^{q_f q_i} O_S^{q_f q_i} + C_P^{q_f q_i} O_P^{q_f q_i} + \text{primed}] + \text{H.c.}, \tag{A35}$$

where the operators (together with their primed counterparts) are defined as

$$\begin{aligned}
\mathcal{O}_V^{q_f q_i} &= (\bar{q}_f \gamma_\mu P_L q_i)(\bar{\ell}_B \gamma^\mu \ell_A), & \mathcal{O}_A^{q_f q_i} &= (\bar{q}_f \gamma_\mu P_L q_i)(\bar{\ell}_B \gamma^\mu \gamma_5 \ell_A),\\
\mathcal{O}_V^{\prime q_f q_i} &= (\bar{q}_f \gamma_\mu P_R q_i)(\bar{\ell}_B \gamma^\mu \ell_A), & \mathcal{O}_A^{\prime q_f q_i} &= (\bar{q}_f \gamma_\mu P_R q_i)(\bar{\ell}_B \gamma^\mu \gamma_5 \ell_A),\\
\mathcal{O}_S^{q_f q_i} &= (\bar{q}_f P_L q_i)(\bar{\ell}_B \ell_A), & \mathcal{O}_P^{q_f q_i} &= (\bar{q}_f P_L q_i)(\bar{\ell}_B \gamma_5 \ell_A),\\
\mathcal{O}_S^{\prime q_f q_i} &= (\bar{q}_f P_R q_i)(\bar{\ell}_B \ell_A), & \mathcal{O}_P^{\prime q_f q_i} &= (\bar{q}_f P_R q_i)(\bar{\ell}_B \gamma_5 \ell_A).
\end{aligned} \tag{A36}$$

Making use of the hadronic matrix elements

$$\langle 0|\bar{q}_f \gamma_\mu \gamma_5 q_i|PS\rangle = i f_{PS} p_{PS}^\mu, \qquad \langle 0|\bar{q}_f \gamma_5 q_i|PS\rangle = -i f_{PS} \frac{M_{PS}^2}{(m_{q_f} + m_{q_i})}, \tag{A37}$$

one obtains the branching ratio

$$\begin{aligned}
\mathcal{B}[PS(\bar{q}_f q_i) \to \ell_A^+ \ell_B^-] = \frac{G_F^4 M_W^4}{32\pi^5} f(x_A^2, x_B^2) M_{PS} f_{PS}^2 (m_{l_A} + m_{l_B})^2 \tau_{PS} \Bigg\{ \Bigg| \frac{M_{PS}^2 (C_P^{q_f q_i} - C_P^{\prime q_f q_i})}{(m_{q_f} + m_{q_i})(m_{l_A} + m_{l_B})} - (C_A^{q_f q_i} - C_A^{\prime q_f q_i}) \Bigg|^2 \\
\times [1 - (x_A - x_B)^2] + \Bigg| \frac{M_{PS}^2 (C_S^{q_f q_i} - C_S^{\prime q_f q_i})}{(m_{q_f} + m_{q_i})(m_{l_A} + m_{l_B})} + \frac{(m_{l_A} - m_{l_B})}{(m_{l_A} + m_{l_B})} (C_V^{q_f q_i} - C_V^{\prime q_f q_i}) \Bigg|^2 \\
\times [1 - (x_A + x_B)^2] \Bigg\},
\end{aligned} \tag{A38}$$

where the function $f(x_i, x_j)$ and the ratio x_i are defined as [160]

$$f(x_i, x_j) = \sqrt{1 - 2(x_i + x_j) + (x_i - x_j)^2}, \qquad x_i = \frac{m_{\ell_i}}{M_{PS}}.$$

a. Wilson coefficients

(i) Tree-level neutral Higgs contributions to $PS(\bar{q}_f q_i) \to \ell_A^+ \ell_B^-$ in the 2HDM of type III

(ii) The nonvanishing Wilson coefficients of the operators in Eq. (A35) induced through tree-level neutral Higgs ($H_k^0 = H^0, h^0, A^0$) exchange read

$$\begin{aligned}
C_S^{q_f q_i} &= \frac{\pi^2}{2G_F^2 M_W^2} \sum_{k=1}^{3} \frac{1}{m_{H_k^0}^2} (\Gamma_{\ell_B \ell_A}^{LR\,H_k^0} + \Gamma_{\ell_B \ell_A}^{RL\,H_k^0}) \Gamma_{q_f q_i}^{RL\,H_k^0},\\
C_P^{q_f q_i} &= \frac{\pi^2}{2G_F^2 M_W^2} \sum_{k=1}^{3} \frac{1}{m_{H_k^0}^2} (\Gamma_{\ell_B \ell_A}^{LR\,H_k^0} - \Gamma_{\ell_B \ell_A}^{RL\,H_k^0}) \Gamma_{q_f q_i}^{RL\,H_k^0},\\
C_S^{\prime q_f q_i} &= \frac{\pi^2}{2G_F^2 M_W^2} \sum_{k=1}^{3} \frac{1}{m_{H_k^0}^2} (\Gamma_{\ell_B \ell_A}^{LR\,H_k^0} + \Gamma_{\ell_B \ell_A}^{RL\,H_k^0}) \Gamma_{q_f q_i}^{LR\,H_k^0},\\
C_P^{\prime q_f q_i} &= \frac{\pi^2}{2G_F^2 M_W^2} \sum_{k=1}^{3} \frac{1}{m_{H_k^0}^2} (\Gamma_{\ell_B \ell_A}^{LR\,H_k^0} - \Gamma_{\ell_B \ell_A}^{RL\,H_k^0}) \Gamma_{q_f q_i}^{LR\,H_k^0}.
\end{aligned} \tag{A39}$$

(iii) Loop-induced charged Higgs contributions to $B_s \to \mu^+ \mu^-$ in the 2HDM of type II.

As mentioned earlier, we also include in our analysis the 2HDM of type-II loop-induced charged Higgs contributions to $B_s \to \mu^+ \mu^-$ from Ref. [52]:

$$C_S^{bs} = C_P^{bs} = -\frac{m_b V_{tb}^* V_{ts}}{2} \frac{m_\mu}{2M_W^2} \tan^2\beta \frac{\log(m_H^2/m_t^2)}{m_H^2/m_t^2 - 1}, \tag{A40}$$

where m_b and m_t are understood to be running masses evaluated at the matching scale.

8. Flavor-changing lepton decays

The general expressions for the branching ratios of $\tau^- \to e^- \mu^+ \mu^-$ and $\tau^- \to \mu^- \mu^+ \mu^-$ have the form

$$\mathcal{B}[\tau^- \to e^- \mu^+ \mu^-] = \frac{m_\tau^5}{12(8\pi)^3\Gamma_\tau}\left(\left|\frac{\Gamma_{\tau e}^{LRH_k^0\star}\Gamma_{\mu\mu}^{LRH_k^0}}{m_{H_k^0}^2}\right|^2 + \left|\frac{\Gamma_{e\tau}^{LRH_k^0\star}\Gamma_{\mu\mu}^{LRH_k^0}}{m_{H_k^0}^2}\right|^2 + \left|\frac{\Gamma_{\tau e}^{LRH_k^0}\Gamma_{\mu\mu}^{LRH_k^0}}{m_{H_k^0}^2}\right|^2 + \left|\frac{\Gamma_{e\tau}^{LRH_k^0}\Gamma_{\mu\mu}^{LRH_k^0}}{m_{H_k^0}^2}\right|^2\right),$$

$$\mathcal{B}[\tau^- \to \mu^- \mu^+ \mu^-] = \frac{m_\tau^5}{12(8\pi)^3\Gamma_\tau}\frac{1}{2}\left(2\left|\frac{\Gamma_{\tau\mu}^{LR\,H_k^0\star}\Gamma_{\mu\mu}^{LRH_k^0}}{m_{H_k^0}^2}\right|^2 + 2\left|\frac{\Gamma_{\mu\tau}^{LR\,H_k^0\star}\Gamma_{\mu\mu}^{LR\,H_k^0}}{m_{H_k^0}^2}\right|^2 + \left|\frac{\Gamma_{\tau\mu}^{LR\,H_k^0}\Gamma_{\mu\mu}^{LR\,H_k^0}}{m_{H_k^0}^2}\right|^2 + \left|\frac{\Gamma_{\mu\tau}^{LR\,H_k^0}\Gamma_{\mu\mu}^{LR\,H_k^0}}{m_{H_k^0}^2}\right|^2\right). \tag{A41}$$

Note that the (not explicitly denoted) sum over the Higgses must be performed before taking the various absolute values in Eq. (A41).

9. Input parameters

In this section we list our input parameters in Tables IX and X.

TABLE IX. Top: Input values for the quark masses used in our article. In the numerical analysis, we used the NNLO expressions in α_s for the running (see for example Ref. [163]) in order to obtain the quark-mass values at higher scales. Bottom: Electroweak parameters and the strong coupling constant used in our analysis. Concerning the running of α_s we used NNLO expressions (given for example in Ref. [70]).

Parameter	Value (GeV)
$\bar{m}_u$ (2 GeV)	0.00219 ± 0.00015 [94]
$\bar{m}_d$ (2 GeV)	0.00467 ± 0.00020 [94]
$\bar{m}_s$ (2 GeV)	0.095 ± 0.006 [94]
$\bar{m}_c(m_c)$	1.28 ± 0.04 [164]
$\bar{m}_b(m_b)$	4.243 ± 0.043 [103]
$\bar{m}_t(m_t)$	$165.80 \pm 0.54 \pm 0.72$ [14]

Parameter	Value
M_W	80.40 GeV
M_Z	91.19 GeV
$\alpha_s(M_Z)$	0.119
G_F	1.16637×10^{-5} GeV^{-2}
α_{em}^{-1}	137
v	174.10 GeV

TABLE X. Top: Values for decay constants of Ref. [14] obtained by averaging the lattice results of Refs. [80–93]. Bottom: Meson masses according to the particle data group (see online update of Ref. [70]).

Parameter	Value
f_{B_s}/f_B	$1.221 \pm 0.010 \pm 0.033$ [14]
f_D	218.9 ± 11.3 MeV [80]
f_{D_s}	$249 \pm 2 \pm 5$ MeV [14]
f_{D_s}/f_D	1.188 ± 0.025 [80]
f_K	$156.3 \pm 0.3 \pm 1.9$ MeV [14]
f_K/f_π	1.193 ± 0.005 [94]

Meson masses	Values (GeV)
$m_{B^\pm(B^0)}$	5.279
m_{B_s}	5.367
$m_{D^\pm(D^0)}$	1.870 (1.865)
m_{D_s}	1.969
$m_{K^\pm(K^0)}$	0.494 (0.498)
$m_{\pi^\pm(\pi^0)}$	0.140 (0.135)

[1] T. Lee, Phys. Rev. D **8**, 1226 (1973).
[2] J. F. Gunion, H. E. Haber, G. L. Kane, and S. Dawson, Front. Phys. **80**, 1 (2000).
[3] G. Branco, P. Ferreira, L. Lavoura, M. Rebelo, M. Sher, and J. P. Silva, Phys. Rep. **516**, 1 (2012).
[4] J. E. Kim, Phys. Rep. **150**, 1 (1987).
[5] R. Peccei and H. R. Quinn, Phys. Rev. Lett. **38**, 1440 (1977).
[6] M. Trodden, arXiv:hep-ph/9805252.
[7] H. E. Haber and G. L. Kane, Phys. Rep. **117**, 75 (1985).
[8] B. Aubert *et al.*, Phys. Rev. Lett. **109**, 101802 (2012).
[9] J. Lees *et al.*, arXiv:1303.0571.
[10] J. Lees *et al.*, arXiv:1207.0698.
[11] B. Aubert *et al.*, Phys. Rev. D **81**, 051101 (2010).
[12] K. Hara *et al.*, Phys. Rev. D **82**, 071101 (2010).
[13] I. Adachi *et al.*, Phys. Rev. Lett. **110**, 131801 (2013).
[14] J. Charles, A. Höcker, H. Lacker, S. Laplace, F. R. Diberder, J. Malclés, J. Ocariz, M. Pivk, and L. Roos, Eur. Phys. J. C **41**, 1 (2005).
[15] G. D'Ambrosio, G. F. Giudice, G. Isidori, and A. Strumia, Nucl. Phys. **B645**, 155 (2002).
[16] A. Crivellin, C. Greub, and A. Kokulu, Phys. Rev. D **86**, 054014 (2012).
[17] A. J. Buras, M. V. Carlucci, S. Gori, and G. Isidori, J. High Energy Phys. 10 (2010) 009.
[18] G. Blankenburg and G. Isidori, Eur. Phys. J. Plus **127**, 85 (2012).
[19] C. Hamzaoui, M. Pospelov, and M. Toharia, Phys. Rev. D **59**, 095005 (1999).
[20] K. S. Babu and C. F. Kolda, Phys. Rev. Lett. **84**, 228 (2000).
[21] M. S. Carena, D. Garcia, U. Nierste, and C. E. Wagner, Nucl. Phys. **B577**, 88 (2000).
[22] G. Isidori and A. Retico, J. High Energy Phys. 11 (2001) 001.
[23] A. J. Buras, P. H. Chankowski, J. Rosiek, and L. Slawianowska, Nucl. Phys. **B659**, 3 (2003).
[24] L. Hofer, U. Nierste, and D. Scherer, J. High Energy Phys. 10 (2009) 081.
[25] G. Isidori and A. Retico, J. High Energy Phys. 09 (2002) 063.
[26] A. Crivellin, Phys. Rev. D **83**, 056001 (2011).
[27] D. Noth and M. Spira, J. High Energy Phys. 06 (2011) 084.
[28] A. Crivellin and C. Greub, Phys. Rev. D **87**, 015013 (2013).
[29] Y. Okada, M. Yamaguchi, and T. Yanagida, Prog. Theor. Phys. **85**, 1 (1991).
[30] H. E. Haber and R. Hempfling, Phys. Rev. Lett. **66**, 1815 (1991).
[31] J. R. Ellis, G. Ridolfi, and F. Zwirner, Phys. Lett. B **257**, 83 (1991).
[32] A. Brignole, Phys. Lett. B **277**, 313 (1992).
[33] P. H. Chankowski, S. Pokorski, and J. Rosiek, Nucl. Phys. **B423**, 437 (1994).
[34] A. Dabelstein, Z. Phys. C **67**, 495 (1995).
[35] A. Pilaftsis and C. E. Wagner, Nucl. Phys. **B553**, 3 (1999).
[36] M. S. Carena, J. R. Ellis, A. Pilaftsis, and C. Wagner, Nucl. Phys. **B586**, 92 (2000).
[37] A. Freitas, E. Gasser, and U. Haisch, Phys. Rev. D **76**, 014016 (2007).
[38] M. Gorbahn, S. Jager, U. Nierste, and S. Trine, Phys. Rev. D **84**, 034030 (2011).
[39] A. Crivellin, L. Hofer, and J. Rosiek, J. High Energy Phys. 07 (2011) 017.
[40] J. Rosiek, Phys. Rev. D **41**, 3464 (1990).
[41] S. L. Glashow and S. Weinberg, Phys. Rev. D **15**, 1958 (1977).
[42] T. Miki *et al.*, arXiv:hep-ph/0210051.
[43] A. W. E. Kaffas, P. Osland, and O. M. Ogreid, Phys. Rev. D **76**, 095001 (2007).
[44] O. Deschamps, S. Descotes-Genon, S. Monteil, V. Niess, S. T'Jampens, and V. Tisserand, Phys. Rev. D **82**, 073012 (2010).
[45] S. Bertolini, F. Borzumati, A. Masiero, and G. Ridolfi, Nucl. Phys. **B353**, 591 (1991).
[46] M. Ciuchini, G. Degrassi, P. Gambino, and G. Giudice, Nucl. Phys. **B527**, 21 (1998).
[47] F. Borzumati and C. Greub, Phys. Rev. D **58**, 074004 (1998).
[48] M. Misiak, H. Asatrian, K. Bieri, M. Czakon, A. Czarnecki *et al.*, Phys. Rev. Lett. **98**, 022002 (2007).
[49] T. Hermann, M. Misiak, and M. Steinhauser, J. High Energy Phys. 11 (2012) 036.
[50] X. He, T. Nguyen, and R. Volkas, Phys. Rev. D **38**, 814 (1988).
[51] W. Skiba and J. Kalinowski, Nucl. Phys. **B404**, 3 (1993).
[52] H. E. Logan and U. Nierste, Nucl. Phys. **B586**, 39 (2000).
[53] W.-S. Hou, Phys. Rev. D **48**, 2342 (1993).
[54] A. Akeroyd and S. Recksiegel, J. Phys. G **29**, 2311 (2003).
[55] S. Fajfer, J. F. Kamenik, and I. Nisandzic, Phys. Rev. D **85**, 094025 (2012).
[56] M. Tanaka, Z. Phys. C **67**, 321 (1995).
[57] U. Nierste, S. Trine, and S. Westhoff, Phys. Rev. D **78**, 015006 (2008).
[58] A. Akeroyd, Prog. Theor. Phys. **111**, 295 (2004).
[59] A. Akeroyd and C. H. Chen, Phys. Rev. D **75**, 075004 (2007).
[60] A. Akeroyd and F. Mahmoudi, J. High Energy Phys. 04 (2009) 121.
[61] M. Antonelli *et al.*, Nucl. Phys. B, Proc. Suppl. **181–182**, 83 (2008).
[62] M. Baak, M. Goebel, J. Haller, A. Hoecker, D. Ludwig *et al.*, Eur. Phys. J. C **72**, 2003 (2012).
[63] A. Pich and P. Tuzon, Phys. Rev. D **80**, 091702 (2009).
[64] M. Jung, A. Pich, and P. Tuzon, J. High Energy Phys. 11 (2010) 003.
[65] F. Mahmoudi and O. Stal, Phys. Rev. D **81**, 035016 (2010).
[66] E. Iltan, Phys. Rev. D **64**, 013013 (2001).
[67] T. Cheng and M. Sher, Phys. Rev. D **35**, 3484 (1987).
[68] R. Aaij *et al.*, Phys. Rev. Lett. **110**, 021801 (2013).
[69] G. Isidori and R. Unterdorfer, J. High Energy Phys. 01 (2004) 009.
[70] J. Beringer *et al.*, Phys. Rev. D **86**, 010001 (2012).
[71] A. J. Buras, J. Girrbach, D. Guadagnoli, and G. Isidori, Eur. Phys. J. C **72**, 2172 (2012).
[72] T. Inami and C. Lim, Prog. Theor. Phys. **65**, 297 (1981).
[73] M. Ciuchini, E. Franco, V. Lubicz, G. Martinelli, I. Scimemi, and L. Silvestrini, Nucl. Phys. **B523**, 501 (1998).
[74] A. J. Buras, M. Misiak, and J. Urban, Nucl. Phys. **B586**, 397 (2000).
[75] M. Bona *et al.*, J. High Energy Phys. 03 (2008) 049.

[76] D. Becirevic, M. Ciuchini, E. Franco, V. Gimenez, G. Martinelli, A. Masiero, M. Papinutto, J. Reyes, and L. Silvestrini, Nucl. Phys. **B634**, 105 (2002).
[77] M. Ciuchini, V. Lubicz, L. Conti, A. Vladikas, A. Donini *et al.*, J. High Energy Phys. 10 (1998) 008.
[78] V. Lubicz and C. Tarantino, Nuovo Cimento Soc. Ital. Fis. **123B**, 674 (2008).
[79] D. Becirevic, V. Gimenez, G. Martinelli, M. Papinutto, and J. Reyes, Nucl. Phys. B, Proc. Suppl. **106–107**, 385 (2002).
[80] A. Bazavov *et al.*, Phys. Rev. D **85**, 114506 (2012).
[81] B. Blossier *et al.*, J. High Energy Phys. 07 (2009) 043.
[82] C. Bernard, C. E. DeTar, L. Levkova, S. Gottlieb, U. Heller *et al.*, Proc. Sci., LAT2007 (2007) 090 [arXiv:0710.1118].
[83] E. Follana, C. Davies, G. Lepage, and J. Shigemitsu, Phys. Rev. Lett. **100**, 062002 (2008).
[84] C. Aubin, J. Laiho, and R. S. Van de Water, Proc. Sci., LATTICE2008 (2008) 105 [arXiv:0810.4328].
[85] S. Beane, P. Bedaque, K. Orginos, and M. Savage, Phys. Rev. D **75**, 094501 (2007).
[86] S. Durr, Z. Fodor, C. Hoelbling, S. Katz, S. Krieg, T. Kurth, L. Lellouch, T. Lippert, A. Ramos, and K. K. Szabó, Phys. Rev. D **81**, 054507 (2010).
[87] C. Bernard, S. Datta, T. DeGrand, C. DeTar, S. Gottlieb, U. Heller, C. McNeile, K. Orginos, R. Sugar, and D. Toussaint, Phys. Rev. D **66**, 094501 (2002).
[88] A. Bazavov *et al.*, Proc. Sci., LAT2009 (2009) 249 [arXiv:0912.5221].
[89] C. Davies, C. McNeile, E. Follana, G. Lepage, H. Na, and J. Shigemitsu, Phys. Rev. D **82**, 114504 (2010).
[90] P. Dimopoulos *et al.*, J. High Energy Phys. 01 (2012) 046.
[91] E. Gamiz, C. T. Davies, G. P. Lepage, J. Shigemitsu, and M. Wingate, Phys. Rev. D **80**, 014503 (2009).
[92] C. McNeile, C. Davies, E. Follana, K. Hornbostel, and G. Lepage, Phys. Rev. D **85**, 031503 (2012).
[93] C. Albertus, Y. Aoki, P. Boyle, N. Christ, T. Dumitrescu *et al.*, Phys. Rev. D **82**, 014505 (2010).
[94] G. Colangelo, S. Durr, A. Juttner, L. Lellouch, H. Leutwyler *et al.*, Eur. Phys. J. C **71**, 1695 (2011).
[95] M. Ciuchini, G. D'Agostini, E. Franco, V. Lubicz, G. Martinelli, F. Parodi, P. Roudeau, and A. Stocchi, J. High Energy Phys. 07 (2001) 013.
[96] A. Lenz, U. Nierste, J. Charles, S. Descotes-Genon, A. Jantsch, C. Kaufhold, H. Lacker, S. Monteil, V. Niess, and S. T'Jampens, Phys. Rev. D **83**, 036004 (2011).
[97] M. Bona *et al.*, J. High Energy Phys. 10 (2012) 068.
[98] K. Hayasaka, K. Inami, Y. Miyazaki, K. Arinstein, V. Aulchenko *et al.*, Phys. Lett. B **687**, 139 (2010).
[99] U. Bellgardt *et al.*, Nucl. Phys. **B299**, 1 (1988).
[100] S. Stone, at the *International Conference on High Energy Physics (ICHEP 2012)* (Melbourne, Australia, 2012).
[101] B. Collaboration, Phys. Rev. D **86**, 112008 (2012).
[102] J. Lees *et al.*, Phys. Rev. D **86**, 052012 (2012).
[103] Y. Amhis *et al.*, arXiv:1207.1158.
[104] M. Benzke, S. J. Lee, M. Neubert, and G. Paz, J. High Energy Phys. 08 (2010) 099.
[105] T. Hurth and M. Nakao, Annu. Rev. Nucl. Part. Sci. **60**, 645 (2010).
[106] P. del Amo Sanchez *et al.*, Phys. Rev. D **82**, 051101 (2010).
[107] W. Wang, arXiv:1102.1925.
[108] A. Crivellin and L. Mercolli, Phys. Rev. D **84**, 114005 (2011).
[109] A. Ali, H. Asatrian, and C. Greub, Phys. Lett. B **429**, 87 (1998).
[110] T. Hurth, E. Lunghi, and W. Porod, Nucl. Phys. **B704**, 56 (2005).
[111] B. Aubert *et al.*, Phys. Rev. Lett. **104**, 021802 (2010).
[112] K. Hayasaka *et al.*, Phys. Lett. B **666**, 16 (2008).
[113] J. Adam *et al.*, arXiv:1303.0754.
[114] J. J. Hudson, D. M. Kara, I. J. Smallman, B. E. Sauer, M. R. Tarbutt, and E. A. Hinds, Nature (London) **473**, 493 (2011).
[115] G. Bennett *et al.*, Phys. Rev. D **80**, 052008 (2009).
[116] K. Inami *et al.*, Phys. Lett. B **551**, 16 (2003).
[117] C. Baker, D. Doyle, P. Geltenbort, K. Green, M. van der Grinten *et al.*, Phys. Rev. Lett. **97**, 131801 (2006).
[118] J. Hisano, M. Nagai, P. Paradisi, and Y. Shimizu, J. High Energy Phys. 12 (2009) 030.
[119] M. Passera, J. Phys. G **31**, R75 (2005).
[120] M. Passera, Nucl. Phys. B, Proc. Suppl. **155**, 365 (2006).
[121] M. Davier, Nucl. Phys. B, Proc. Suppl. **169**, 288 (2007).
[122] K. Hagiwara, A. Martin, D. Nomura, and T. Teubner, Phys. Lett. B **649**, 173 (2007).
[123] A. J. Buras, G. Isidori, and P. Paradisi, Phys. Lett. B **694**, 402 (2011).
[124] D. A. Demir, O. Lebedev, K. A. Olive, M. Pospelov, and A. Ritz, Nucl. Phys. **B680**, 339 (2004).
[125] M. Pospelov and A. Ritz, Phys. Rev. D **63**, 073015 (2001).
[126] D. A. Demir, M. Pospelov, and A. Ritz, Phys. Rev. D **67**, 015007 (2003).
[127] K. A. Olive, M. Pospelov, A. Ritz, and Y. Santoso, Phys. Rev. D **72**, 075001 (2005).
[128] M. Antonelli, V. Cirigliano, G. Isidori, F. Mescia, M. Moulson *et al.*, Eur. Phys. J. C **69**, 399 (2010).
[129] R. Decker and M. Finkemeier, Phys. Lett. B **316**, 403 (1993).
[130] S. Banerjee, arXiv:0811.1429.
[131] J. F. Kamenik and F. Mescia, Phys. Rev. D **78**, 014003 (2008).
[132] J. Korner and G. Schuler, Z. Phys. C **38**, 511 (1988).
[133] J. Korner and G. Schuler, Phys. Lett. B **231**, 306 (1989).
[134] J. Korner and G. Schuler, Z. Phys. C **46**, 93 (1990).
[135] P. Heiliger and L. Sehgal, Phys. Lett. B **229**, 409 (1989).
[136] X.-Y. Pham, Phys. Rev. D **46**, R1909 (1992).
[137] S. Fajfer, J. F. Kamenik, I. Nisandzic, and J. Zupan, Phys. Rev. Lett. **109**, 161801 (2012).
[138] N. Deshpande and A. Menon, J. High Energy Phys. 01 (2013) 025.
[139] X.-G. He and G. Valencia, Phys. Rev. D **87**, 014014 (2013).
[140] A. Celis, M. Jung, X.-Q. Li, and A. Pich, J. High Energy Phys. 01 (2013) 054.
[141] M. Tanaka and R. Watanabe, Phys. Rev. D **87**, 034028 (2013).
[142] J. A. Bailey, A. Bazavov, C. Bernard, C. Bouchard, C. DeTar *et al.*, Phys. Rev. Lett. **109**, 071802 (2012).
[143] A. Datta, M. Duraisamy, and D. Ghosh, Phys. Rev. D **86**, 034027 (2012).
[144] D. Becirevic, N. Kosnik, and A. Tayduganov, Phys. Lett. B **716**, 208 (2012).

[145] P. Ko, Y. Omura, and C. Yu, J. High Energy Phys. 03 (2013) 151.
[146] P. Biancofiore, P. Colangelo, and F. De Fazio, Phys. Rev. D **87**, 074010 (2013).
[147] Y. Sakaki and H. Tanaka, Phys. Rev. D **87**, 054002 (2013).
[148] B. A. Dobrescu and A. S. Kronfeld, Phys. Rev. Lett. **100**, 241802 (2008).
[149] J. Alexander *et al.*, Phys. Rev. D **79**, 052001 (2009).
[150] P. Onyisi *et al.*, Phys. Rev. D **79**, 052002 (2009).
[151] G. Burdman, J. T. Goldman, and D. Wyler, Phys. Rev. D **51**, 111 (1995).
[152] J. N. Simone, Int. J. Mod. Phys. Conf. Ser. **02**, 92 (2011).
[153] V. G. M. J. Barranco, D. Delepine, and L. Lopez-Lozano, arXiv:1303.3896.
[154] A. Masiero and P. Paradisi, J. Phys. Conf. Ser. **53**, 248 (2006).
[155] A. Dedes, J. R. Ellis, and M. Raidal, Phys. Lett. B **549**, 159 (2002).
[156] A. Dedes, J. Rosiek, and P. Tanedo, Phys. Rev. D **79**, 055006 (2009).
[157] D. Boubaa, A. Datta, M. Duraisamy, and S. Khalil, arXiv:1211.5168.
[158] G. Passarino and M. Veltman, Nucl. Phys. **B160**, 151 (1979).
[159] W. Altmannshofer, A. J. Buras, and D. Guadagnoli, J. High Energy Phys. 11 (2007) 065.
[160] P. H. Chankowski and L. Slawianowska, Phys. Rev. D **63**, 054012 (2001).
[161] T. Aaltonen *et al.*, Phys. Rev. Lett. **102**, 201801 (2009).
[162] B. Aubert *et al.*, Phys. Rev. D **77**, 091104 (2008).
[163] A. J. Buras, arXiv:hep-ph/9806471.
[164] B. Blossier, P. Dimopoulos, R. Frezzotti, V. Lubicz, M. Petschlies, F. Sanfilippo, S. Simula, and C. Tarantino, Phys. Rev. D **82**, 114513 (2010).
[165] S. Chatrchyan *et al.*, Phys. Lett. B **713**, 68 (2012).